# The Role of Chd3 in Murine Cortical Development

Anneka Schoeppe

Supervisor: Dr. David J. Picketts

A thesis submitted to the Department of Biochemistry, Microbiology, and Immunology

University of Ottawa

In partial fulfilment of the requirements for the degree of Master of Science in Biochemistry with specialization in Human and Molecular Genetics

Submitted: July 2023

# Abstract

The nucleosome remodeling and deacetylase (NuRD) complex makes use of Chromodomain Helicase DNA binding protein 3 (CHD3) to remodel chromatin. Of the three CHD proteins NuRD may incorporate (CHD3/4/5); the function of CHD3 within the brain is the only one to have not been studied through gene knockout. Chd3 mutations in humans cause a neurodevelopmental disorder (SNIBCPS) characterized by intellect and speech deficits, but limited work has been done to describe a phenotype in mice. We have generated mice with fore-brain specific deletion of Chd3 to characterize its impact on embryonic and postnatal cortical development. To analyze the consequence of Chd3 ablation on cortical lamination, layer-specific staining was performed and showed a decreased number of cells in layers II-IV. Neuronal birthdating has demonstrated that this is due to a defect in migration, causing the cells to be retained in the lower layers. Behaviour testing has also indicated defect in fear learning and memory in heterozygote males. These initial indications of defects in cortical development and behavioural deficits in the Chd3 mutant mice suggest that the animals are a good first model of the SNIBCP syndrome.

# Acknowledgements

Firstly to Dave, thank you for giving me a chance when I came in with no experience. The past two years have been quite a learning curve and you have always guided me with patience and kindness. I will be forever grateful for my time in your lab and all I was able to learn from you.

To Pierre, Diane, the Mattar lab, and the Picketts lab, thank you for all of the discussion and direction along the way. It's easy to follow the wrong trail and I think you kept me on the right track.

To Keqin and Valerie, I am the first person in my family to go to grad school. I had no idea how anything worked or if I was doing the right things when I started. You both were the first to show me what I needed to know and throughout the completion of this thesis were always there to help me when I needed it. I never could have made it here without either of you and I am glad to call you my friends.

To Pranisha and Mat, a friend is someone who is there when you need them, you are both friends personified. Grad school is quite an experience and you made the hard days not so hard. I have always been able to lean on you both when my fifth attempt at an experiment still isn't working or the weight of deadlines was crushing me. I hope I have been the same to you.

To my family thank you for caring for me and being patient with my crazy schedules throughout the completion of this thesis. I am so thankful for each and every one of you.

Finalmente, a mi amor. Esta tesis es tanto mía como tuya. Nunca podría poner en palabras lo agradecido que estoy por ti. Siempre has sido tan paciente y comprensivo, especialmente en estos largos días de escritura. Estoy aquí gracias a ti y podré seguir adelante por la misma razón. Gracias por todo lo que eres.

And finally a reminder to myself and anyone who may read this; I impart the biggest lesson I learned these past two years: You're going to drop some balls, you just have to know which ones are rubber and which are glass.

# Table of Contents

# List of Abbreviations

ACF = ATP-utilizing Chromatin Assembly and Remodeling Factor
ADD = ATRX-DNMT3-DNMT3L
ALT = Alternative Lengthening of Telomeres
ARPs = Actin Related Proteins
ASD = Autism Spectrum Disorder
ATRX = alpha thalassemia/mental retardation syndrome X-linked
BAF = BRG1/BRM-associated factor
BPTF = Bromodomain PHD finger Transcription Factor
BRG1 = Brahma Related Gene 1
BRM = Brahma
BRD7 = Bromodomain Containing 7
BRD9 = Bromodomain Containing 9
BRK = Brahma Kismet
cDNA= Complementary DNA
CENP-A= Centromere protein A
CERF = CECR2-containing remodeling factor complex
CHARGE = Coloboma, Heart Disease, Atresia of the Choanae, Retarded Growth and Mental Development, Genital Anomalies, and Ear Malformations
CHD = Chromodomain Helicase DNA-binding
CHRAC = Chromatin Assembly Complex
cHTs = Conditional Heterozygotes
CKOs = Conditional Knockouts
CP = Cortical Plate
CSD = Canadian Survey on Disability
CSF = Cerebrospinal Fluid
CSS = Coffin-Siris Syndrome
CR= Cajal-Retzius
Ctip2= COUP-TF-interacting protein 2
DAPI = 4',6-diamidino-2-phenylindole
DAXX = Death Associated Protein 6
DNA= Deoxyribonucleic acid
Dnmt = DNA Methyltransferase
DSB = Double Stranded Break
EE = Epileptic Encephalopathy
ECL= Enhanced Chemiluminescence
EDTA= Ethylenediamine tetraacetic acid
EdU = 5-ethynyl-2′-deoxyuridine
GAPDH = Glyceraldehyde 3-Phosphate Dehydrogenase
GATAD2A/2B = GATA Zinc Finger Domain Containing 2A/2B
GLTSCR1 = Glioma Tumor Suppressor Candidate Region Gene 1
GOF = Gain of Function
GYF = Glycine-Tyrosine-Phenylalanine
H3K9me = Lysine 9 Methylation on Histone H3
H3K9ac = Lysine 9 Acetylation on Histone H3
HAT = Histone Acetyltransferases

HDAC1/2 = Histone Deacetylase 1/2
HRP = Horseradish Peroxidase
HSA = Helicase-SANT-Associated
IF = Immunofluorescence
INO80 = INOsitol-requiring Mutant 80
IPCs = Intermediate Progenitor Cells
ISWI = Imitation SWItch
ITI = Intertrial Interval
IZ = Intermediate Zone
KMT = Lysine Methyltransferase
lncRNAs = Long Non-Coding RNAs
MBD2/3 = Methyl-DNA Binding Protein 2/3
mPFC= Medial Prefrontal Cortex
MRI = Magnetic Resonance Imaging
mRNA= Messenger RNA
MTA1/2/3 = Metastasis Associated 1/2/3
ncBAF = Non-Canonical BRG1/BRM-associated factor
NCBRS = Nicolaides-Baraitser Syndrome
NEDDFL = Neurodevelopmental Disorder with Dysmorphic Facies and Distal Limb Anomalies
NMD = Nonsense-Mediated Decay
NoRC = Nucleolar Remodeling Complex
NPC = Neural Progenitor Cell
NSCs = Neural Stem Cells
NTC = Non-template control
NuRD = Nucleosome Remodeling and Deacetylase Complex
NURF = Nucleosome Remodeling Factor
OCT = Optimal Cutting Temperature
PBAF = Polybromo-Associated BAF
PBRM1 = Polybromo 1
PBS = Phosphate Buffered Saline
PFA = Paraformaldehyde
PHD = Plant Homeodomain
pHH3= Phospho-histone H3
PML= Promyelocytic leukemia
PMNDS = Parenti-Mignot Neurodevelopmental Syndrome
PTC= Premature Termination Codon
PTM = Post-Transcriptional Modifications
PVDF = Polyvinylidene Fluoride
RBBP4/7 = Retinoblastoma Binding Protein 4/7
rDNA= Ribosmal DNA
RGC = Radial Glial Cells
RIPA = Radio-Immunoprecipitation Assay
RNA = Ribonucleic acid
RSF = Remodeling and Spacing Factor
Satb2 = Special AT-rich sequence-binding protein 2
scRNA-seq = single cell RNA sequencing

SDS = Sodium Dodecyl Sulfate
shRNA = Short Hairpin RNA
SIHIWES = Sifrim-Hitz-Weiss Syndrome
SMARCA1= SWI/SNF Related, Matrix Associated, Actin Dependent Regulator of Chromatin, Subfamily A, Member 1
SMARCA2 = SMARCA2 (SWI/SNF Related, Matrix Associated, Actin Dependent Regulator of Chromatin, Subfamily A, Member 2
SMARCA4 = SMARCA2 (SWI/SNF Related, Matrix Associated, Actin Dependent Regulator of Chromatin, Subfamily A, Member 4
SMARCA5 = SWI/SNF Related, Matrix Associated, Actin Dependent Regulator of Chromatin, Subfamily A, Member 5
SMARCC2 = SWI/SNF-Related Matrix-Associated Actin-Dependent Regulator of Chromatin Subfamily C Member 2
SNIBCPS = Snijders Blok-Campeau Syndrome
SRCAP = Snf2-Related CREBBP Activator Protein
SVZ = Subventricular Zone
SWI/SNF = SWItch/Sucrose Non-Fermentable
Tbr1 = T-box brain transcription factor 1
TBS-T = Tris-Buffered Saline with 0.1% Tween
TSS = Transcriptional Start Sites
VZ = Ventricular zone
WICH = WSTF (Williams Syndrome Transcription Factor) and ISWI (Imitation Switch)
WT = Wild Type

# List of Figures

# List of Tables

# 1. Introduction

## 1.1 Cortical Development

Developmental disability represents a significant burden on the Canadian health care system with approximately 2% of the population affected (1). The 2017 Canadian Survey on Disability (CSD) saw 64% of respondents reporting having “severe” or “very severe” disability and 87% described their mental health as less than “very good” compared to 30% of the general population (2). Of the 1616 genes definitively linked to developmental disabilities, 10% of the genes encode epigenetic regulators (3). Dynamic chromatin regulation is a critical aspect of neurogenesis as genes are activated and repressed throughout developmental time (4).

Murine corticogenesis begins with the formation of radial glia cells (RGCs), a multipotent neural stem cell, from neuroepithelial cells in the ventricular zone (VZ) around embryonic day 10.5 (E10.5) (5). RGCs may divide symmetrically (i.e., with the plane of cell division perpendicular to the ventricle) to form two daughter RGCs or asymmetrically (i.e., with the plane of cell division parallel or oblique to the ventricle) to form an RGC and a committed neuron or an intermediate progenitor cell (IPC). The IPCs are more restricted and largely divide symmetrically to produce two neurons. Nonetheless, both RGCs and IPCs receive external cues and change their intrinsic expression profile to expression different transcription factors that subsequently alter their competency to form deep or upper layer neurons with this switch occurring around E14.5 (6). These progenitors experience a competency switch again at E17.5 to begin the production of glial cells.

By E12.5, Cajal-Retzius (CR) cells are generated and these form layer I of the cortex. At this time, the progenitors also start differentiation of the neurons which will populate the cortical

plate (CP) (7). Layer VI cells are the first formed and thus the first to enter the CP. Layer V is generated next and must travel through the layer VI cells to take their position in the cortex. This process continues in the so-called inside-out fashion until the final layer, layer II, is filled. The timing of production of each layer occurs in a concerted fashion with each occurring in approximately one day (Figure 1).

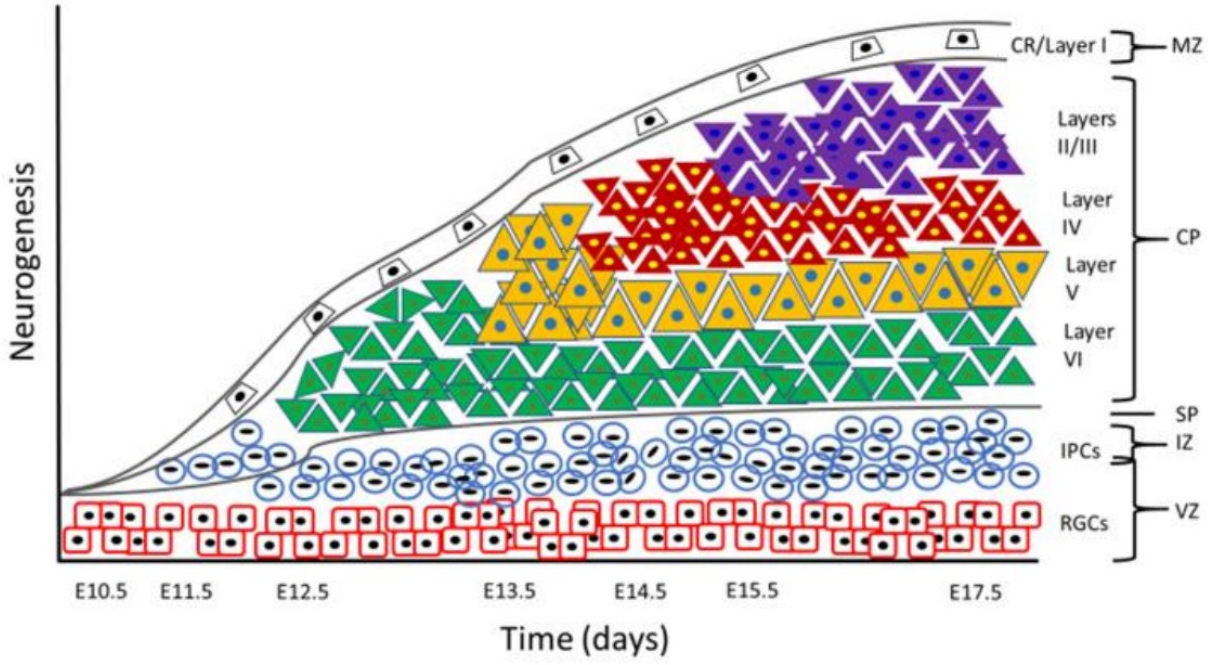


**Figure 1. Embryonic development of the murine cortex.** Murine corticogenesis occurs in a concerted inside-out manner. Layer I comprised of CR cells is formed by E12.5. Layer VI begins formation at the same time and each subsequent day another layer is added. Figure adapted from Adnani *et al.* (5).

## 1.2. Chromatin

The full diploid complement of the human genome contains roughly 6.4 billion nucleotides (8). This requires over 1.8 m of DNA to fit within a nucleus that is on average 5 μm across (9). In order to achieve the necessary compaction, the DNA is wrapped around eight positively charged histone proteins – two copies each of histones H2A, H2B, H3, and H4, forming a nucleosome which holds 147 base pairs (10). A chromatosome is formed with the association of the linker histone H1 which binds the DNA as it enters the nucleosome. Additionally, histones only partially reduce the negative charge of the DNA thus repulsion is still experienced with other regions of the DNA. The incorporation of H1 proteins along with cations and other positively charged proteins allow for further folding (11).

The next level of compaction still has yet to be fully resolved. The folding of nucleosomes into a regular fibre with a diameter of 30 nm (the "30-nm fibre") was first described in 1976 (12). This structure has been regularly observed *in vitro* with debate over the exact folding of the fibre as it is not readily formed under conditions appropriate for high-resolution structural analyses (13). The solenoid or "one-start" model has been observed in the presence of histone H5 (14), while on long reconstituted nucleosome arrays the two-start zigzag model has been seen (15). The zigzag tetranucleosomal model was revealed with x-ray crystallography – formed by two stacks of nucleosomes attached by a segment of linker DNA (16). Although resolution of the 30-nm fibre can provide insight into the electrostatic interactions of nucleosomes, increasing evidence has suggested that the native chromatin has a much more dynamic "liquid-like" structure (17-19). Furthermore, the regular folding of the 30-nm fiber is seen under low salt conditions whereas physiological salt concentrations are much higher, leading to irregular folding described as supramolecular globular structures (19-21). For the

molecular biologist, the conceptualization of this folding is perhaps more pertinent insofar as the understanding of the function and regulation of genes *in vivo*.

### 1.2.1. Histone Tails

An additional level of structural control is provided by the positively charged N-terminal tails of the histone proteins. The tails of histones H3 and H4 regulate higher order folding by binding to DNA or acidic regions of other nearby nucleosomes (22-24). Histone tails vary in length and importantly undergo considerable posttranslational modification (PTM). There are three main groups of proteins which are involved with the histone PTM landscape (25). Readers have domains designed to recognize or "read" specific PTMs. Writers are enzymes which add PTMs onto histone tails. Erasers are enzymes that remove PTMs. More than two dozen possible modifications have been described, but an exhaustive review of these PTMs is beyond the scope of this thesis. However, it is comprehensible that this large number of modifications which may be present in thousands of possible combinations provides the need for the several hundred histone-modifying enzymes that have been described thus far (26). Here, I briefly review the two most common modifications, histone acetylation and histone methylation which are typically involved in chromatin decompaction/compaction, respectively.

Acetylation does indeed result in decompaction. Addition of acetyl groups to lysines of histone H3 – strongly associated with transcriptional start sites (TSS) – or H4 – variable in genomic location – by histone acetyltransferase (HAT) results in loosening of the nucleosomes (27-29). This is due to the acetyl groups neutralizing the positive charge of the lysine residues, thus reducing the attraction to the negatively charged DNA backbone (30).

Although methylation can result in increased packaging of chromatin it may also reduce it depending on the location and number of methyl groups added. All basic histone residues can

be methylated, though the most extensively studied is the methylation of lysine (31-34). Histone lysine methyltransferases (KMTs) can catalyze the transfer of one, two, or three methyl groups (35). Di-methylation and tri-methylation of H3 lysine 9 or 27 cause repression of the local DNA region (36-37). However, mono-methylation of H3 lysine 4, 9, 27, or 79, di-methylation of H3 lysine 79, and tri-methylation of H3 lysine 4 and 36 all correspond with gene activation (29, 37-39). This variable effect on chromatin accessibility is unlike acetylation in that methylation does not have the same effect on electrostatic interactions, but rather the epigenetic marks present can act as recognition sites for chromatin remodelers or inhibit binding of transcription factors (40).

### 1.2.2. Histone Variants

The core canonical histones have paralogs (variants) that can take their place in the nucleosome, thus providing a different structural or functional capability. One of the key differences between canonical histones and their variants is that they are synthesized during S-phase to be added immediately following replication while the variants are replication-independent and therefore can be synthesized throughout the cell cycle (41). Additionally, eukaryotic core histones are well conserved whereas the variants have a large disparity between species (42). Common variants with well described roles include H3.3, H2AZ, and CENP-A. More variants likely have yet to be described and some that have been identified are not well understood (43, 44). While there is still much to be learned it is clear that on the whole histone variants confer further temporal and spatial transcriptional control.

### 1.2.3. Additional Mechanisms of Chromatin Modification

Beyond modifications to histones, the DNA itself may also be modified. Transfer of a methyl group onto the fifth carbon of a cytosine by DNA methyltransferase (Dnmt) forms 5-methylcytosine (5mC) (45). This occurs on cytosines within CpG dinucleotides and regulates

gene expression by blocking binding of transcription factors or by recruiting repressive enzymes. Patterns of DNA methylation may be inherited from parental chromosomes or *de novo* alterations may be made. Dnmt activity is high in developing embryos but reduces drastically by the time a cell reaches terminal differentiation. However, postmitotic neurons still experience elevated Dnmt activity. Neurons are thus able to modulate their DNA methylation landscape in response to internal and external stimuli, thereby altering the gene expression as necessary.

Additionally, there exists a form of RNA which may modulate chromatin structure known as long non-coding RNAs (lncRNAs). 16000 lncRNA genes have been identified, however some estimate that the total number exceeds 100000 (46, 47). The negative charge of the lncRNA may neutralize the positive charges of the histone tails to encourage chromatin decompaction (48). This is believed to provide a mechanism for rapid control of gene expression – either by new association of an lncRNA to initiate or increase expression or dissociation to return the compaction from histone tails. These lncRNAs may act in *cis* or *trans* directly with the DNA, however they may also help recruit or prevent binding of chromatin modifiers (49).

### 1.3. Chromatin Remodelers

While the contents of genes are important, chromatin remodelers may be considered equally important as they act to control the expression of the genes. Chromatin remodeler proteins not only alter the accessibility of chromatin by making covalent changes to the histones or exchanging histone variants, but also through nucleosome sliding. ATP-dependent chromatin remodeling proteins contain ATP-dependent helicase domains (ATPases) which hydrolyze ATP to facilitate the movement of the nucleosomes by disrupting the contacts between the histones and DNA (50). Chromatin remodeling proteins frequently operate in remodeler complexes, of which there are 5 main classes: imitation switch (ISWI), switching defective/sucrose non-

fermenting (SWI/SNF), inositol requiring 80 (INO80), alpha thalassemia/mental retardation syndrome X-linked (ATRX), and chromodomain helicase DNA binding (CHD) (51). These remodelers all belong to the helicase superfamily 2 (SF2) characterized by their bi-lobed Snf2 ATPase comprising two tandem RecA-like folds. Each family is distinguished by the additional conserved chromatin motifs and by the distance between the helicase and ATPase domains which alter the sliding activity. Additionally, these proteins lack the wedge domain found in other remodeler superfamilies which enables strand separation and as such only act as DNA translocases (52). These families have all been implicated in neurodevelopmental disorders, summarized in Table 1 below and described in detail in the following sections.

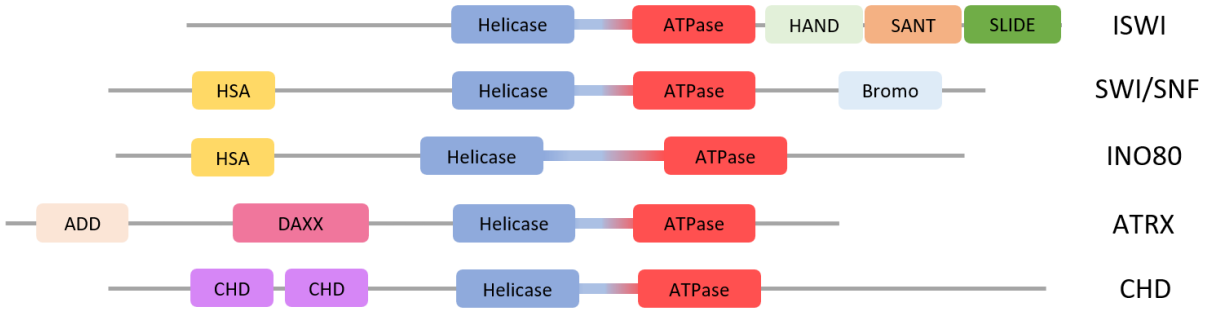


**Figure 2. Schematic representation of chromatin remodeler families.** All families share the helicase-ATPase domain. Conserved characteristic domains of each family are also displayed.

**Table 1. List of SF2-associated neurodevelopmental disorders described in this thesis.**

| Class | Gene | Associated Disease(s) | Reference |
|---|---|---|---|
| ISWI | *SMARCA5* | Developmental delay, microcephaly, short stature | Li *et al*. (2021) |
| | *SMARCA1* | CSS-like, Rett syndrome-like, schizophrenia | Karaca *et al*. (2015); Homann *et al*. (2016); Lopes *et al*. (2016) |
| | *BPTF* | NEDDFL | Stankiewicz *et al*. (2017) |
| SWI/SNF | *BAF250B* | CSS | Wieczorek *et al.* (2013) |
| | *SMARCA4* | CSS, ASD | Tsurusaki *et al.* (2012); Qian *et al.* (2022) |
| | *SMARCA2* | CSS, NCBRS, schizophrenia | Tsurusaki *et al.* (2012); Miyake *et al.* (2016); Koga *et al.* (2009) |
| INO80 | *INO80* | Intellectual disability, developmental delay, microcephaly | Alazami *et al.* (2014) |
| | *SRCAP* | Floating-Harbor syndrome | Hood *et al.* (2012) |
| ATRX | *ATRX* | ATR-X Syndrome | Gibbons *et al.* (2000) |
| CHD | *CHD1* | Pilarowski-Bjornsson syndrome | Pilarowski *et al.* (2018) |
| | *CHD2* | EE, ASD, *CHD2*-related neurodevelopmental disorder | Lamar *et al.* (2018); Yasin *et al.* (2020); Carvill *et al.* (2021) |
| | *CHD3* | SNIBCPS | Snijders Blok *et al*. (2018) |
| | *CHD4* | SIHIWES | Sifrim *et al.* (2016); Weiss *et al.* (2016) |
| | *CHD5* | PMNDS | Parenti *et al.* (2021) |
| | *CHD7* | CHARGE syndrome | Hittner *et al.* (1979) |
| | *CHD8* | ASD, Zahir-Friedman syndrome | Weissberg *et al.* (2021); Yasin *et al.* (2019) |

### 1.3.1. ISWI

Like all chromatin remodelers, ISWI proteins contain a highly conserved ATPase domain. ISWI have a SWI2/SNF2 family ATPase domain along with their characteristic HAND-SANT-SLIDE domains which possess the proteins' DNA binding activity (52). The HAND domain performs both histone and DNA binding and recognition, the SANT domain interacts with unmodified histone tails, and the SLIDE domain binds the DNA of the nucleosome that is present at the dyad axis (53).

Though ISWI was originally first identified in *Drosophila*, these proteins are highly conserved in eukaryotes (54). Mammals have two ISWI proteins: Snf2h encoded by the gene *Smarca5* and Snf2l encoded by the gene *Smarca1* (55). These proteins have been found to associate in 8 different chromatin remodeling complexes: ATP-utilizing chromatin assembly and remodeling factor (ACF), chromatin assembly complex (CHRAC), SNF2H-cohesin, remodeling and spacing factor (RSF), nucleolar remodeling complex (NoRC), WSTF-ISWI chromatin remodeling complex (WICH), CECR2-containing remodeling factor (CERF), and nucleosome remodeling factor (NURF) (56-68). These complexes have been classically described as 6 containing Snf2h and 2 containing Snf2l, however it has been found that both co-purify with all interactors, suggesting that either gene may be incorporated into any of the complexes (69).

#### 1.3.1.1. ISWI-associated Neurodevelopmental Disorders

As these proteins operate in a multitude of complexes, it can be difficult to connect the loss of functioning of any one directly to the phenotype observed in related neurodevelopmental disorders. Indeed, it could be a combinatorial effect between the loss of multiple complexes. Nevertheless, mutations in the genes themselves have been associated with a few neurodevelopmental disorders.

Snf2h has been shown to have a critical role in mammalian development. In mice, constitutive knockouts die early *in utero* and conditional knockouts have shown to have reduced body size and cerebellar hypoplasia (70). Pathogenic *SMARCA5* germline variants have been identified in 12 patients across 10 families (71). All individuals present with mild developmental delay, microcephaly, short stature, and facial dysmorphisms. Of note, this disorder was found to be transmissible across at least three generations which is not commonly seen with pathogenic variants in chromatin remodelers (72, 73).

While *SMARCA1* has not been directly linked to any one neurodevelopmental disorder, variants have been found in genetic screens in three different conditions: Coffin-Siris syndrome-*like* phenotype, Rett syndrome-*like* phenotype, and schizophrenia spectrum disorders (74-76). Interestingly, a broad range of phenotypes were seen across all identified *SMARCA1* mutations.

Aside from the ISWI proteins themselves, several ISWI partner proteins have also been implicated in neurodevelopmental disorders. For example, the bromodomain PHD finger transcription factor (BPTF) protein of the NURF complex is causative for Neurodevelopmental disorder with dysmorphic facies and distal limb anomalies (NEDDFL), characterized by intellectual disability and microcephaly (77).

#### 1.3.1.2. Current ISWI Neurodevelopmental Disorder Mouse Models

Given that there is no distinct mechanism of action in the ISWI-associated neurodevelopmental disorders it can be difficult to conceptualize a treatment or cure. Of course, the location and type of mutation in the gene can result in different aberrant functions or complete loss of function, making it more difficult to understand the pathogenesis. However, even general model systems provide direction and give better insight into the actions of a gene.

*Smarca5* has been characterized in three conditional knockouts (cKOs). The first is using the Emx1-Cre driver which results in forebrain deletion (78). These mice saw increased cell death and a decrease in Tbr2+ intermediate progenitor cells (IPCs) and FoxG1+ post-mitotic neurons, which resulted in a deficit of the upper-layer neurons (79). The loss of cells produced a reduction in the size of the cortex which was also observed in human patients (see above). A hyperactivity phenotype was also observed. A central and peripheral nervous system Cre driver (80) – Nestin-Cre – showed a significant reduction in body weight and cKOs died before reaching maturity (70). These mice had cerebellar hypoplasia and severe motor defects. Finally,

PCP2-Cre is active in postmitotic Purkinje cells after postnatal day 10 (P10). Behavioural assays of PCP2-Cre cKOs suggested impaired associative learning and reduced sociability. Importantly, these mouse models demonstrated a compensatory mechanism of Snf2l under Snf2h loss. Though it is difficult to characterize an intellectual disability in mice, these models demonstrate the molecular mechanisms that result in the microcephaly seen in the *SMARCA5* variants. It is likely that these alterations in brain development provide the underpinnings of the developmental delay as well.

*Smarca1* mice were generated with a constitutive exon 6 deletion of the gene (81). Exon 6 contains the ATP-binding motif of the SNF2 domain. These animals generate an internally truncated Snf2l protein that lacks the ability to bind or hydrolyze ATP but can still interact with its partner proteins. Unlike the hypoplasia seen in *Smarca5* models, exon 6 deleted animals saw an increase in brain size with hypercellularity observed as early as E15.5 due to an increase in progenitor self-renewal. Though *SMARCA1* mutations are not associated with a unique condition, none of the associated disorders have described patients with macrocephaly. This is perhaps due to a disparity between the model allele and those of patient mutations. While these mutants provide important insights into the mechanisms of the gene, they are not an ideal model of the human phenotype.

Though *Bptf* mice cannot survive knockout with *Nestin*-Cre, a model generated with *Emx1*-Cre demonstrated severe cortical hypoplasia (82). It was found that these mice had a loss of layer V neurons due to increased cell cycle length and cell death within the progenitor pool. Additionally, molecular studies identified Bptf target genes involved in fate determination, neural development, and apoptotic signaling. This is an exemplary mouse model. The *Bptf Emx1*

cKO mice display the NEDDFL phenotype and upon analysis demonstrate a clear and distinct mechanism of the phenotype. They provide an excellent resource in the study of NEDDFL.

### 1.3.2. SWI/SNF

The first ATP-dependent chromatin remodeler described was the yeast SWI/SNF complex (83, 84). In mammals, there are two SWI/SNF homologs – brahma (BRM) and brahma-related gene 1 (BRG1). The SWI/SNF family has a characteristic bromodomain which targets acetylated histone tails (85). They also contain a helicase-SANT-associated (HSA) domain which binds actin or actin related proteins (ARPs) which is thought to facilitate remodeling, histone binding, complex assembly and stability, or regulating ATPase activity (86-88). Recently, it has been demonstrated that the removal of the HSA domain from the SWI/SNF protein Brahma-related gene 1 (BRG1) results in a severe reduction in chromatin remodeling capabilities likely due to disruptions in stable chromatin binding (89).

The SWI/SNF complex is highly dynamic with composition varied between cell types and tissues (90). In mammals, three SWI/SNF complexes have been found: BRG1/BRM-associated factor (BAF), polybromo-associated BAF (PBAF), and non-canonical BAF (ncBAF or GBAF) (91, 92). All contain one of the two SWI/SNF chromatin remodelers BRG1 (*SMARCA4*) or BRM (*SMARCA2*). BAF is a large complex comprised of 13 subunits (93). The other two complexes are highly similar, except for some key differences. In PBAF, the core BAF subunit ARID1A is replaced with its paralog ARID2. Additionally, it contains the proteins bromodomain containing 7 (BRD7) and polybromo1 (PBRM1). In the ncBAF complex the ARID1A subunit is replaced with the glioma tumour suppressor candidate region gene 1 (GLTSCR1). It is also smaller due to a lack of three BAF proteins: SWI/SNF related, matrix associated, actin dependent regulator of chromatin subfamily C member 2 (SMARCC2),

SMARCE1 (subfamily E member 1), and SMARCB1 (subfamily B member 1). However, it uniquely contains bromodomain containing 9 (BRD9). These distinct compositions allow for specificity to enhancers and promoters that is not shared between complexes (94).

#### 1.3.2.1. SWI/SNF-associated Neurodevelopmental Disorders

Many of the SWI/SNF complex subunits are implicated in neurodevelopmental disorders. *BAF250b* is the most frequently mutated gene in Coffin-Siris syndrome (CSS), appearing in up to 68% of patients in some cohorts (95, 96). However, the chromatin remodelers themselves, *SMARCA4* and *SMARCA2*, have also been reported to have variants that are pathogenic for CSS (96). Missense *SMARCA2* mutations were found within the ATPase domain, likely affecting proper ATP hydrolysis (97). Missense and in-frame deletions were also found in the ATPase domain of *SMARCA4* mutants in CSS, though these have been suggested to function through a gain-of-function (GOF) or dominant-negative effect (98). Aside from CSS, *SMARCA4* has also been implicated in autism spectrum disorder (ASD) (99, 100).

Though both proteins have a 74% amino acid similarity, only *SMARCA2* mutations are seen in Nicolaides-Baraitser syndrome (NCBRS), an intellectual disability characterized by severe intellectual disability, speech delay, seizures, growth retardation, and characteristic facial dysmorphisms (101-105). Additionally, *SMARCA2* has uniquely been linked to Schizophrenia (106, 107).

Some argue that SWI/SNF-associated disorders exist on a spectrum based on the alterations to the genes (100, 108). This spectrum would see ASD on the end of milder features with CSS of increasing severity forming the middle of the spectrum and NCBRS as the most severe.

#### 1.3.2.2. Current SWI/SNF Neurodevelopmental Disorder Mouse Models

Given that the SWI/SNF remodelers were the first identified, many mouse models have been generated to characterize their roles. *Smarca2*-null mice are available for purchase from the Jackson Laboratory and the International Mouse Phenotyping Consortium only characterize them as having hyperactivity in females (109). However, a group at the University of Tsukuba have found that *Smarca2* knockout mice have impaired social interaction and prepulse inhibition (106). Moreover, psychotogenic drugs lowered the *Smarca2* expression in the brain while antipsychotic drugs lead to an increase.

In stark contrast to the *Smarca2*-null mice, *Smarca4*-null mice die in the peri-implantation stage (110). As such, numerous *Smarca4* conditional knockouts have been generated with three of note examining cortical development (111). *Nestin*-Cre cKOs showed a defect in self-renewal and maintenance of neural stem cells (NSCs) along with astrocytic differentiation (112-114). *Glast*-Cre affects adult NSCs and astrocytes, leading to a defect in adult NSC neurogenesis in the subventricular zone (SVZ) and astrogenesis (112, 115).

*Arid1A Emx1*-Cre cKOs have also demonstrated critical roles of the protein in cortical development. These mutants were found to have corpus callosum agenesis and mistargeting of intracortical axons (116). Another group saw a reduction in cortical thickness due in part to inhibition of proliferation of RGCs as well as an increase in cell death in late cortical development (117). It was found that the mutants had dysregulation of expression of genes associated with proliferation and differentiation. These results could explain the intellectual deficits and microcephaly observed in CSS patients, however further work is required to better describe the mechanisms behind these phenotypes and elucidate the impact on the functioning of the mice.

Further, Baf155 cKO with *Emx1*-Cre displayed a loss of IPCs due to loss of Pax6-dependent transcription (118). This resulted in loss of cell adhesion of apical RGCs in the ventricular zone (VZ) leading to ectopic basal positioning. In addition, Baf170 which competes with Baf155 for incorporation into the complex, can produce cortical overgrowth in cKOs or a reduction of the cortex when overexpressed (119). Baf170 also associates with Pax6 to regulate IPC proliferation. This proposed model comprises Baf170 overexpression leads to repression of IPC genes causing RGCs to be the direct contributor to the neuronal population leading to underdevelopment of the cortex. In the absence of Baf170, Baf155 must compensate and causes overexpression of the IPC genes leading to an overgrowth of the cortex. This provides important insight into the control of corticogenesis. Further, behaviour analysis of Baf170 cKOs found spatial learning deficits likely due to the loss of radial glial-like progenitors in the hippocampus (120). The behaviour results are more demonstrative of the intellectual disability seen in human patients, indicating that the aberrant function of molecular mechanisms observed in the mice may have a role in the patients as well though further analysis is needed.

### 1.3.3. INO80

The Ino80 family gets its name from its functional role of regulating inositol-responsive gene expression in yeast (121). The mammalian Ino80 family comprises a homologous INO80 protein and the Snf2-related CREBBP activator protein (SRCAP), each forming a unique complex (52). These proteins contain an HSA domain like the SWI/SNF, as well as a characteristic spacer region that splits the ATPase domain. The spacer region was found to bind RuVB-like subunits and ARPs (122).

The presence of the RuVB-like helicases in the INO80 complexes are indeed involved in DNA repair. The complex associates with γ-H2AX at double stranded breaks (DSBs) in DNA

and helps with nucleosome eviction of the surrounding area (123-125). Another significant role is histone variant loading. The SRCAP complex is responsible for replacing H2A with the histone variant H2A.Z for the regulation of gene expression (126-128).

#### 1.3.3.1. INO80-associated Neurodevelopmental Disorders

Missense mutations in *INO80* have been found to cause intellectual disability due to a global developmental delay and primary microcephaly (129). As loss of DNA damage repair is frequently seen with microcephaly, it is thought that loss of repair from the INO80 complex is what underlies the microcephaly in these patients.

In *SRCAP*, truncating mutations are causative for Floating-Harbor syndrome, characterized by language deficits, short stature, delayed ossification, and distinctive facial dysmorphisms (130). For individuals who had parental DNA available, all mutations were found to be *de novo*. Interestingly, the five mutations between the thirteen identified patients all clustered within 111 codons of the final exon.

#### 1.3.3.2. Current INO80 Neurodevelopmental Disorder Mouse Models

*Ino80*-null mice die before reaching weaning age (131). Due to this, most characterization has been performed on the *Ino80*+/- mice. It was found that they have decreased locomotor activity, decreased novel environment exploration, and increased aggression. Additionally, females have abnormal vocalization and males have abnormal seminal vesicle morphology. Conditional knockout of *Ino80* in neural progenitor cells (NPCs) with *Neurod6*-Cre lead to apoptosis and microcephaly due to the loss of DNA repair in symmetric, but not asymmetric NPC divisions (132). This represents a thorough characterization, providing exceptional insight into the mechanisms of the *INO80*-associated neurodevelopmental disorder. The analysis of the NPCs confirms the hypothesis of the microcephaly being caused by the loss

of these cells to repair DNA damage. The addition of the behavioural assays better conveys the consequences of alterations to the brain that could be seen in human patients. The reiteration of some aspects of the disorder in the mice warrants further exploration into their behaviour. For example, mouse models of intellectual disability have shown difficulties in assays requiring learning and memory which were not explored here (133).

While conditional knockouts of *Srcap* have been performed in other organ systems (134-137), no neural mouse models have been described.

### 1.3.4. ATRX

As previously mentioned, ATRX is an orphan chromatin remodeler. Though it has no true paralogs, like the other families it contains the conserved helicase-ATPase domain characteristic of the SNF2 superfamily (138). In addition, it has an ATRX-DNMT3-DNMT3L (ADD) domain which reads the repressive H3K9me3 marks characteristic of constitutive heterochromatin and is blocked by the euchromatic signature of H3K4 methylation (139-144). It then follows that ATRX has been found to mostly localize to regions such as pericentric heterochromatin, telomeres, and G-rich repeats that can form G4 quadruplex structures (145, 146). It is believed that ATRX plays a key role in maintaining genome integrity by keeping these regions compacted. Additionally, alternative lengthening of telomeres (ALT) positive cancers (~15% of cancers) have been found to have somatic loss of ATRX (147, 148). These cancers utilize recombination to maintain telomere length through the ALT pathway, taking advantage of the loss of ATRX which is thought to inhibit recombination at telomeres. ALT+ cancers account for some of the most notoriously difficult to treat, such as glioblastoma multiforme. Beyond heterochromatin, ATRX has also been found to have roles in gene regulation and localization with promyelocytic leukemia (PML) nuclear bodies (149-151).

ATRX forms a complex with death domain associated protein (DAXX) through its DAXX binding domain (152, 153). DAXX acts as a histone chaperone to the variant H3.3. The ATRX/DAXX complex deposits H3.3 in nucleosomes present in pericentric heterochromatin and telomeric repeats (154, 155). H3.3-null cell lines have demonstrated its role in maintaining genome integrity by supporting constitutive heterochromatic structures (156).

There also exists a notable truncated isoform of ATRX known as ATRXt. This protein does not have intron 11 spliced from the primary transcript thereby creating a premature stop codon and making it 80 kDa smaller than ATRX (157, 158). The isoform retains its ADD domain, but not its DAXX or ATPase domain, indicating that it should still be able to bind DNA but not perform its canonical functional roles. Though the sequence has been described, its function has yet to be elucidated.

#### 1.3.4.1. ATRX Syndrome

ATR-X syndrome is a rare neurodevelopmental disorder primarily affecting males. Most mutations identified are missense changes that are functional hypomorphs while complete loss of ATRX function is believed to be incompatible with life. Afflicted individuals present with intellectual disability, hypotonia, hematological abnormalities, urogenital anomalies, skeletal alterations, and characteristic facial dysmorphisms (159-162). Of the reported clinical features, only intellectual disability is shared between all patients. As the syndrome is X-linked, females are usually asymptomatic carriers with a large skewing of X inactivation for the chromosome carrying the pathogenic *ATRX* copy (163). In two cases where females presented with mild symptoms, they had X inactivation skewing toward the wildtype allele (164-166).

#### 1.3.4.2. Current ATRX Syndrome Mouse Models

In mouse development, ATRX expression has been noted at the time of fertilization making knockouts more difficult to produce (167). Even a conditional knockout with *Gata1*-Cre causes embryonic lethality (168). Overexpression of human ATRX in mice caused growth retardation, neural tube defects, and frequently embryonic lethality (169). Those that did survive to birth had an increased occurrence of perinatal death, seizures, and craniofacial dysmorphisms.

Mice with the forebrain-specific *Foxg1*-Cre had a substantial reduction in the forebrain with the largest reduction in the caudal-medial area due to significant neuronal loss in the early stages of corticogenesis (170). It was found that these mice had an increased occurrence of apoptosis. Later work identified the association of ATRX with PML bodies which are known regulators of apoptosis. It is possible that the loss of ATRX leads to dysregulation of apoptotic genes leaving the cells more sensitive to proapoptotic signals (138). Other studies suggest that the RGCs are prone to replication stress in the absence of ATRX and this results in a high incidence of mitotic catastrophe and cell death (171-173). This is an effective demonstration of the importance of mouse models in their ability to illuminate disease mechanisms that would otherwise be difficult to resolve.

Knockouts specific to the excitatory neurons of the forebrain using the *αCaMKII*-Cre driver led to impaired spatial learning and memory in males (174). It is believed that this phenotype was produced due to impairments in a hippocampal pathway associated with learning and memory, however the exact pathway was not determined. Hippocampal defects were also seen in mice with exon 2 deletions of *Atrx* (175). It was found that these mice demonstrated reduced contextual memory likely related to the reduction of long-term potentiation in the CA1 region along with reduction of phosphorylation of αCaMKII and the glutamate receptor GluR1.

Further study of these mice found abnormal dendritic spine formation in the medial prefrontal cortex (mPFC) likely caused by aberrant αCaMKII activity (176). The hippocampus and mPFC along with the amygdala form the triad of brain regions in the circuit of fear memory (177). Further work found that Atrx binds to G4 quadruplexes in the *Xlr3B* gene to regulate its expression by recruiting methyltransferases as overexpression of the gene disturbs proper αCaMKII expression (178). Moreover, it was demonstrated that 5-ALA treatment is able to rescue this effect in ATR-X model mice. These impairments could explain how the loss of ATRX in ATR-X syndrome contributes to intellectual disability and therefore warrant further exploration.

Recently, an alternative approach was taken whereby mice with the mouse homolog R245C of the most common patient mutation R246C were generated in place of a conditional knockout (179). This knock-in model better exemplifies the alterations seen in the ATRX syndrome phenotype. These mice have craniofacial defects, microcephaly, and impaired neurologic functioning. Furthermore, the knock-in mice had deficits in spatial memory, novelty recognition, and contextual fear memory. It was found that the mutant protein is less stable and has disability in binding to heterochromatin, likely explaining the pathogenicity of this variant. The extensive characterization of these mice and the strong overlap with the patient phenotype indicate that this is an indispensable model in testing therapeutics for the syndrome.

### 1.3.5. CHD

The CHD subfamily contains 9 proteins divided into three subfamilies: CHD1 and CHD2 comprise subfamily I, CHD3/4/5 make up subfamily II, and CHD6-9 are in subfamily III (52, 180). Aside from the conserved ATPase domain, the family is characterized by their tandem

chromodomains which recognize the histone PTMs or certain transcription factors or proteins. The specific binding of the chromodomains (CHDs) is relative to each protein. Each subfamily then has their own characteristic domains as well. Subfamily I is the only group to contain no other distinctive domains (181, 182). Whereas subfamily II has tandem N-terminal plant homeodomains (PHD). Notably, these PHDs are used for recognition of H3K9me and H3K9ac in place of the CHDs. Instead, their CHDs are thought to support ATPase activity by binding to DNA directly as has been demonstrated in *Drosophila* (182). In subfamily III there are two extra domains. First a SANT domain which interacts with unmodified histone tails following the ATPase domain, followed by tandem Brahma Kismet (BRK) domains (183). While the function of the BRK domains is unknown, similarity was found in the structure to the glycine-tyrosine-phenylalanine (GYF) domain which acts as a protein-protein interaction module. For this thesis, we will elaborate more on the role of subfamily II.

#### 1.3.5.1. Subfamily II and the Nucleosome Remodeling and Deacetylase Complex

All members of subfamily II may be incorporated into the nucleosome remodeling and deacetylase (NuRD) complex in a mutually exclusive manner with the exact subunit utilized dependent on physiological conditions or cell type (184). In addition to the CHD proteins, the NuRD complex also contains a combination of GATA zinc finger domain containing 2A or 2B (GATAD2A/2B), methyl-CpG-binding domain protein 2 or 3 (MBD2/3), retinoblastoma binding protein 4 and/or 7 (RBBP4/7), metastasis-associated protein 1, 2, or 3 (MTA1/2/3), and histone deacetylase 1 or 2 (HDAC1/2) (45). In conjunction with the deacetylase subunits the NuRD complex has a demonstrated role in transcriptional repression (185-196).

A study of subfamily II in the murine cortex has made great strides to elucidate the CHD/NuRD complex's role in cortical development (197). Through Chd3 knockdown with a

small hairpin RNA (shRNA) construct at E13.5, it was observed that upper layer cells were being retained in the lower layers. Electroporation of the shChd3 along with a human CHD3 rescue construct was able to resolve the phenotype. Moreover, co-electroporation of shChd3 and human CHD5 also demonstrated a rescue of the phenotype. The Chd4 mice were not knocked down but rather conditionally knocked out using *Nestin*-Cre. It was found that these mice had microcephaly due to a reduction in cortical thickness. The NPCs in the Chd4 cKOs were prematurely exiting the cell cycle and thus dying before differentiation. Analyses at E18.5 suggested these were progenitors destined for the upper layers. Finally, electroporation with shChd5 at E13.5 caused cells to be retained in the intermediate zone (IZ) rather than reaching the cortical plate (CP). Again, co-electroporation with human CHD5 rescued the phenotype, however mouse Chd4 and human CHD3 rescue constructs failed in this regard.

#### 1.3.5.2. CHD-associated Neurodevelopmental Disorders

Due to their important regulatory roles, nearly all CHD proteins have been implicated in neurodevelopmental disorders. Mutations in *CHD1* are causative for Pilarowski-Bjornsson syndrome – a condition characterized by developmental delay, hypotonia, speech apraxia, seizures, and characteristic facial dysmorphisms (198). Pathogenic deletions in *CHD2* were originally described in cases of epileptic encephalopathy (EE) or ASD (199-201). Yet recently suggested guidelines for genetic counselors and clinicians have been updated for establishing a diagnosis of "*CHD2*-related neurodevelopmental disorder" in individuals who present with early-onset EE and intellectual disability and/or ASD (202).

For subfamily III, no neurodevelopmental disorder has been connected to *CHD6* mutations. However, at least one patient has been found with intellectual disability, ASD, and epilepsy with the causative mutation mapped to a 700 bp deletion within exon 1 of *CHD6* (203).

Contrarily, *CHD7* was the first CHD gene linked to a developmental disorder and is responsible for a syndrome named after the common phenotypes – coloboma, heart defects, atresia choanae, retardation of growth, genital abnormalities, and ear abnormalities (CHARGE) (204-206). Though it should be noted that as neurological phenotypes are not distinguishing in CHARGE syndrome, it is not primarily considered to be a neurodevelopmental disorder. *CHD8* is perhaps the most well-known CHD protein due to its strong association with ASD (207-211). In addition, Zahir-Friedman syndrome is distinguished by developmental delay, cognitive impairment, and dysmorphic features due to haploinsufficiency of CHD8 (212). Though *CHD9* does not have an established associated with any neurodevelopmental disorders it is becoming more frequently described as a candidate gene for ASD (213-216).

#### 1.3.5.2.1. Subfamily II Neurodevelopmental Disorders

As of 2021, all subfamily II genes have been found to be the cause of a neurodevelopmental disorder. De novo *CHD4* variants were first found in five patients with congenital heart defects (217). With more than 25 additional identified individuals this condition is now known as Sifrim-Hitz-Weiss syndrome (SIHIWES) (218, 219). In the majority of cases, afflicted individuals experience a developmental delay including a speech delay and motor delay, intellectual disability, brain anomalies, heart anomalies, and ophthalmic anomalies. In the 96% of SIHIWES patients with brain anomalies, 55% had ventriculomegaly and 32% had Arnold-Chiari 1 malformation. Additionally, 65% of males had cryptorchidism and/or a microphallus. Many patients had a large forehead, square face, and periorbital fullness with distinctive characteristics being more noticeable before puberty. The vast majority of pathogenic mutations were missense mutations or in-frame indels within the ATPase-helicase domain. Of the three patients who carried truncating mutations, few symptoms were noted outside of the nervous

system. ATPase studies showed that variants in the PHD and CHD domains decreased the activity by 30-50% and a selected helicase variant yielded a significant decrease in nucleosome remodeling capabilities.

Snijders Blok Campeau syndrome (SNIBCPS) was the next described (220-222). The first cohort comprises 35 patients with *de novo* mutations in *CHD3*. All individuals had an intellectual disability or developmental delay. Common features include a speech delay or disorder, hypotonia, macrocephaly, and characteristic facial dysmorphisms such as frontal bossing and widely spaced eyes (Figure 3). Similarly to SIHIWES, SNIBCPS mutations cluster within the ATPase-helicase domain. Between 35 patients, 23 unique mutations were identified with 19 being missense mutations. This indicates the presence of mutational hotspots. In six children from five families, they contained the p.Arg985Trp mutation and two other individuals had p.Arg985Glu mutations in the same location. Further analysis of the ATPase mutations found no difference from wildtype in subcellular localizations of CHD3. However, ATPase assays in dsDNA or recombinant nucleosomes showed varying results. Of six representative mutations chosen, two had a significant reduction in both substrates (R1121P, R1172Q) and one had a significant reduction only in the presence of dsDNA (N1159K). While two others had no significant difference (R1187P, W1158R), the final mutation (L915P) had a significant increase in activity in both conditions. Furthermore, combining mutant and wildtype protein together showed no impact on the function of the wildtype protein. Chromatin remodeling assays of restriction enzyme accessibility to nucleosomal DNA recapitulated these phenotypes, except for W1158R which this time showed a reduction in remodeling capabilities. Of course, many factors affect the impact of a given mutation including the type of mutation and location. Changes in the electrostatic characteristics from the wildtype amino acid to the mutant could

have major implications in one position with limited changes in another. For example, the non-significant R1187P variant has the same mutation as R1121P which had one of the most significant reductions in activity in both assays.

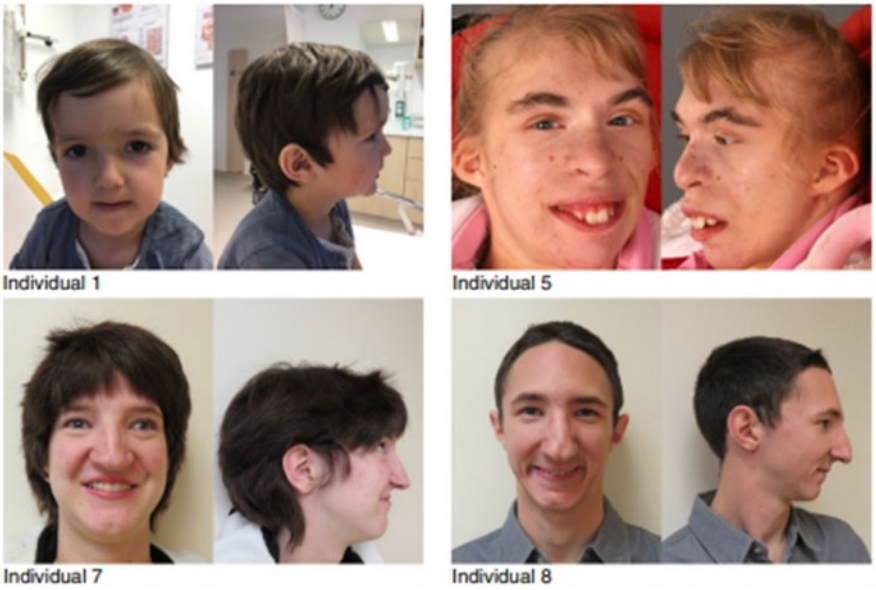


**Figure 3. SNIBCPS patients share characteristic facial dysmorphisms**. Characteristic facial dysmorphisms include frontal bossing, widely spaced eyes, and a broad nasal bridge. Individual 1: truncation following amino acid 457, global developmental delay including speech and motor, macrocephaly. Individual 5: p.Gly921Glu, global developmental delay with inability to speak or walk, microcephaly. Individual 7: p.Arg985Trp, global developmental delay including speech and motor, macrocephaly. Individual 8: p.Arg985Trp, global developmental delay including speech and motor, macrocephaly. Individuals 7 and 8 are siblings with the mother mosaic for the mutation. Images represent individuals from the first identified cohort (213).

Interestingly, a separate cohort of SNIBCPS patients whose variants were inherited have been examined (72). While mutations were still present in the ATPase-helicase domain, these individuals had a much more even spread across the functional domains (Figure 4). As most of the carrier parents were female (71%), it has been suggested that a female protective effect could be what shields the parents from the syndrome's phenotype though this is questionable as there is a slight skew towards females in *de novo* SNIBCPS patients (55%) as well as in the inherited

variant cohort (57%). However, despite suggesting incomplete penetrance, the presence of carriers for a syndrome of only heterozygous afflicted individuals warrants further investigation.

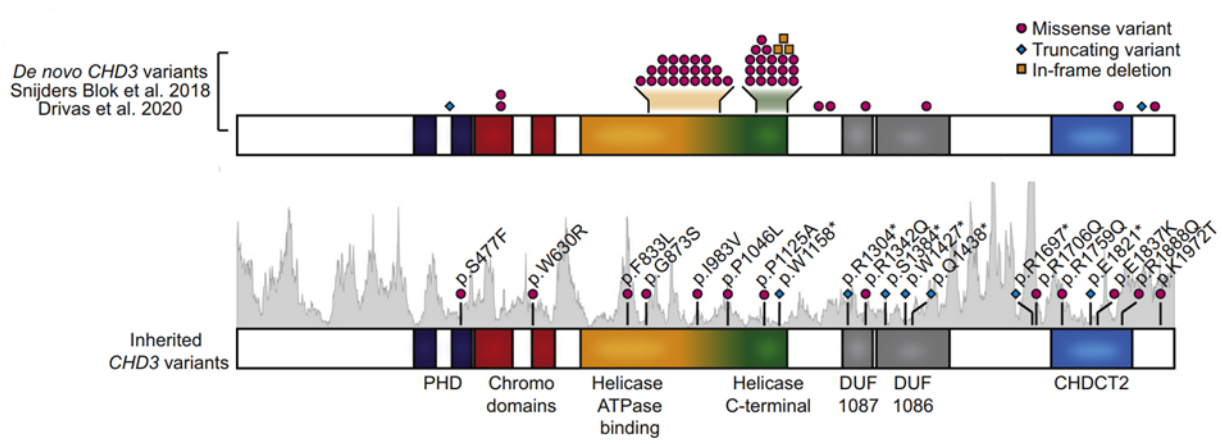


**Figure 4. Schematic representation of *de novo* and inherited SNIBCPS variants.** The *de novo* variants show a clear clustering within the ATPase-helicase domain. Though the inherited variants do not share this trait, they still cluster within functional domains. Figure adapted from Drivas *et al.* (71).

Finally, *CHD5* missense and truncating mutations have been identified as causative for a syndrome now called Parenti-Mignot neurodevelopmental syndrome (PMNDS) (223, 224). Twelve of the cohort of 16 have *de novo* mutations comprising ten missense and two splice site variants. Three familial mutations had nonsense or missense variants and one of unknown inheritance had a frameshift variant. PMNDS patients frequently display intellectual disability, speech delay, motor delay, behavioural problems, and epilepsy. While pathogenic mutations do

not cluster in the ATPase-helicase domain, it can be seen that they indeed cluster in functional domains (Figure 4). This could be due to the fact that the ATPase-helicase clustering is seen when comparing SIHIWES and SNIBCPS *de novo* variants, whereas mere functional domain clustering was seen in inherited variant SNIBCPS. Furthermore, it was found that PMNDS inherited variants presented with variable phenotypes. Taken with the presence of unaffected carriers it could indicate an incomplete penetrance – though it has been acknowledged that the lack of a full clinical history of the carriers could be a contributing factor to this observation.

#### 1.3.5.2. Current CHD Subfamily II Neurodevelopmental Disorder Mouse Models

Both *Chd3* and *Chd5* can be constitutively deleted and produce surviving adults, yet *Chd4* cannot (225, 226). However, many *Chd4* conditional knockouts have been studied. Deletion in granule neurons of the cerebellar cortex with *G6r*-Cre showed that the presence of Chd4 is necessary to turn off a set of developmental genes to allow for proper efferent connectivity of the granule neurons (227). By far the greatest strides in generating a SIHIWES mouse model has been done with a study comparing both *Cmv*-Cre (germline deletions) and *Emx1*-Cre cKOs (228). As to be expected, *Cmv*-Cre knockouts experienced embryonic lethality so heterozygotes were examined in their stead, though this better recapitulates SIHIWES as patients are heterozygous as well. These mice displayed impaired spatial and motor learning. The *Emx1*-Cre cKO mice displayed a different phenotype. Multiple behavioural assays showed anxiety in the cKOs and the marble burying test revealed a female-driven repetitive behaviour phenotype. The conditional heterozygotes (cHTs) also showed the female-driven repetitive behaviour phenotype along with social deficits. It was found that the cKOs had a significant reduction of the cortex with a loss of late-born upper layer cells. While these models give a

greater understanding of the role of Chd4 in brain development they also underscore the utility of patient mutation knock-in mice in modeling disease phenotypes.

As *Chd5*-null mice are viable they would be able to be characterized directly. Unfortunately, full-body *Chd5* deletion produced infertile males due to their inability to produce sperm (229). Instead, *Nestin*-Cre cKOs were generated and bred to produce the *Chd5*-/- mice (230). These mice displayed behavioural abnormalities including impaired social interactions and neophobic behaviours across multiple assays. Though the main focus of the characterization of these mice was on behaviour, RNA-seq results indicated a possible defect of dendritic arborization. Primary cultured cortical neurons demonstrated it was indeed the case as cells displayed altered dendritic arborization resulting in a decrease in the dendritic intersections. As repeatedly mentioned, behavioural assays help to connect molecular phenotypes to the human syndrome being modeled. The reiteration of the behavioural phenotypes in PMNDS in the *Chd5*-/- mice is a good indication human *CHD5* variants may experience alterations in dendritic arborization as well and as such these mice may be useful in studying potential PMNDS therapies.

Generation of *Chd3*-null mice from an allele that initially had LoxP sites flanking exons 12-21 (containing the ATPase-helicase domain) showed a partial lethality in KOs before weaning (231). Aside from confirming a high expression of Chd3 in the brain, these mice were only studied for vascular development and no nervous system analyses were performed.

## 1.4. Gaps in Knowledge of *Chd3*

Chromatin remodelers have been implicated in all aspects of cortical development. They may impact the generation of the progenitor pool or the transition from RGC to IPC through a variety of mechanisms including altered cell cycle kinetics or increased susceptibility to

proapoptotic factors. Additionally, cell death or migration deficits may be seen within the cortical plate. Despite the significant burden of intellectual disabilities on the health care system and the large number of neurodevelopmental disorders caused by mutations in these genes, there still remains an overwhelming amount left to be understood.

Preliminary mouse work has suggested that *Chd3* may drive migration (197), however this was in an acute knock-down model which have been seen to diverge from knockout phenotypes for some genes (232). Moreover, as demonstrated with other CHD proteins as well as with other chromatin remodelers, mouse models are invaluable not only in defining gene function but also in elucidating disease pathogenesis. There exists no model to study the pathogenesis of SNIBCPS which is the focus of this thesis. As such, we have generated and characterized *Emx1*-Cre conditional knockout mice with the *Chd3*-flox allele to help address the gaping hole in the understanding of both *CHD3* and SNIBCPS.

## 1.5. Hypothesis and Aims

It is hypothesized that *Chd3* ablation will reproduce the neurological phenotypes of SNIBCPS patients due to disruption of cortical lamination caused by defects in late-stage neural migration. This is examined with the following two aims:

1. Elucidate the pathogenesis of *Chd3* ablation on the developing cortex.
2. Define any behavioural alterations and compare to SNIBCPS clinical presentations.

# 2. Methods

## 2.1. *Chd3* Transgenic Mice

### 2.1.1. Animal Husbandry

All animals were housed in the University of Ottawa animal facilities. Animal breeding and experimental protocols following the Canadian Council for Animal Care guidelines were approved by the University of Ottawa Animal Care Committee. Mice were kept on the standard 12-hour light/dark cycle in cages of no more than 5 adult mice with food and water provided *ad libitum*.

### 2.1.2. Timed Breeding

For collection of embryos at a desired timepoint timed breeding was performed. Female mice were placed into a male's cage in the evening and replaced into their own cage the following morning. At the necessary day, the pregnant female was sacrificed with $CO_2$ asphyxiation and the embryos were dissected from her womb. The complete dissection of the embryos is described in subsequent sections according to the use of the tissue.

### 2.1.3. Chd3-flox Mice

*Chd3-flox* alleles were generously provided by Dr. Courtney Griffin (Oklahoma Medical Research Foundation) and were designed using LoxP sites flanking exons 13 to 20, as previously described (231). The *Chd3-flox* mice were obtained on a mixed C57BL/6 and C3H/HeJ background and subsequently backcrossed with C57BL/6 for 8 generations.

### 2.1.4. Emx1-Cre Mice

*Emx1-Cre* mice were purchased from The Jackson Laboratory (stock #005628). They contain the Cre sequence inserted downstream of the *Emx1* stop codon. As such, Cre expression

begins at E10.5 along with *Emx1* (70). These mice were provided on a pure C57BL/6 background.

### 2.1.5. Genotyping

Tissue samples taken were approximately 1mm by 5 mm. A forelimb was used for embryonic samples, a tail snip for P0, and an ear snip for P21 and older. The tissue was added to 75 µL of a lysis buffer containing 1N NaOH and 0.5M EDTA at pH 8.0. Tubes were loaded into a thermal cycler (Eppendorf Mastercycler EP Gradient 96 well thermal cycler) and run at 90°C for 60 minutes. An equivalent amount of neutralization buffer containing 1M Tris-HCl at pH 8.0 was added to each tube. 1 µL per sample was used for each PCR genotyping reaction. All reactions followed a standard PCR reaction protocol as follows: 2-minute hot start at 94°C, 35 cycles of 20 second denaturation at 94°C, 20 second annealing at relevant temperature, 20 second elongation at 72°C with a final elongation after the cycles for 5 minutes. All samples were run on a 1.5% agarose gel at 100V for 30 minutes. Expected annealing temperatures are given below in Table 2.

**Table 2. Primers used for genotyping.**

| Gene Name | 5'-3' Sequence | Annealing Temperature (ºC) |
|---|---|---|
| Chd3 flox - F | GGGTGGAGGTGGAAAGTGTA | 55 |
| Chd3 flox - R | AGAGGACAGGTCACAGGACAA | 55 |
| Cre - F | ATGCTTCTGTCCGTTTGCCG | 60 |
| Cre - R | CCTGTTTTGCACGTTCACCG | 60 |
| Sry - F | TTGTCTAGAGAGCATGGAGGGCCATGTCAA | 60 |
| Sry - R | CCACTCCTCTGTGACACTTTAGCCCTCCGA | 60 |

### 2.1.6. Behaviour Testing

All mice began behaviour testing at 6 weeks of age at the University of Ottawa Animal Behaviour and Physiology Core facilities. Cages were changed one week before testing began and two days before the Morris Water Maze test. No mice were individually housed. For tests that were required to be performed in groups, males were tested before females to avoid confounding effects from any lingering female scent. The order of tests performed was: Beambreak, Rotarod, Open Field, Adult Social Interaction, Morris Water Maze, and Fear Conditioning. The second cohort was only able to complete up to the Open Field test due to limitations in equipment availability. Testing of the first two cohorts was performed by Anneka Schoeppe, while that of the latter three was done by Animal Behaviour and Physiology Core staff. All testing was performed blinded in regard to genotype. Animal Care and Veterinary Service Standard Operating Procedures were used for each test with relevant parameters altered as necessary. All statistical analysis used a one-way ANOVA (though the beambreak used a two-way ANOVA) with post-hoc Tukey-Kramer test due to the uneven sample sizes.

#### 2.1.6.1. Beambreak

Mice were habituated for 1 hour under normal light conditions. They were then individually loaded into shoebox cages on a Micromax Analyzer with food and water in a metal hopper but no cage enrichment. Interruptions of infrared beams perpendicular to the length of the cage were recorded for 48 hours under the standard 12-hour light cycle of 07:00 on until 19:00 off and exported in 1-hour bins. Genotypes were compared at each hour using a two-way ANOVA with post-hoc Tukey-Kramer test, while total number of beam breaks were compared with a one-way ANOVA with post-hoc Tukey-Kramer test. Analyses were repeated for both sexes as well.

#### 2.1.6.2. Rotarod

Mice were habituated for 30 minutes under normal light conditions. The Ugo Basile rotarod was used testing 4-5 mice at a time. A ramp protocol of 4-40 rpm over the first minute for a maximum of 5 minutes was performed for four trials with an intertrial interval (ITI) of 10 minutes. The computer records the latency to fall for each mouse which was later analyzed with a one-way ANOVA with post-hoc Tukey-Kramer test. Analyses were performed on each sex as well.

#### 2.1.6.3. Open Field

Mice were habituated for 30 minutes under normal light conditions. Four mice were tested at a time – being placed in the middle of the arena with movement tracked by centrepoint for 10 minutes under 300 lux light. The Ethovision tracking software (Ethovision 14, Noldus Information Technologies, Leesburg, VA, USA) recorded the time spend in the centre of the arena and the four corners in addition to the average speed and distance travelled. These measurements were analyzed with a one-way ANOVA with post-hoc Tukey-Kramer test. All analyses were repeated on the data segregated by sex as well.

#### 2.1.6.4. Adult Social Interaction

Mice were habituated for 30 minutes under 100 lux regular light and under red light in the testing room for 30 minutes. Testing was performed under red light. In brief, each mouse was placed in an open field arena with an empty 5.5x9.6x30 cm (WxLxH) wire mesh cage holder for 5 minutes. The mouse was returned to a holding cage for an ITI of 5 minutes. During this time a gender- and strain-matched mouse of relatively the same age was placed in the cage holder. The test mouse was then returned to the box for a trial of 5 minutes. Two interactor mice per sex were used for all trials in the day with a maximum of 5 trials per interactor. The Ethovision tracking

software (Ethovision 14, Noldus Information Technologies, Leesburg, VA, USA) was used to measure the distance travelled and time and frequency in the interaction zone. Results were analyzed with a one-way ANOVA with post-hoc Tukey-Kramer test. All analyses were repeated on the data segregated by sex as well.

#### 2.1.6.5. Morris Water Maze

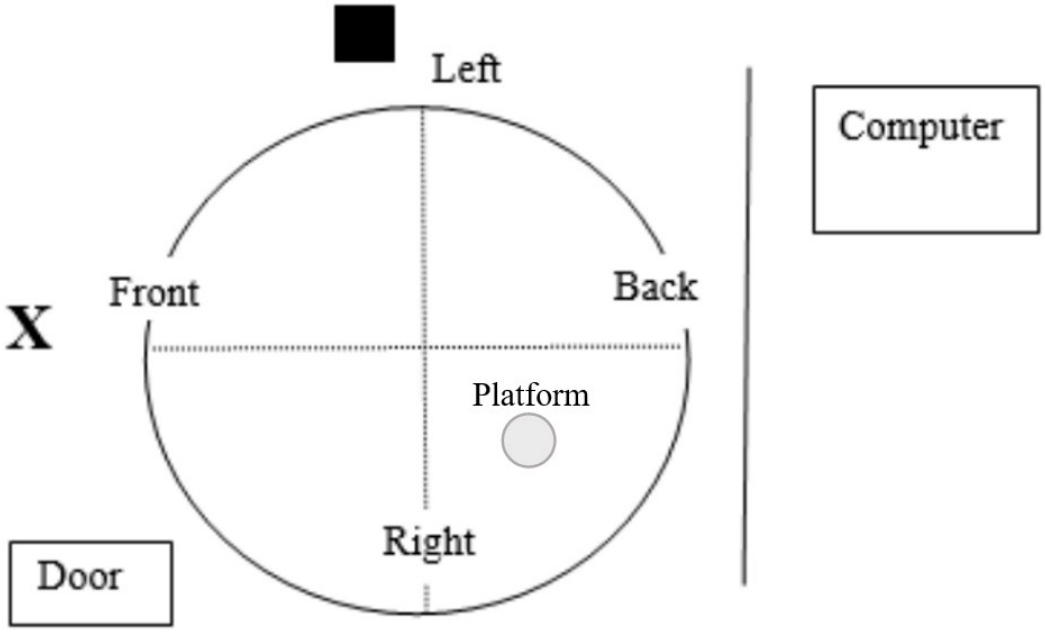


**Figure 5. Room set up of Morris Water Maze test.** A black X and black square were used as visual cues. The submerged platform was placed in quadrant BR. A screen next to the back side of the water tub blocked view of the computer, tester, and other mice. Figure adapted from ACVS SOP Behav-7 Morris Water Maze.

Mice were habituated in the testing room for 30 minutes. The visual cues used were a black square on the north wall and a black X on the east wall with the platform located in the bottom right quadrant (Figure 5). The mice were given 7 training days. Each day the mice are put into the pool from each end once with each mouse given the same order of entrance to the pool

on a given day and the order changing each day. This gives a total of 4 trials per day to each mouse with a maximum trial time of 60 seconds and an ITI of 20 minutes. On the probe day the platform is removed from the water and each mouse is tested for 60 seconds from a randomly assigned point of entrance. The Ethovision tracking software (Ethovision 14, Noldus Information Technologies, Leesburg, VA, USA) measured the time to the platform on each trial to track the learning of the mice. On the probe day, the time spent in each of the quadrants along with the total distance travelled were measured and analyzed by one-way ANOVA with post-hoc Tukey-Kramer's test. Analyses were repeated by sex.

#### 2.1.6.6. Fear Conditioning

Mice were habituated for 30 minutes in a room separated and away from the testing room. Mice were then placed in phenotyper boxes. After 2 minutes in the boxes, they received 2 tone-shock pairings – a loud 30-second tone delivered with a 2-second foot shock of 0.5 mA – with a minute in between. The test time was a total of 6 minutes and their movement throughout the testing was recorded. On the second day, the mice were placed back in the boxes for the same amount of time but with no tone or shock. On the final day the boxes were altered so that the mice would not recognize them. Inserts were put in to give triangular walls, the shock floor was removed, and a vanilla scent was added. Mice were put in a different box than on the training day, a different disinfectant was used to clean the boxes, a different cart was used to transport the mice, and a different path was taken to the testing room. A total of 6 minutes of testing was performed again, this time with no tone for the first 3 minutes and the tone from the training day played during the last 3 minutes. On each day the Ethovision tracking software (Ethovision 14, Noldus Information Technologies, Leesburg, VA, USA) measured activity and freezing time to

test the response to the stimuli and context. Results were then analyzed by one-way ANOVA with post-hoc Tukey-Kramer's test and repeated by sex.

## 2.2. Structural Analyses

### 2.2.1. EdU-pulse Labelling

EdU-pulse labelling was performed by senior lab technician Keqin Yan on timed breeding (2.1.2.) dams by way of intraperitoneal injections of 300 µL of EdU (10 mg/mL). For analysis of progenitor populations including quantification of cells in S-phase, injections were performed at E15.5 and embryos were collected after one hour (1-hour pulse). For neuronal birthdating, injections were performed at E13.5 to label layer V or E15.5 to label layers II-III with pups collected at P7.

### 2.2.2. Tissue Dissection

#### 2.2.2.1. Embryonic Dissection

Following timed breeding (2.1.2.), pregnant dams were sacrificed with $CO_2$ asphyxiation. Embryo heads were severed at the base of the skull and fixated in 4% PFA (in 1X autoclaved PBS) for 24 hours at 4ºC. Heads were then put in a 30% sucrose solution (in dd$H_2O$ with 0.03% sodium azide) for 7 days at 4ºC.

#### 2.2.2.2. Pup Dissection

Weight measurements were taken on a scale (Mettler-Toledo PB302). Pups then had the brain stem severed with point tweezers and the scalps and calottes were removed. Whole brains were extracted and fixated in 4% PFA for 24 hours at 4ºC. The solution was then switched to 30% sucrose for 7 days at 4ºC.

#### 2.2.2.3. Adult Dissection

Adult mice were sacrificed with $CO_2$ asphyxiation and perfused with 4% PFA to remove blood from the brain vasculature and improve fixation. Heads were then severed and the scalps and calottes were removed whereby brains were extracted and fixated in 4% PFA for 24 hours at 4ºC. The solution was then switched to 30% sucrose for 7 days at 4ºC.

### 2.2.3. Tissue Embedding

30 mL of methylbutane (Sigma M32631) was cooled for 15 minutes in a beaker on dry ice along with tweezers and labelled tin foil sections. Heads or brains were dried of excess sucrose solution and submerged in the methylbutane until bubbles were no longer produced. They were then removed and wrapped in the relevant tin foil section and stored at -80ºC.

### 2.2.4. Cryosectioning

All cryosectioning was performed on a Leica CM1850 cryostat. Brains were left in the cryostat set to –28°C for 1 hour before sectioning. They were then embedded on the chuck in optimal cutting temperature (OCT) compound (Fisher Scientific 23-7300-571). Sections were cut to 14 µm for Nissl staining (2.2.5.) or 12 µm for immunofluorescent staining (2.2.6.) and collected on SuperFrost slides (Thermo Fisher Scientific). Slides were left at room temperature for 30 minutes for drying and then stored at -20ºC until staining.

### 2.2.5. Nissl Staining

Slides were dried in an incubator at 37ºC for 30 minutes prior to staining. Sections were rehydrated in decreasing concentrations of ethanol as follows: 95% for 10 minutes, 70% for 1 minute, and 50% for 1 minute followed by two 5-minute washes in water. Slides were then placed in 0.25% cresyl violet acetate (0.25g cresyl violet (Thermo Fisher Scientific 405760100), 100 mL water, 1 mL acetic acid) for approximately 15 minutes. Excess stain was washed off

with two 5-minute washes in water. Dehydration of sections was then performed in increasing concentrations of ethanol: 50% for 2 minutes, 70% for 10 seconds, 95% for 2 minutes, 100% for 5 minutes twice, followed by three 5-minute washes in xylene. The xylene was dried from the slides and mounted with Permount Mounting Medium (Fisher Chemical SP15-100) with 22x50 mm cover slips (Fisherbrand 12545E). Stained sections were imaged on a ZEISS Axio Scan slide scanner (ZEISS Axio Scan.Z1) under brightfield.

### 2.2.6. Immunofluorescent Staining

Slides were removed from -20ºC and put in an incubator at 37ºC for 15 minutes. Sections were next rehydrated with three 5-minute washes in phosphate-buffered saline (PBS). Sodium citrate solution (pH 6.0) was heated to boiling in a microwave. The slides were added to the solution for antigen retrieval and put in the microwave for 10 minutes on level 0. Once finished, slides were allowed to cool for 30 minutes. Sections were traced with Dako pen (Agilent S2002) and 300 µL of 10% horse serum (in PBS) was added to each slide for 1 hour for blocking. Following blocking, 300 µL of 10% horse serum containing the applicable dilution of primary antibody (Table 3) was added to each slide and left overnight at 4ºC. Three 5-minute washes in PBS were performed and 300 µL of 10% horse serum containing a 1:500 dilution of the relevant species secondary antibody conjugated with Alexa Fluor (Table 3) was added to each slide for 1 hour. Slides underwent three 5-minute PBS washes again. If EdU staining was required, slides were put into an EdU click chemistry solution (100 µL 1.M Tris-HCl (pH 7.2), 100 µL 100mM ascorbic acid, 20 µL 2 mM $CuSO_4$, 2 µL fluorescent azide (Cy-5-Azide, Sigma 777323-1MG), 778 µL dd$H_2O$) for 1 hour and then washed three times for 5 minutes in PBS before moving to DAPI staining. Otherwise, slides went directly into a 1:20000 (in PBS) solution of DAPI for 15 minutes. After a final three 5-minute washes in PBS, slides were mounted with DAKO mounting

media (Agilent s3023) and coverslips were sealed with clear nail polish. Stained sections were imaged on the widefield upright Zeiss AxioImager M2 microscope with the Zen imaging package (Zen Blue). Images were produced using a Z-stack and tiling under the 20x objective. Post-imaging processing included stitching (Zen Blue) and five iteration deconvolution (AutoQuant X3). Images were finally prepared and quantified in Image J (Fiji).

**Table 3. Primary and secondary antibodies used in immunofluorescent staining.**

| | Antibody | Host | Dilution | Company | Catalog Number |
|---|---|---|---|---|---|
| Primary | Chd3 | Rabbit | 1:300 | Abcam | Ab109195 |
| | Ctip2 | Rat | 1:300 | Abcam | Ab18465 |
| | Pax6 | Rabbit | 1:200 | BioLegend | 901301 |
| | pHH3 | Rabbit | 1:500 | EMD Millipore | 06-570 |
| | Satb2 | Mouse | 1:300 | Abcam | Ab51502 |
| | Tbr1 | Rabbit | 1:100 | Abcam | Ab31940 |
| | Tbr2 | Rabbit | 1:200 | Abcam | Ab23345 |
| Secondary | Alexa Fluor 488 | Mouse | 1:500 | Invitrogen | A-21202 |
| | Alexa Fluor 555 | Rat | 1:500 | Invitrogen | A-48263 |
| | Alexa Fluor 594 | Rabbit | 1:500 | Cederlane | 711-585-152 |
| | Alexa Fluor 647 | Rabbit | 1:500 | Invitrogen | A-31573 |

## 2.3. Protein Analysis

### 2.3.1. Tissue Dissection

Embryos were euthanized as per 2.2.2.1. or pups as per 2.2.2.2. Brains were extracted and cortices were put into liquid nitrogen in CryoPure tubes (Sarstedt 72.380) for flash freezing. Samples were then stored at -80ºC until required.

### 2.3.2. Protein Extraction

Brain samples were removed from -80ºC and kept on dry ice. They were then moved to cell lysis tubes containing 1 mL RIPA buffer (50mM Tris-HCl pH 7.5, 1% NP-40, 1% Triton-X-100, 150mM NaCl, 12mM Na-deoxycholate, 0.05% sodium dodecyl sulfate (SDS), 2mM EDTA, 1mM DTT) with 5 µL protease inhibitor (Sigma P8340) on ice for 1 minute. After, each cortex was homogenized using setting 1 of the Tissue Tearor (Biospec Products 985-370). Following 20-minute incubation on ice, lysates were moved to Eppendorf tubes for centrifuge at 14500 rpm for 10 minutes at 4ºC. The supernatant was removed and stored at -80ºC.

### 2.3.3. Bradford Protein Assay

A 1:5 dilution of Bio-Rad protein assay dye reagent (cat #5000006) in dd$H_2O$ was prepared. Thawed cortical lysates were mixed to ensure even protein distribution before adding 1uL of lysate to 1 mL of protein assay solution in cuvettes (Sigma-Aldrich C5416). The absorbances were measured from a Ultrospec 3100 pro spectrophotometer (Pharmacia Biotech 80-2106-25) at 595 nm and subsequently used to calculate the protein concentration from a standard curve.

### 2.3.4. Western Blot

Protein samples were diluted to a total of 20 µg of protein as necessary in RIPA buffer based on Bradford assay results. All samples had a total of 7 µL of protein dye with 5% β-mercaptoethanol (Sigma M3148) to a total volume of 20 uL and were then boiled for 5 minutes at 95ºC. The samples were then loaded onto a 6% SDS-PAGE gel flanked by protein ladder (FroggaBio PM008-0500) on either side in SDS running buffer (25mM Tris-HCl, 192mM glycine and 0.1% SDS). The gel was run at 180V for 5 minutes and then 150V until the 75 kDa band was the lowest visible band on the protein ladder. The protein was then transferred to

polyvinylidene fluoride (PVDF) membranes at 100 volts for 90 minutes in transfer buffer (39mM glycine, 48mM Tris-HCl and 20% methanol). Following transfer, the membranes were cut at about 180 kDa and put into a blocking solution of 5% milk in TBS-T (150 mM NaCl, 50mM Tris, pH 7.4, 0.05% Tween 20, pH 7.4) for 1 hour. Primary antibodies were prepared by adding the relevant concentration (Table 4) to the 5% milk solution and membranes were incubated overnight a 4ºC with agitation. On the second day, membranes were washed for 5 minutes thrice in TBS-T and then incubated in the relevant concentration of the matched animal HRP conjugated secondary antibody in 5% milk solution for 1 hour. After another 3x 5-minute wash in TBS-T the membranes were incubated with Clarity Western ECL Substrate (Bio-Rad 1705061) prepared by manufacturer guidelines for 1 minute. The membranes were then exposed to X-ray film and developed for visualization.

**Table 4. Primary and secondary antibodies used in western blot.**

| Antibody | Host | Dilution | Company | Catalog Number |
|---|---|---|---|---|
| 1° Chd3 | Rabbit | 1:7500 | Abcam | Ab109195 |
| 1° Vinculin | Rabbit | 1:10000 | Abcam | Ab129002 |
| 2° HRP | Rabbit | 1:15000 | Jackson Immunoresearch | 111-035-003 |

## 2.4. RNA Analyses

### 2.4.1. RNA Extraction

Frozen cortices were placed immediately on ice from -80ºC and 1 mL of TRIzol was added to each tube. Samples were homogenized using setting 1 of the Tissue Tearor (Biospec Products 985-370). Tubes were then left at room temperature for 5 minutes to allow for complete dissociation of the nucleoprotein complex. 200 µL of chloroform was added to each tube and shaken vigorously for approximately 15 seconds before another room temperature incubation for 3 minutes. The samples were centrifuged for 15 minutes at 4ºC at 12000 x g. The upper aqueous

phase was then removed and the organic phase discarded. Each tube had 500 µL of 100% isopropanol added and were left to incubate at room temperature for 10 minutes. Tubes were again centrifuged for 15 minutes at 4ºC at 12000 x g. The supernatant was removed from the tubes and the remaining pellets were washed with 1 mL of 75% ethanol. After vortexing, tubes were centrifuged at 7500 x g for 5 minutes at 4ºC. The wash step was repeated twice. The final supernatants were again removed and the pellets were left to air dry under careful watch to prevent desiccation. The dried pellets were resuspended in 30 µL of HPLC water and incubated in a heat block for 1 minute at 70ºC. Samples were finally stored at -80ºC or immediately underwent cDNA synthesis.

### 2.4.3. cDNA Synthesis

Previously prepared RNA samples first underwent a DNAse treatment as per the manufacturer's instructions using the DNAse kit for cDNA (Fisher AM1906). Total RNA concentrations were quantified with the NanoDrop One (Thermo Scientific 13-400-518) and 2 µg of total RNA was added to 2 µl of 10X DNAse buffer, 1 µl DNAse 1 and HPLC water up to 20 µl and incubated at 37ºC for 30 minutes in a thermal cycler. Afterwards, 2 µl of inactivation buffer was added to each tube and incubated at room temperature for 2 minutes. After a quick spin in a mini centrifuge (VWR), 15 µl of supernatant was used for cDNA synthesis. Each RNA sample had 1 µl of 100 ng/µL random hexamers (Thermo Fisher Scientific #SO142) added and the tubes were put in a thermal cycler at 70ºC for 5 minutes to allow for denaturation. Upon completion, they were left on ice for 2 minutes and 9 µl of a master mix containing 5 µl of 5X buffer, 0.6 µL of RNAse out, 2.5 µl 10 mM dNTPs, and 1 µL of RevertAid reverse transcriptase (Thermo Fisher Scientific) per sample was added to each of the tubes. Tubes were loaded into a thermal cycler (Eppendorf Mastercycler EP Gradient 96 well thermal cycler) with the protocol as

follows: 25°C for 5 minutes, 42°C for 60 minutes, and 70°C for 15 minutes. 1/10 dilutions were stored at -20ºC and used for further testing while extract stocks were stored at -80ºC.

### 2.4.4. RT-PCR

The same protocol used for genotyping (2.1.5.) was repeated for RT-PCR except with 1 µL of cDNA per sample and primers as described in Table 5 below.

### 2.4.5. RT-qPCR

The master mix was prepared using 6 µL of 2X SYBR green advantage qPCR Premix (Clontech 639676), 0.5 µL of each primer (10 µM), and 5 µL of water per sample. A 96-well plate had 10 µL of master mix loaded per well with three wells per sample and one non-template control (NTC) for each master mix. Then 1 µL of sample was added to each of the relevant wells. In the Applied Biosystems 7500 Real-Time Fast PCR thermocycler, the standard 3-step PCR protocol was used with an annealing temperature of 55ºC and an extension time of 30 seconds. For analysis, samples were normalized to their respective GAPDH results and calculated using the ΔΔCT method. Primers are described below.

**Table 5. Primers used for RT-PCR and RT-qPCR.**

| Gene Name | 5'-3' Sequence | Annealing Temperature (ºC) | Expected Band Size (bp) |
|---|---|---|---|
| Chd3 Exons 12-21 - F | ATCCCAGAGTACGACGACA | 54 | WT – 1359 cKO – 158 |
| Chd3 Exons 12-21 - R | GAAGCGATCAATGGCCTCT | 55 | |
| Chd3 Exons 16-17 F | GAGGCTCATCGACTCAAGAAC | 55 | 87 |
| Chd3 Exons 16-17 R | CCCCGTCAGCAACAACTTATG | 55 | |
| Gapdh - F | CGGCAAATTCAACGGCACAG | 60 | 183 |
| Gapdh - R | TCACAAACATGGGGGCATCG | 60 | |

## 2.5. Statistics

Mendelian ratios were analyzed with the Chi-square test and birthweights with the one-way ANOVA. All staining protocol analyses were performed on triplicates unless otherwise stated. Number of biological replicates varied between test and genotype for the behavioural assays and are given in figure captions. As the number of replicates was consistent across groups for staining protocols, one-way ANOVA with post-hoc Dunnett's test was performed for analyses. Behavioural analyses are listed by test but used one-way ANOVA with post-hoc Tukey-Kramer's test, except for the beam break test which used two-way ANOVA with post-hoc Tukey-Kramer's test. The Tukey-Kramer's test was used to account for the difference in sample size across genotypes in the behaviour assays. Significant P values are signified in figures as follows: * $\leq$ 0.05, ** $\leq$ 0.01, *** $\leq$ 0.001, **** $\leq$ 0.0001.

# 3. Results

The *Chd3* allele used to assess forebrain development (Figure 6) was designed in the Courtney Griffin laboratory at the Oklahoma Medical Research Foundation. LoxP sites flank exons 13 to 20 such that introduction of Cre will result in excision of the ATPase-helicase domain and generate a loss of function allele caused by a frameshift.

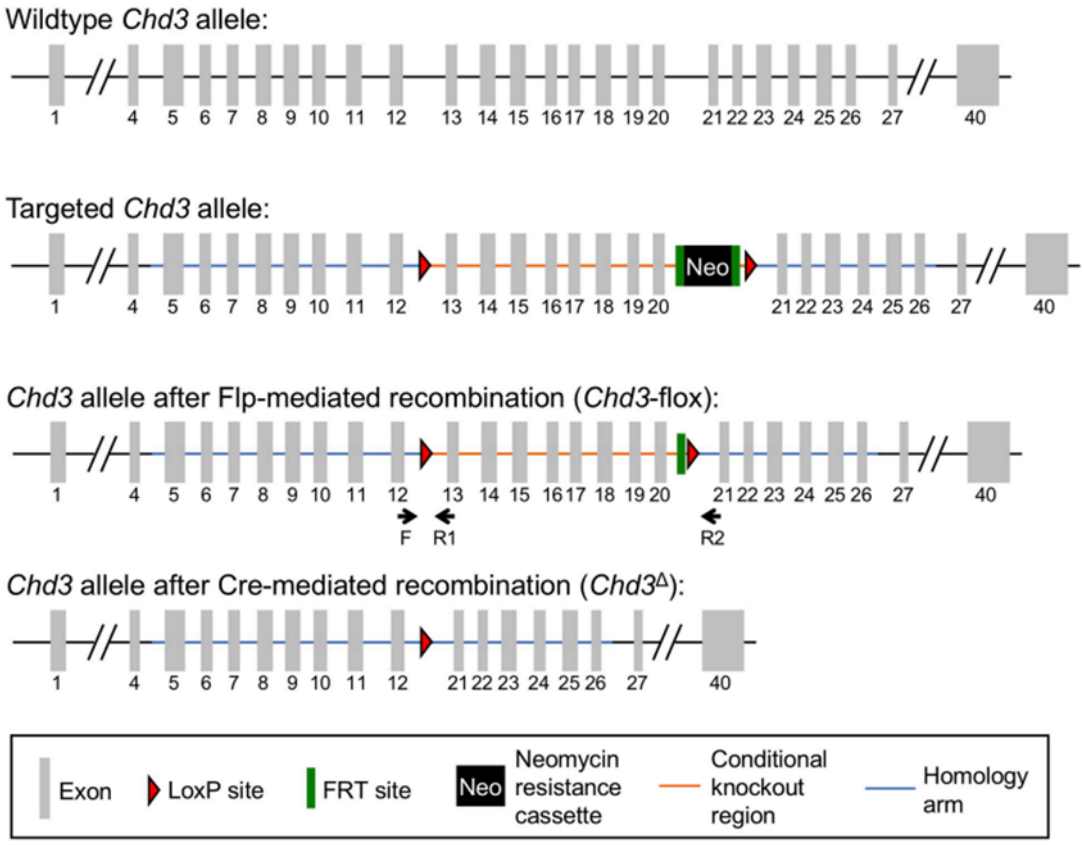


**Figure 6. *Chd3* floxed allele design.** The *Chd3* allele was designed so that upon Cre-mediated recombination exons 13 through 20 are excised. This removes the ATPase-helicase region of the protein and is predicted to cause a frameshift resulting in loss of function – adapted from Xie *et al.* (226).

The Emx1-Cre driver was chosen to conditionally knockout the *Chd3* gene. Emx1 expression turns on at E10.5 and is extensively expressed both in proliferative and postmitotic populations of the lateral, medial, and dorsal pallia by E12.5 (78). The use of this Cre-driver ensures that *Chd3* will be excised before radial glial cells (RGCs) begin their expansion and generation of the neocortex. Additionally, Emx1+ progenitor pools contribute minimally to structures outside of the telencephalon. This confirms that any observed phenotype can be attributed to the cortex or nearby regions.

Using primers designed by the Griffin laboratory for the *Chd3*-flox allele (Table 2), PCR genotyping confirmed that the wildtype allele generated a PCR product of 152 base pairs (bp) and that the floxed allele produced a product of 213 bp (Figure 7), allowing one to discriminate between wildtype, heterozygous and homozygous floxed alleles.

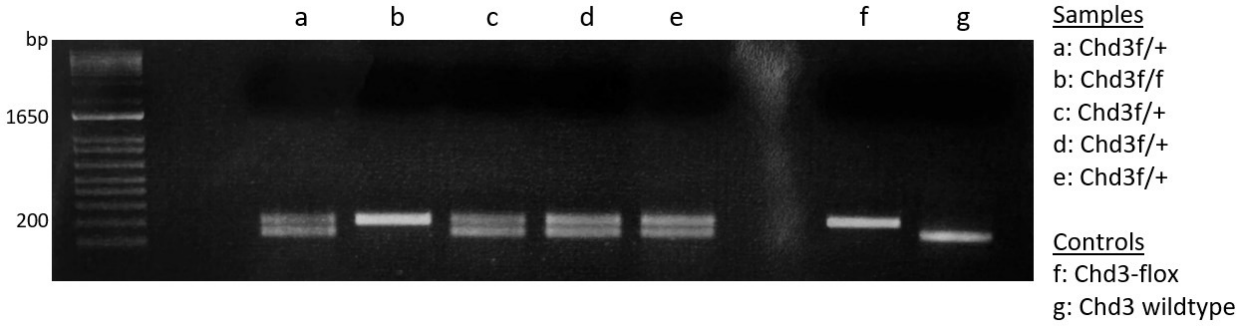


**Figure 7. Genotyping results from an experimental litter.** Samples were genotyped using Chd3-flox primers designed by the Griffin laboratory (Table 6.A.1.). PCR products were run on a 1.5% agarose gel for 35 minutes at 90V. The Chd3-flox band appears at 213 bp and the wildtype Chd3 band appears at 152 bp.

### 3.1. Confirmation of Excision

Before characterization of forebrain *Chd3* ablation could begin, the expected excision first had to be validated. Protein extracted from P0 cortical lysates displayed a reduction in Chd3 protein levels (Figure 8). RT-PCR analyses were designed such that the forward primer was in exon 12 and the reverse in exon 21. Alleles that had undergone recombination would produce a 158 bp band as the exons would be connected, while the wildtype allele would have a much larger amplicon size of 1359 bp. The excision was observed in both conditional heterozygotes (cHTs) and the conditional knockouts (cKOs) but not the wildtype samples and there was an approximately 2-fold enrichment in cKOs compared to the cHTs (Figure 9). For RT-qPCR experiments, the primers were designed to span exons 16 to 17 which are excised upon Cre recombination. This experiment showed a decreased amplification in the cHT and cKO animals although the expected 2:1:0 ratio of WT:cHT:cKO was not seen because the interneurons present in the cortical RNA samples provide wildtype transcripts to amplify thus skewing the ratio from the expectation (see below). Further, immunofluorescent staining of P0 cortical sections showed a depletion of Chd3+ cells in the cKO animals (Figure 10). While there are some Chd3+ cells remaining (9.77% ± 0.52%), these are almost certainly interneurons which migrate tangentially from the ganglionic eminences and do not express the Cre protein. It is consistently seen that about 5-10% of DAPI+ cells remain marker positive as well in *Emx1*-Cre models (79, 82).

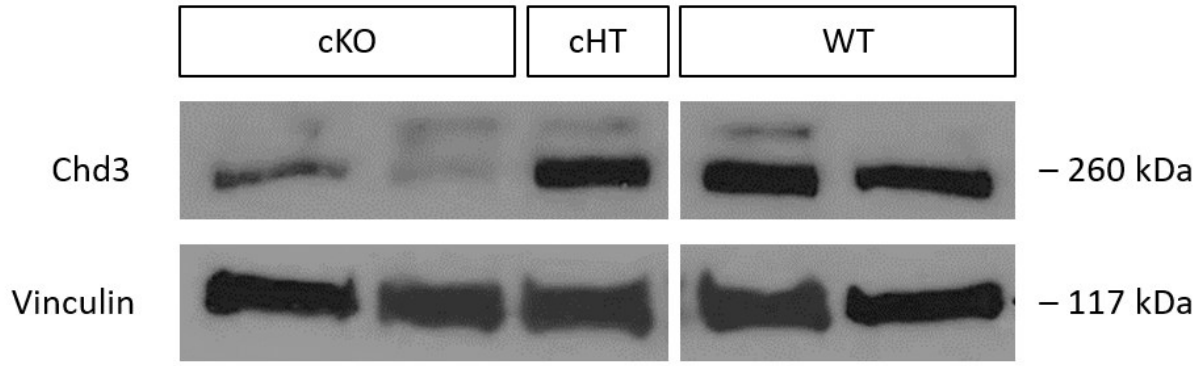


**Figure 8. Western blot of P0 cortical lysates.** Protein extracted at P0 demonstrated a loss of Chd3 protein in the cKO mice. Cre excision does not occur in interneurons which likely accounts for any remaining Chd3 protein levels in cKO samples.

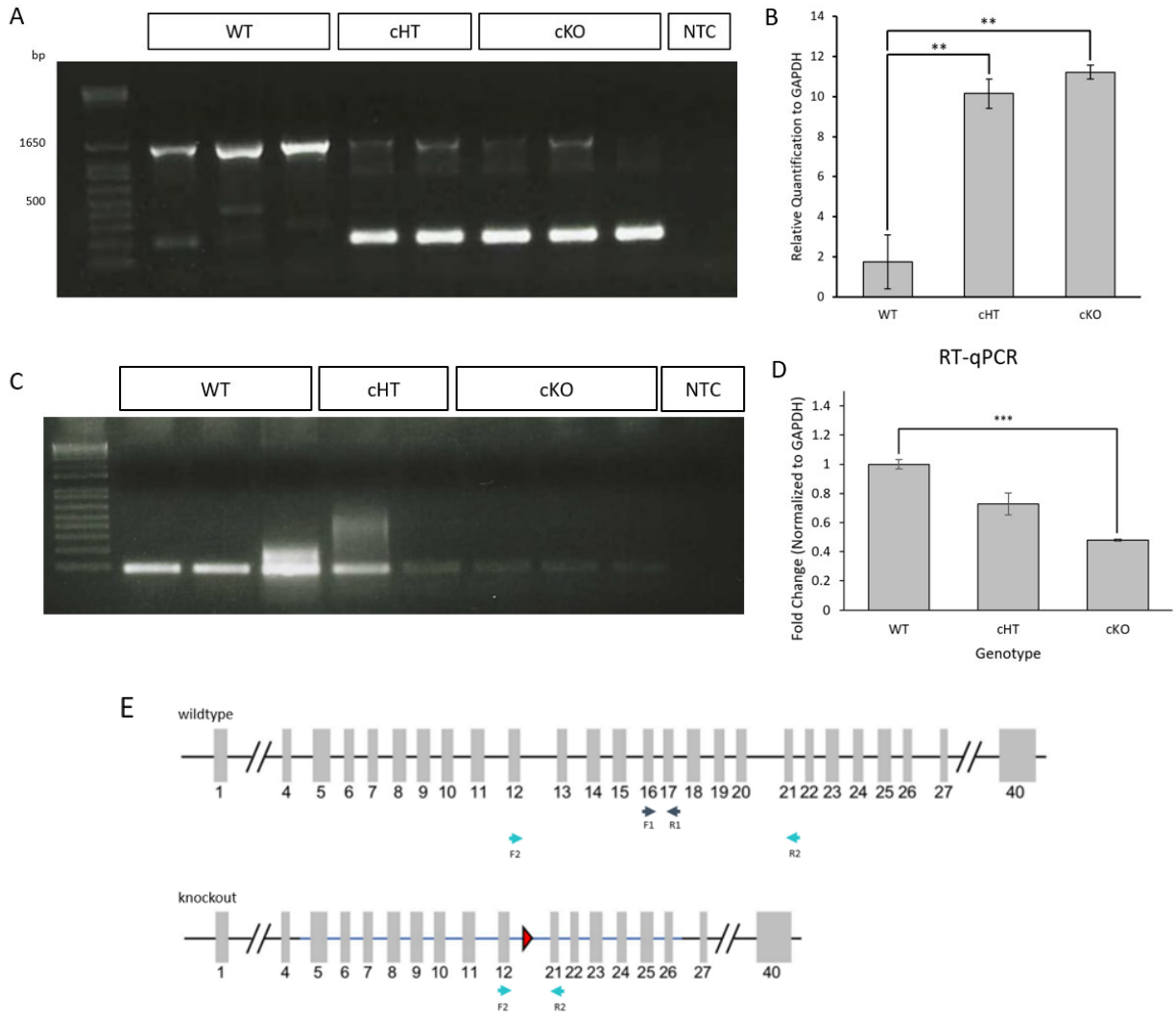


**Figure 9. RT-PCR and RT-qPCR of cDNA produced from RNA extracted from P0 cortical lysates.** For the RT-PCR each genotype produces their expected bands (A) with some non-specific bands present due to the slightly cooler than optimal annealing temperature necessary for the housekeeping gene control primer set. Nonetheless, compared to wildtype, the cHT and cKO have significant increase over wildtype in densitometry analyses (B). The RT-qPCR showed the expected band size (C) with a significant reduction in the presence of the exon 16-17 band in the cKOs (D). A schematic for the Chd3 primer design shows the set 1 used for RT-qPCR and set 2 used for RT-PCR (E) (n = 3, one-way ANOVA with post-hoc Dunnett's test).

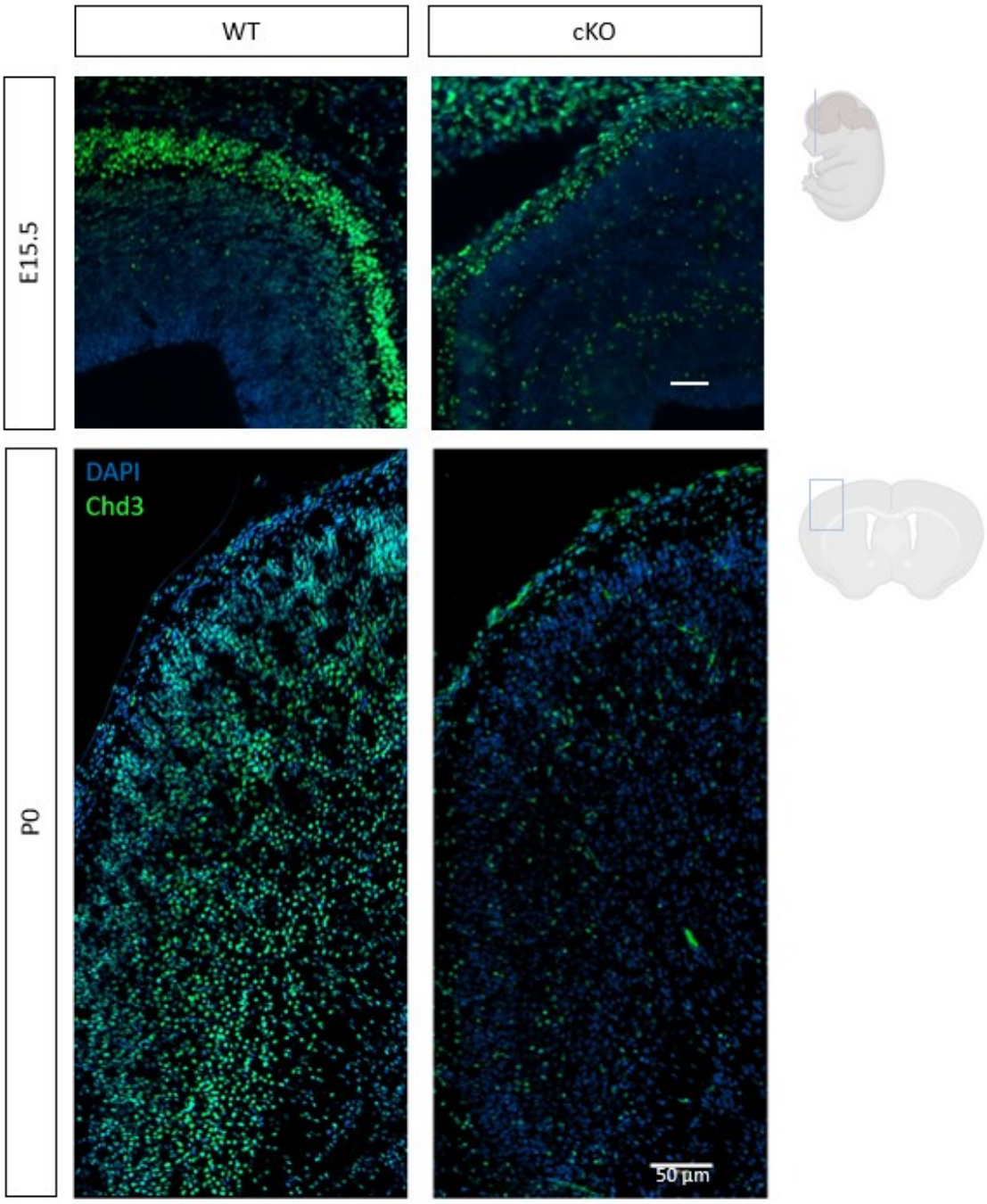


**Figure 10. Immunofluorescent staining of E15.5 and P0 coronal sections.** Staining with an αChd3 antibody displays the loss of Chd3 in the cKO cortex (right) as compared to the wildtype cortex (left) (scale = 50 µm). Schematic diagrams on the right indicate the location of the sections corresponding to the images shown.

### 3.2. Knockout Viability

Knockout animals were indistinguishable by eye from wildtype mice (Figure 11). When aged to P100 there was no noticeable difference in their ability to survive nor any issue with cohabitation with cHT or wildtype mice. Litters contained all genotypes in the expected mendelian ratios (Table 6), and birthweights were consistent across genotypes even when analyzed by sex (Table 7).

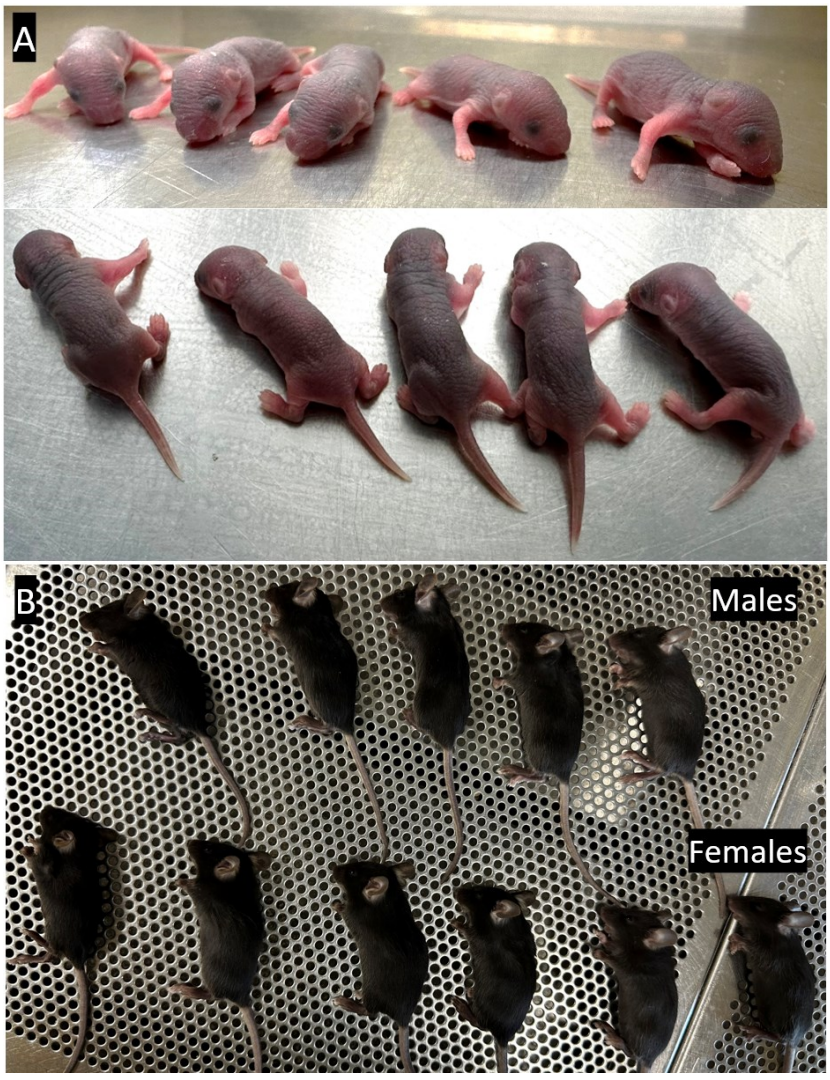


**Figure 11. Whole body images of experimental litters at P4 and P21.** Mice have no noticeable differences either by gross morphology or behaviour. The genotype cannot be known without analysis of tissues.

**Table 6. Genotypic ratios of knockout litters.** While a slightly higher number of wildtype animals with only one floxed *Chd3* allele is observed, there is no statistically significant difference between the occurrence of genotypes. (*P>0.9, n=327, chi-square).

| Genotype | Observed Offspring | Expected Mendelian Ratio | Observed Mendelian Ratio* |
|---|---|---|---|
| Chd3f/f; Emx1cre+/– (cKO) | 80 | 25% | 24.5% |
| Chd3f/f; Emx1cre–/– (WT) | 70 | 25% | 21.4% |
| Chd3f/+; Emx1cre+/– (cHT) | 83 | 25% | 25.4% |
| Chd3f/+; Emx1cre–/– (WT) | 94 | 25% | 28.7% |

**Table 7. Perinatal bodyweight measurements of knockout litters.** The average bodyweight of pups at P0 have no statistically significant difference in general or by sex. (*P>0.05, n=158, one-way ANOVA).

| Genotype | Average Body Weight (g)* | Male (g)* | Female (g)* |
|---|---|---|---|
| Chd3f/f; Emx1cre+/– (cKO) | 1.456 | 1.449 | 1.466 |
| Chd3f/f; Emx1cre–/– (WT) | 1.460 | 1.477 | 1.423 |
| Chd3f/+; Emx1cre+/– (cHT) | 1.434 | 1.411 | 1.458 |
| Chd3f/+; Emx1cre–/– (WT) | 1.503 | 1.505 | 1.500 |

Looking at gross structure of the forebrain at E15.5 and P40 by Nissl staining (Figure 12), there were no clear differences observed between genotypes. Overall, it is concluded that brain structure remains relatively consistent between genotypes.

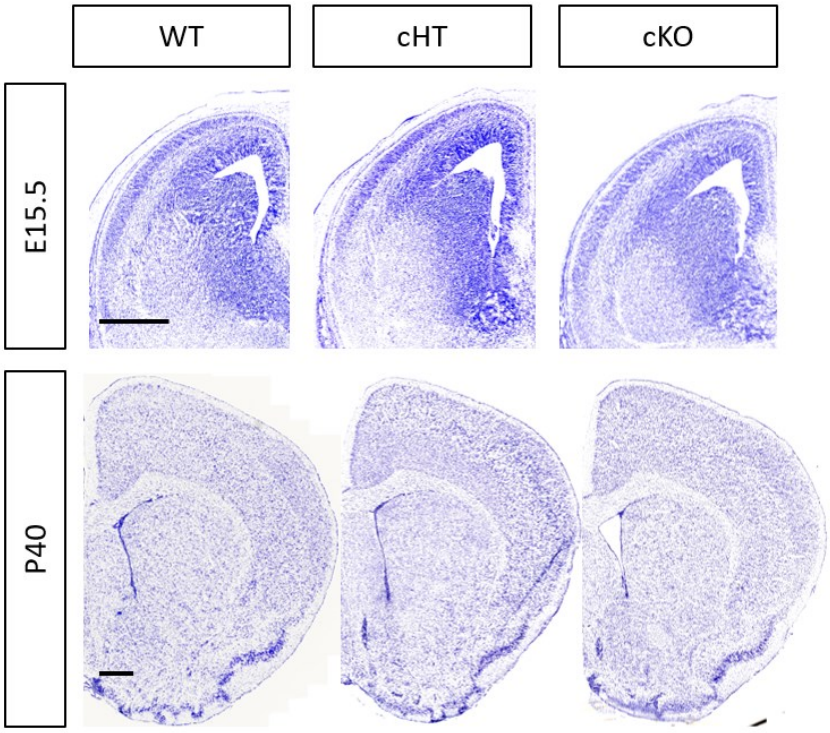


**Figure 12. Nissl staining of embryonic and adult coronal forebrain sections.** Nissl stained E15.5 and P40 representative coronal sections (scale = 1mm).

## 3.3. Progenitor Kinetics and Cortical Lamination

Previous work has suggested that Chd3 protein is expressed at earlier times when progenitors are prevalent (E13.5) (228, 233). To test whether there was any effect on progenitor homeostasis, we examined the proportion of cells in different stages of the cell cycle. E15.5 embryos were sacrificed following a 1-hour EdU pulse[1].To examine the proportion of cells in mitosis, we performed phosphohistone H3 (pHH3) staining on the E15.5 sections (Figure 13). Though there is a slight increase in the number of basal pHH3+ cells (WT: 7.20 ± 0.77; cHT: 7.00 ± 0.40; cKO: 8.40 ± 0.61) as well as with the apical pHH3+ cells (WT: 26.20 ± 3.06; cHT:

[1] All EdU injections were performed by senior lab technician Keqin Yan, MSc.

25.80 ± 3.70; cKO: 27.40 ± 2.24, which may suggest a cell cycle delay in the mutants, the increases were not statistically significant. To look at the proportion of cells in S-phase, the EdU+ stained cells from a1-hour pulse were quantified. A decrease in the proportion of EdU+ cells were seen in the mutant (WT: 23.23% ± 0.69%; cHT: 22.33% ± 0.62%; cKO: 21.48% ± 0.65%) but they do not reach significance. Together these two cell cycle parameters indicate that there are no significant differences in cell cycle kinetics, and that the slight variations observed are likely due to natural variation between animals. Pax6 and Tbr2, which are markers of RGCs and IPCs respectively, were also examined to evaluate any changes in the proportion of these progenitors at E15.5. These stainings produced no noticeable difference.

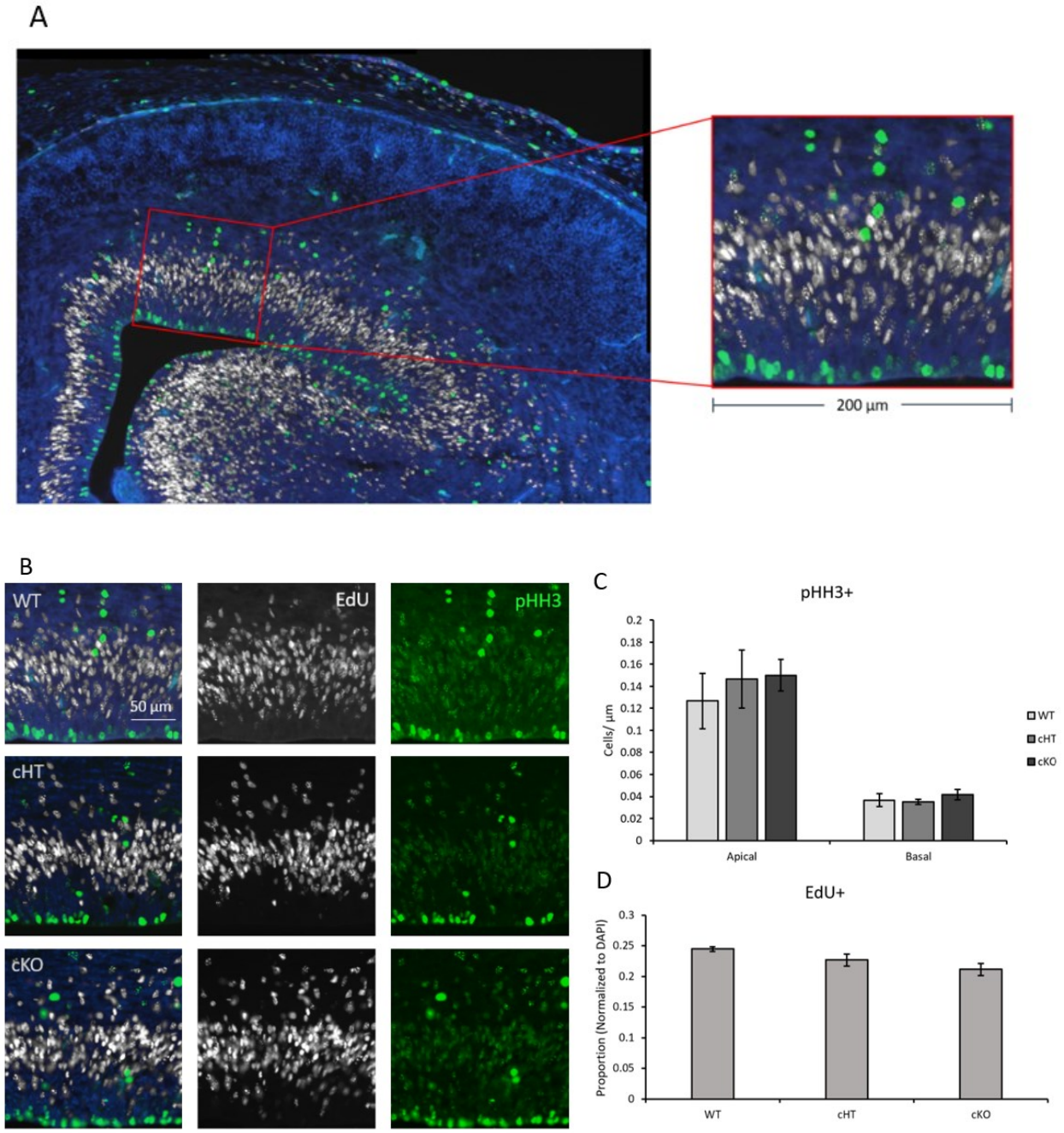


**Figure 13. Phosphohistone H3 staining in E15.5 cortical sections following a 1-hour EdU pulse.** Quantification was performed on 200µm-wide sections covering from the surface of the lateral ventricle to the basal pHH3+ cells (A). Sections show no clear differences (B) which is in line with the quantifications which have no change between genotypes in apical or basal pHH3+ cells (C) nor in EdU+ cells (D). (scale = 50 µm, n = 3, one-way ANOVA).

In line with what was seen in the progenitors, DAPI+ cells were present in equal numbers between all genotypes (WT: 730.14 ± 48.62; cHT: 720.76 ± 42.99; cKO: 696.33 ± 45.56 at P0 and WT: 370.33 ± 16.66; cHT: 406.78 ± 10.60; cKO: 381.78 ± 8.26 at P7). (Figure 14). As such it is taken that any differences observed in the layers are not due to a loss of cells. The difference in raw counts between timepoints is attributed to the difference in size of the representative sections chosen for counting. As P7 cortices are much taller than P0, narrower sections were taken to maintain efficiency during quantification.

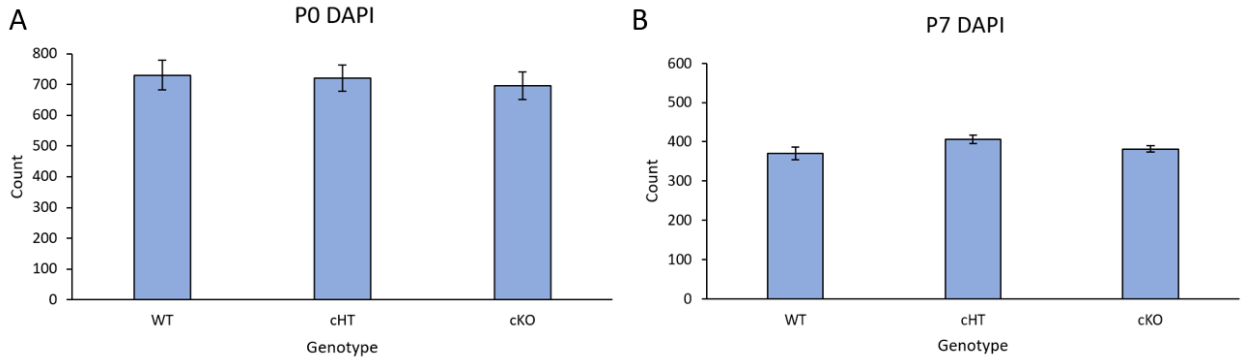


**Figure 14. Raw DAPI counts for cortical sections.** There is no difference in the DAPI counts, i.e., number of cells present in the cortices, at P0 (A) nor P7 (B) between the three genotypes. (n = 3, one-way ANOVA).

In order to assess the cortical lamination of the animals, antibodies against three layer-specific neuronal markers were chosen for IF analysis: Tbr1 which is expressed in layer VI, Ctip2 staining as a marker for layer V neurons, and Satb2 which is primarily expressed in the superficial layers II-IV. While no difference was observed for the deep layer markers (Tbr1, Ctip2), the proportion of Satb2+ cells were decreased in layers II-IV in both heterozygote and knockout cortices (WT: 32.61% ± 1.26%; cHT: 26.06% ± 1.38%; cKO: 22.44% ± 1.22%) Moreover, there was also an increase in the proportion of Satb2+ cells in layer VI at P0 (WT: 24.12% ± 1.82%; cHT: 31.09% ± 1.65%; cKO: 34.71% ± 2.04%) (Figure 15). Although the cells were being retained in layer VI there was no change in the cells co-labelled with Satb2 and Tbr1 between the genotypes, indicating that there is not an error with misexpression. By P7, when all cells should have migrated to their final destination within the cortex, the deficit within upper layer cells observed at P0 remained apparent (WT: 42.41% ± 2.87%; cHT: 31.40% ± 1.63%; cKO: 30.57% ± 1.28%). However, the difference was not as prevalent and at this age a slight decrease in Satb2+ cells was seen in layer V of the cKO animals as well. An improvement of the number of Satb2+ cells remaining in layer VI is also observed albeit it is still near significance (WT: 21.26% ± 1.74%; cHT: 19.37% ± 1.06%; cKO: 26.04% ± 1.41%, P = 0.0645).

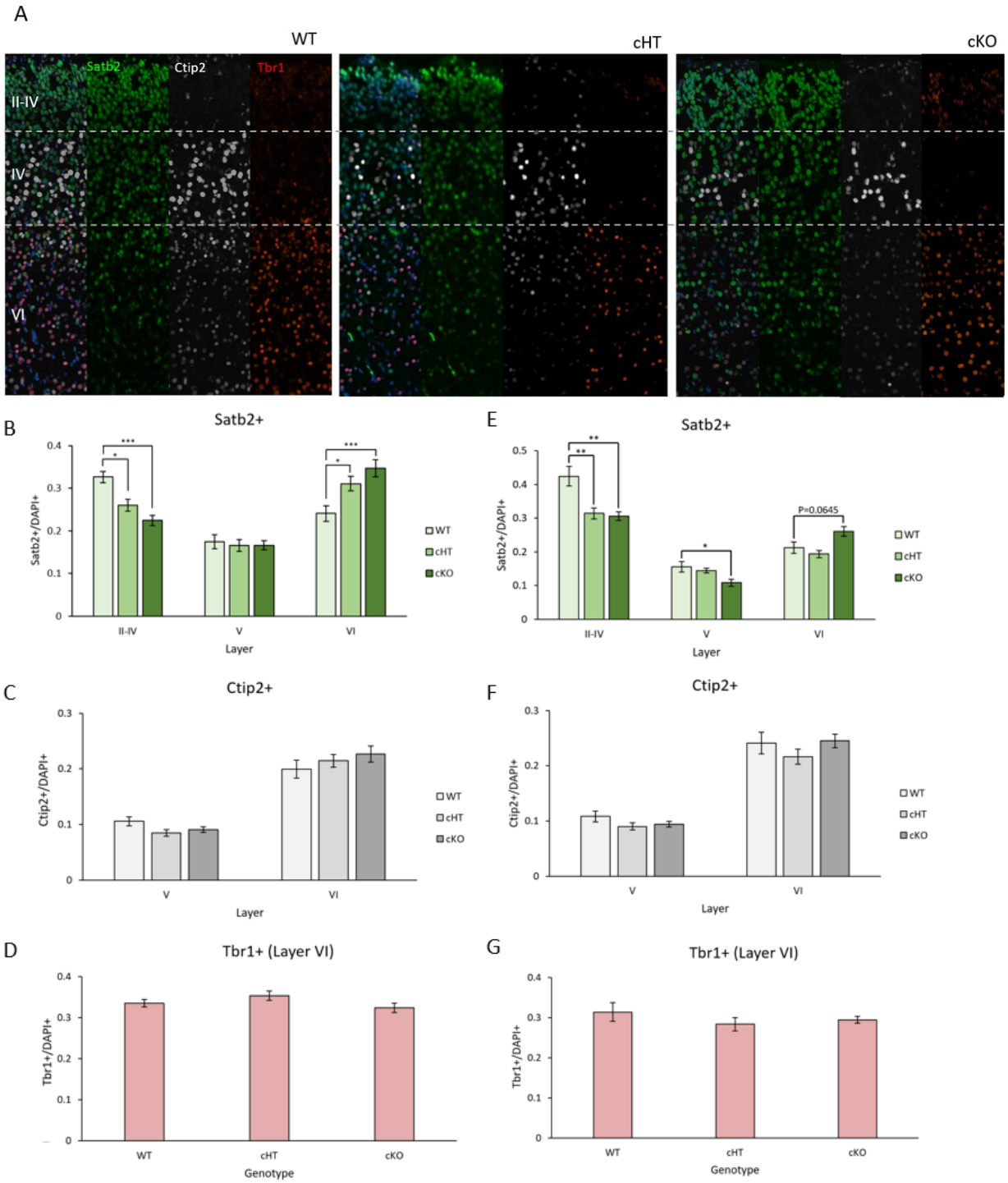


**Figure 15. Cortical lamination of coronal sections.** Cortices were stained with Satb2, Ctip2, and Tbr1 to mark layers II-IV, V, and VI respectively (A). In P0 a reduction of the upper layer cells is observed in mutant animals along with a concurrent rise in the number of Satb2+ cells in layer VI (B). No significant difference was seen between the lower layer proportions (C, D). The same is still observed in P7 with a decrease in Satb2+ cells in the cKO in layers II-V (E) and no difference in Ctip2+ cells (F) nor Tbr1+ cells (G). (n = 3, one-way ANOVA with post-hoc Dunnett's test).

Since no changes in progenitor cell cycle kinetics were observed, we next asked whether there were any defects in migration that could explain the increased number of Satb2+ cells within the lower layers. To examine migration, we performed a neuronal birthdating experiment to track the progression of the upper layer cells (Figure 16). Pregnant dams were injected with EdU[2] at E15.5 and brains were harvested at P7. The cKO and cHT sections showed not only a paucity of EdU+ cells in the upper region (WT: 19.55% ± 1.77%, 16.60% ± 0.99%, 2.39% ± 0.72%; cHT: 10.93% ± 1.71%, 9.33% ± 0.47%,1.16% ± 0.35%; cKO: 10.26% ± 1.85%, 3.12% ± 0.41%, 0.58% ± 0.17%) but a sharp increase in the EdU+ cells at the bottom of the cortex as well (WT: 1.35% ± 0.65%; cHT: 8.13% ± 2.05%; cKO: 7.62% ± 1.98%). When comparing the cells that are co-labelled with EdU and Satb2, the same pattern is seen in the upper layers. The proportion of cells co-labelled is dramatically decreased near the top of the cortex with approximately 40% less co-labelled cells in cHTs and 80% less co-labelled cells in cKOs as compared to wildtype (WT: 20.71% ± 1.18%; cHT: 12.79% ± 1.29%; cKO: 4.44% ± 0.51%) and a ~233% increase in co-labelled cells in cHTs and a ~210% increase in co-labelled cells in cKOs in the lowest region (WT: 0.64% ± 0.18%; cHT: 14.49% ± 2.31%; cKO: 12.60% ± 1.95%). This is supported by the pattern of the nuclei staining with DAPI reduced in the upper region (WT: 146.0 ± 5.9; cHT: 132.3 ± 2.6; cKO: 119.3 ± 5.6) and increased in the lower two regions (WT: 145.0 ± 8.0; cHT: 155.0 ± 1.9; cKO: 174.3 ± 5.5 and WT: 121.3 ± 5.6; cHT: 130.7 ± 6.7; cKO: 153.7 ± 4.6).

[2] EdU injections performed by senior lab technician Keqin Yan, MSc.

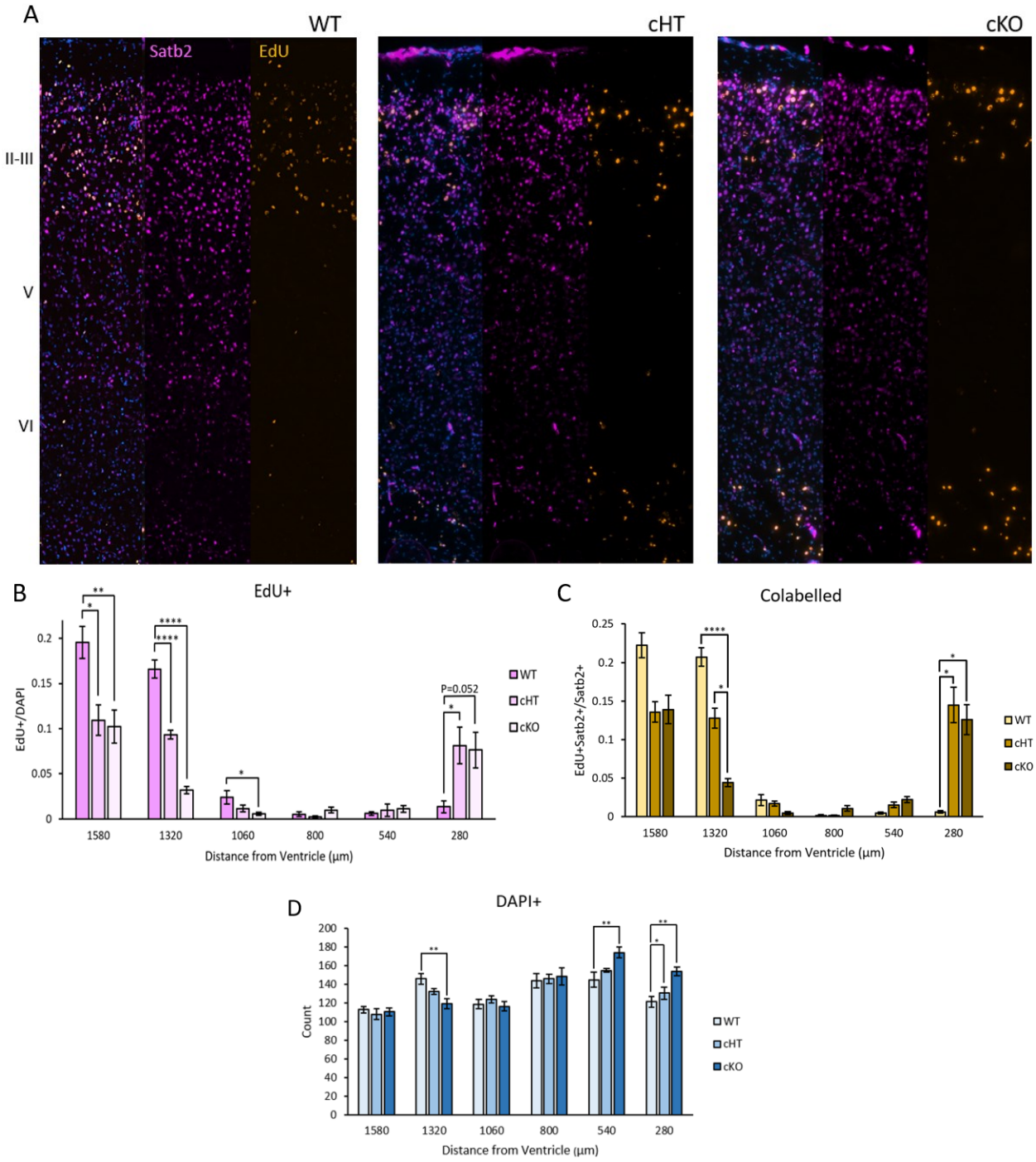


**Figure 16. Neuronal birthdating of layers II-III in P7 cortices.** Quantification was performed on 200 µm-wide sections covering from the border of the white matter to the top of the section. Measurements were performed in bins calculated based on distance from the ventricle starting at a minimum of 280 µm and increasing by 260 µm each bin. The spread of the EdU shows a clear difference between the genotypes (A) with overall EdU (B) recapitulating the phenotype observed in lamination analysis. The same pattern is seen in the EdU+Satb2+ colabelled cells (C) and DAPI+ cells (D) as well. (n = 3, one-way ANOVA with post-hoc Dunnett's test).

### 3.4. Behaviour Analyses

A battery of behavioural assays was performed to assess the impact of the loss of cells in the upper layers on the overall capabilities of the animals. The first test performed was the Beam Break assay. This test looks at general locomotor abilities, habituation to a novel environment, and as it was performed over a period of 48 hours it may find disruptions of the circadian rhythm as well. All mice showed the expected pattern of the highest level of activity during the first few hours as they habituated to the new cages (Figure 17). As they were loaded in the morning, a net drop in activity is seen in all genotypes during the light hours and a following rise in activity during dark hours which is repeated for the second day as well. As mice are nocturnal, this is an expected outcome and indicative of normal circadian rhythms. The majority of subjects place below or around the average curves, however the more active mice greatly increase the scale of the graph, making the curves appear flattened despite the difference in light and dark hours which would otherwise be apparent on a smaller scale. Of note, the cKO curve is consistently below that of the wildtype, only crossing above in 7 of the 48 hours and not by much at these times. This is consistent with the total number of beam breaks seen throughout the course of the test whereby cHTs and cKOs have reduced activity overall (WT: 40793.14 ± 7215.74; cHT: 38561.21 ± 8499.93; 37360.00 ± 7639.37). Analysis of total activity and at each hour showed no significant differences combined nor when data was segregated by sex. This suggests that there are no gross locomotor deficits in the cKO mice and as such can also act as a good control for the rotarod test.

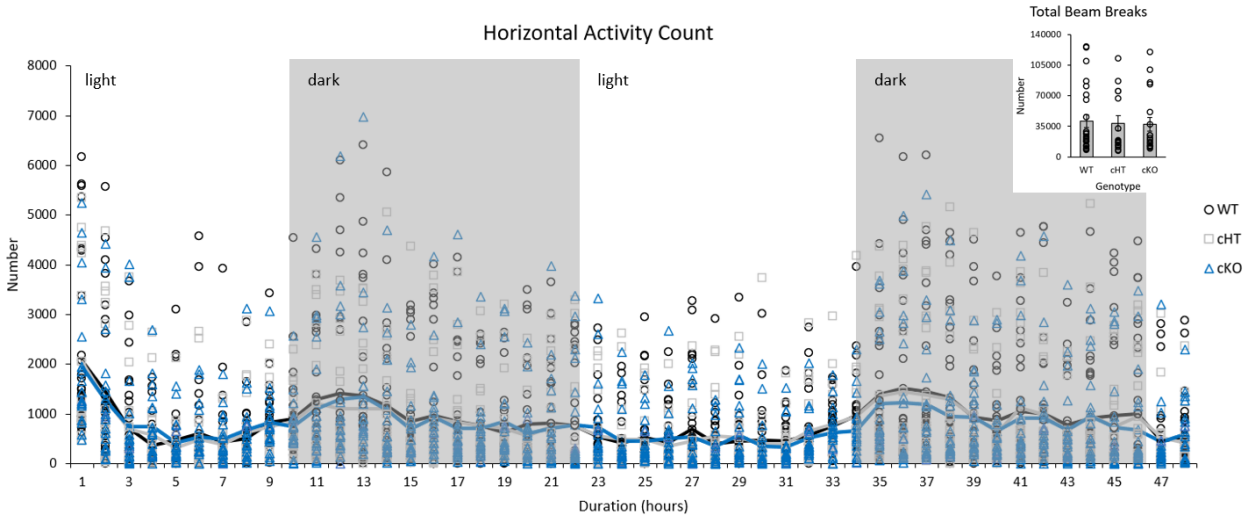


**Figure 17. Horizontal activity count over 48 hours.** All three genotypes follow the same general pattern of activity with the most beam breaks occurring during habituation in the first hour and then a following increase of activity during the dark periods. The curves may appear to not show the expected distinction between light and dark cycles; however, this is due to the subjects above the curve increasing the scale for the number of beam breaks. Inset contains the total average number of beam breaks over the 48 hours of testing. (n= 29, 19, 19 for WT, cHT, cKO respectively, two-way ANOVA with post-hoc Tukey-Kramer test).

For the accelerating rotarod test, which can measure motor coordination and motor learning, mice are placed on a rod that rotates at 4 rpm and increases to 40 rpm during the first minute with up to 5 minutes of testing permitted if they are able to stay on. Mice are tested over four trials a day and for two consecutive days. It is expected that there is an increase in the latency to fall over the course of the first four trials as well as between the two days reflecting the mouse's ability to learn the mechanism of the test and improve their performance accordingly. Unfortunately, the wildtype control animals do not clearly demonstrate the expected motor learning as they show minimal improvement in their ability to remain on the rod on the first day and an overall decrease in ability on the second day (Figure 18A). This would preclude the rest of the data from analysis due to the lack of a proper control. However, it is noted that despite a lack of significance the cKOs show superior performance on both days of testing (Figure 18B) and cHT animals show the greatest improvement on the second day (Figure 18C).

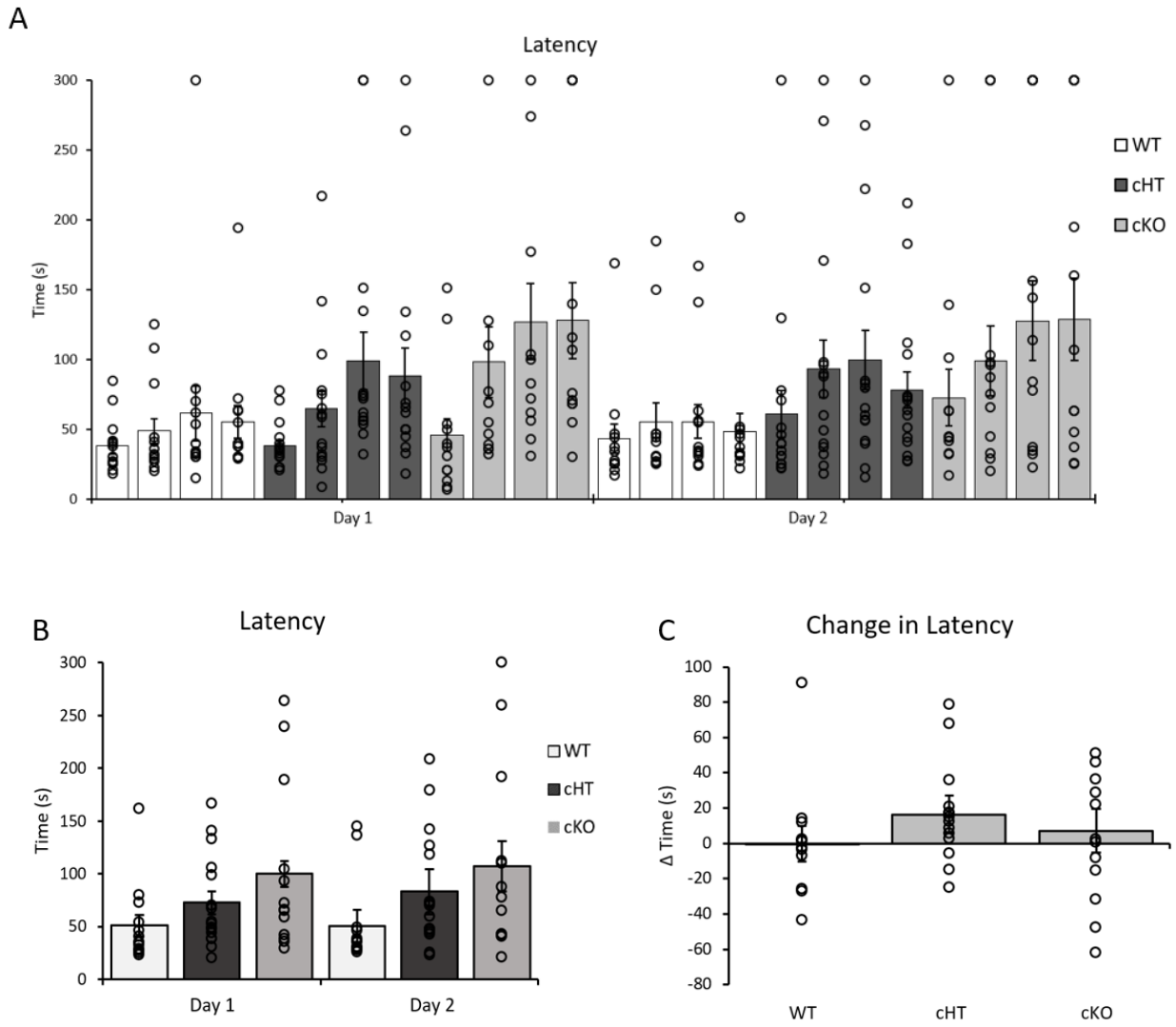


**Figure 18. Comparison of latency to fall for the rotarod test.** Though the knockout animals show clear motor learning, there is a lack of the expected motor learning being demonstrated in the wildtype controls (A). The cKO animals show an increase in latency to fall on both testing days compared to wildtype animal (B) with the cHTs showing the greatest improvement on the second day (C), however there is no significance. (n= 13, 16, 13 for WT, cHT, cKO respectively, one-way ANOVA).

The open field test may also be used to examine motor function or activity levels, but as the beam break and rotarod assays assess these capacities the parameters were set such that anxiety was measured. Throughout the course of the 10-minute test there is a minor but non-significant increase in the average speed of the cKO mice (WT: 4.55 cm/s ± 0.19 cm/s; cHT: 4.49 cm/s ± 0.24 cm/s; cKO: 4.84 cm/s ± 0.33 cm/s) (Figure 19A). This is also seen with the average distance travelled by the animals (WT: 2735.93 cm ± 110.36 cm; cHT: 2695.63 cm ± 14.13 cm; cKO: 2902.64 cm ± 197.98 cm) (Figure 19B). Overall, there were no significant differences in average speed or distance traveled. When comparing the location of the mice during the test, all genotypes spent the majority of the test in the dim corners of the testing arena with cHT spending the most time at 55.9% and the cKO spending the least time at 53.2% (WT: 330.30 s ± 9.79 s; cHT: 335.23 s ± 14.17 s; cKO: 319.49 s ± 14.30 s). Regardless of all animals spending limited time in the brightly lit centre, the cKOs spent the most time at 2.9% and the cHTs spent half of that time at 1.5% (WT: 15.01 s ± 1.99 s; cHT: 8.74 s ± 1.62 s; cKO: 16.78 s ± 2.89 s). Again, despite differences seen on a small scale, no significant differences were observed between genotypes for the proportion of time spent in the dim corners or the bright centre of the arena (Figure 19C, D), suggesting that anxiety levels are unaffected in mutant animals.

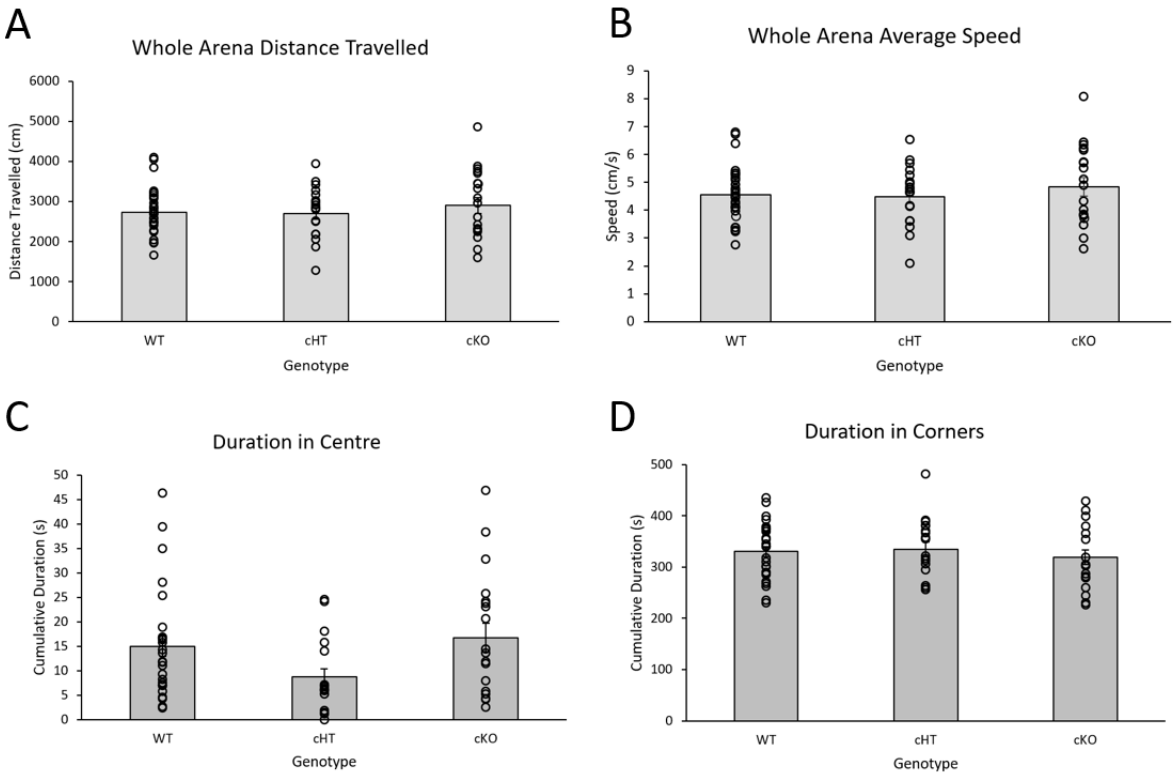


**Figure 19. Open field measurements show no differences between genotypes.** Approximately the same results were seen for wildtype, conditional heterozygote, and conditional knockout animals for the total distance (A), average speed (B), duration in the centre of the arena (C), and the duration in the corners (D). (n= 29, 19, 19 for WT, cHT, cKO respectively, one-way ANOVA).

The adult social interaction test looks at social recognition which may be impacted by alterations to the lateral entorhinal cortex or ventral subiculum in the case of the *Emx1*-Cre cKOs (208-210). When the tested mice are first permitted to survey the empty arena, they are able to explore the small wire cage that the interactor will be placed in. As it is the only object in the arena this allows for generation of a baseline so that the exposure to the interactor mouse is not confounded with exposure to a novel object. It is then expected that at the next trial with the presence of an age- and sex-matched interactor mouse it will lead to an increase in the presence of the test mice in the interaction zone surrounding the wire cage due to normal social recognition capabilities. The results of the testing showed that all genotypes travel less distance overall in the presence of the social target mouse (WT: -632.02 cm ± 82.74 cm; cHT: -493.04 cm ± 97.97 cm; cKO: -731.62 cm ± 90.94 cm) (Figure 20A). Additionally, they all increase the amount of time spent in the interaction zone by approximately the same amount (WT: 14.68 s ± 3.43 s; cHT: 19.77 s ± 4.19 s; cKO: 18.75 s ± 6.10 s) (Figure 20B). Though the same pattern is seen with both sexes, when looking at the frequency of entrance into the interaction zone female wildtype animals expectedly entered the zone more often but the female mutant animals entered the zone less on average (WT: 9.5 ± 2.80; cHT: -4.25 ± 5.21; cKO: -0.43 ± 4.91). Despite this observation, the change between genotypes is not significant.

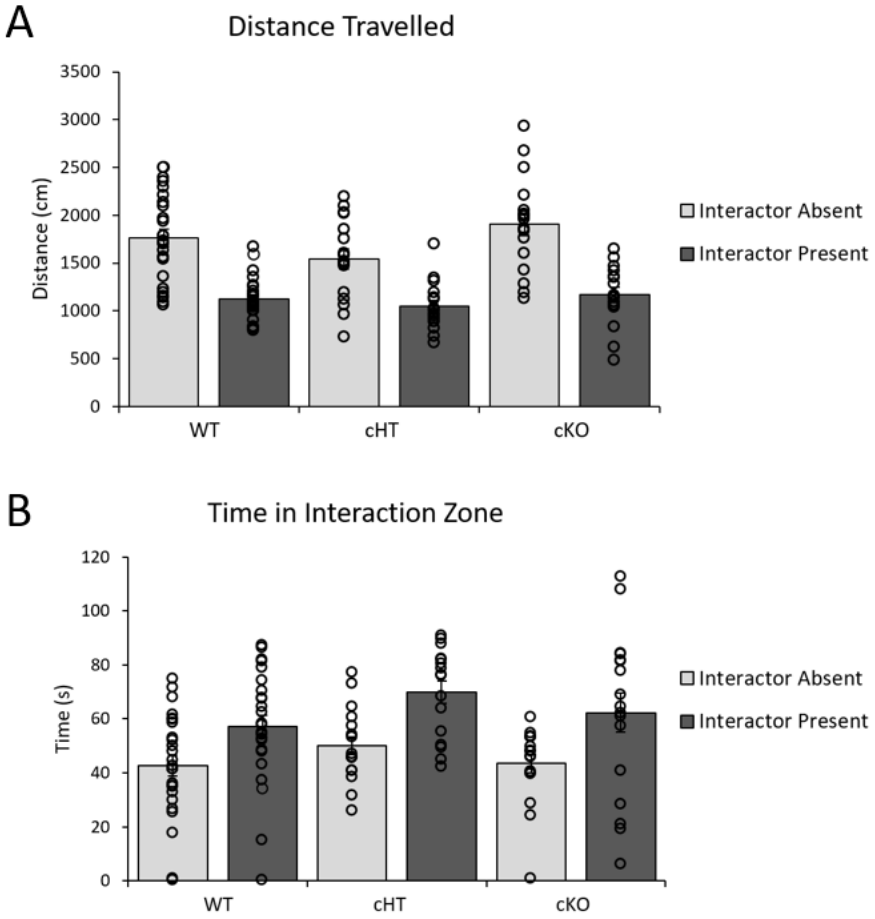


**Figure 20. Concordant sociability is observed in all groups during the adult social interaction test.** There is no change in the total distance travelled (A) nor the time spent in the interaction zone (B) with the interactor mouse absent or present between genotypes. (n= 25, 16, 17 for WT, cHT, cKO respectively).

The last two tests evaluate different forms of learning. The Morris water maze has external visual cues on the walls to help the mice learn the location of a platform slightly below the surface in a tub of water in order to measure spatial learning and memory. The learning curves for each genotype are statistically similar with plateauing at the final days indicating successful training for each group (Figure 21A). When comparing performance on the probe day, there is an equal time spent in the target quadrant (WT: 29.35 s ± 1.55 s; cHT: 24.26 s ± 1.64 s; cKO: 27.66 s ± 2.06 s) along with no difference in the distance travelled (WT: 1329.31 cm ± 35.79 cm; cHT: 1298.68 ± 75.13 cm; cKO: 1163.54 cm ± 70.20 cm). Taken together it suggests that there was no difference between the genotypes in their ability to learn and remember the expected location of the platform (Figure 21B, C). Additionally, the tracking software can measure thigmotaxis. In this context, thigmotaxis refers to an animal circling the perimeter of the pool due to increased anxiety (234, 235). Since increased anxiety can impair learning and memory (236, 237), it follows that these animals which demonstrate no such impairment also have no change in time spent in thigmotaxis (WT: 15.96 s ± 1.69 s; cHT: 15.65 s ± 1.68 s; cKO: 18.68 s ± 2.32 s) (Figure 21D).

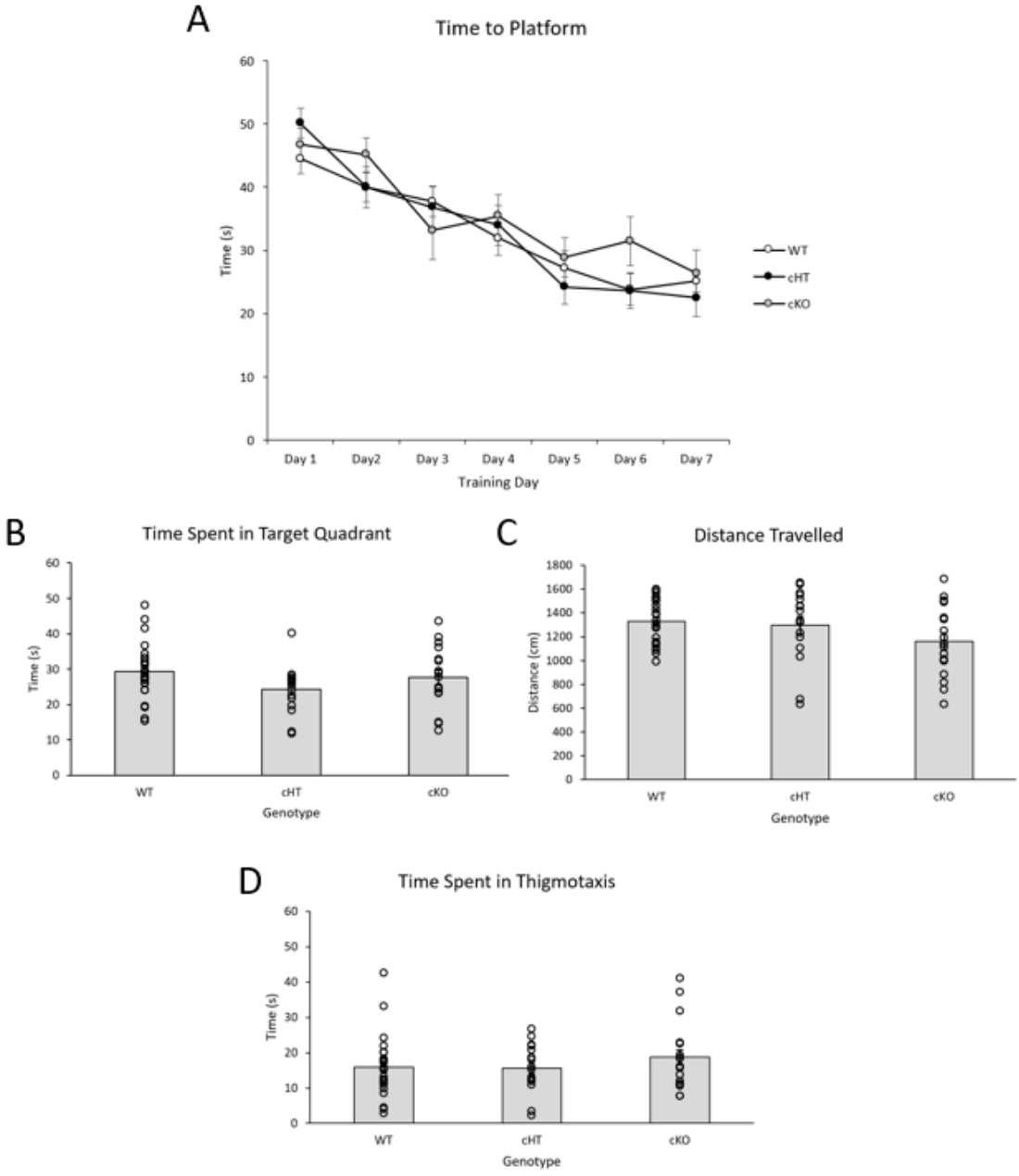


**Figure 21. Mutant animals show outcomes consistent with wildtype during Morris water maze.** All animals learn the platform location in the same amount of time (A). During probe day they then spend the same amount of time in the target quadrant (B), travel the same total distance (C), and spend the same amount of time in thigmotaxis (D) on probe day. (n= 25, 16, 17 for WT, cHT, cKO respectively).

The final test, fear conditioning, looks at both contextual and associative memory. A foot shock is delivered in a phenotyper box at the same time a loud tone is played. The activity beforehand is analyzed to get a baseline activity for the mice and determine if there is a difference between genotypes (Figure 22A). At this point there was no difference in the activity levels between the mice. All mice were active ~80% of the time and freezing only 20% (WT: 82.05% ± 2.56%; cHT: 83.53% ± 2.18%; cKO: 82.16% ± 2.90%). The next day the amount of freezing is measured to see if the mice associate the phenotyper box with the previous day's foot shock. Here, the mice from all 3 genotypes showed an increase in freezing (from 20% day 1 to 60% day 2) demonstrating that they recognized the environment (WT: 61.24% ± 3.87%; cHT: 55.28% ± 3.98%; cKO: 58.27% ± 3.92%). Again, no differences were seen between genotypes when placed in the same context (Figure 22B). On the final day the context is completely changed but the tone is played. The freezing before the tone was played was equally low for each genotype, indicating that none recognized the phenotyper box as desired (WT: 13.39% ± 2.08%; cHT: 13.88% ± 2.44%; cKO: 11.25% ± 2.04%). After the tone was played, the amount of freezing increased to around 70% indicating that they recognized the context of the tone with the same freezing response observed between the genotypes (WT: 79.70% ± 2.04%; cHT: 67.98% ± 6.01%; cKO: 73.13% ± 3.53%) (Figure 22C). However, when compared by sex, the results for the females were consistent with the entire group but the males showed significant differences. Though the initial activity levels on the training day were the same (WT: 76.80% ± 4.89%; cHT: 86.04% ± 1.88%; cKO: 79.73% ± 3.79%), when exposed again to the context wildtype and cKO animals were freezing around 60% of the time but the cHT males were freezing significantly less at ~45% (WT: 62.62% ± 5.57%; cHT: 44.82% ± 2.10%; cKO: 62.17% ± 4.54%) (Figure 22D, E). Further, on the cue day, all males were active around 80-90% of the time before the tone

(WT: 17.75% ± 3.64%; cHT: 9.81% ± 2.20%; cKO: 11.43% ± 2.41%) yet after the tone the freezing of the wildtype and cKO males increased to 70-80% but the cHT males only froze around 50% (WT: 83.83% ± 1.67%; cHT: 52.83% ± 8.28%; cKO: 69.46% ± 4.32%) (Figure 22F). This could indicate either a memory deficit or a reduction in anxiety. Due to the fact that the open field testing conditions were set to assess anxiety and no differences were seen it is supposed that the cHT males have reduced ability in contextual memory and associative memory leading to a reduced instinct to freeze when exposed to previously adverse conditions.

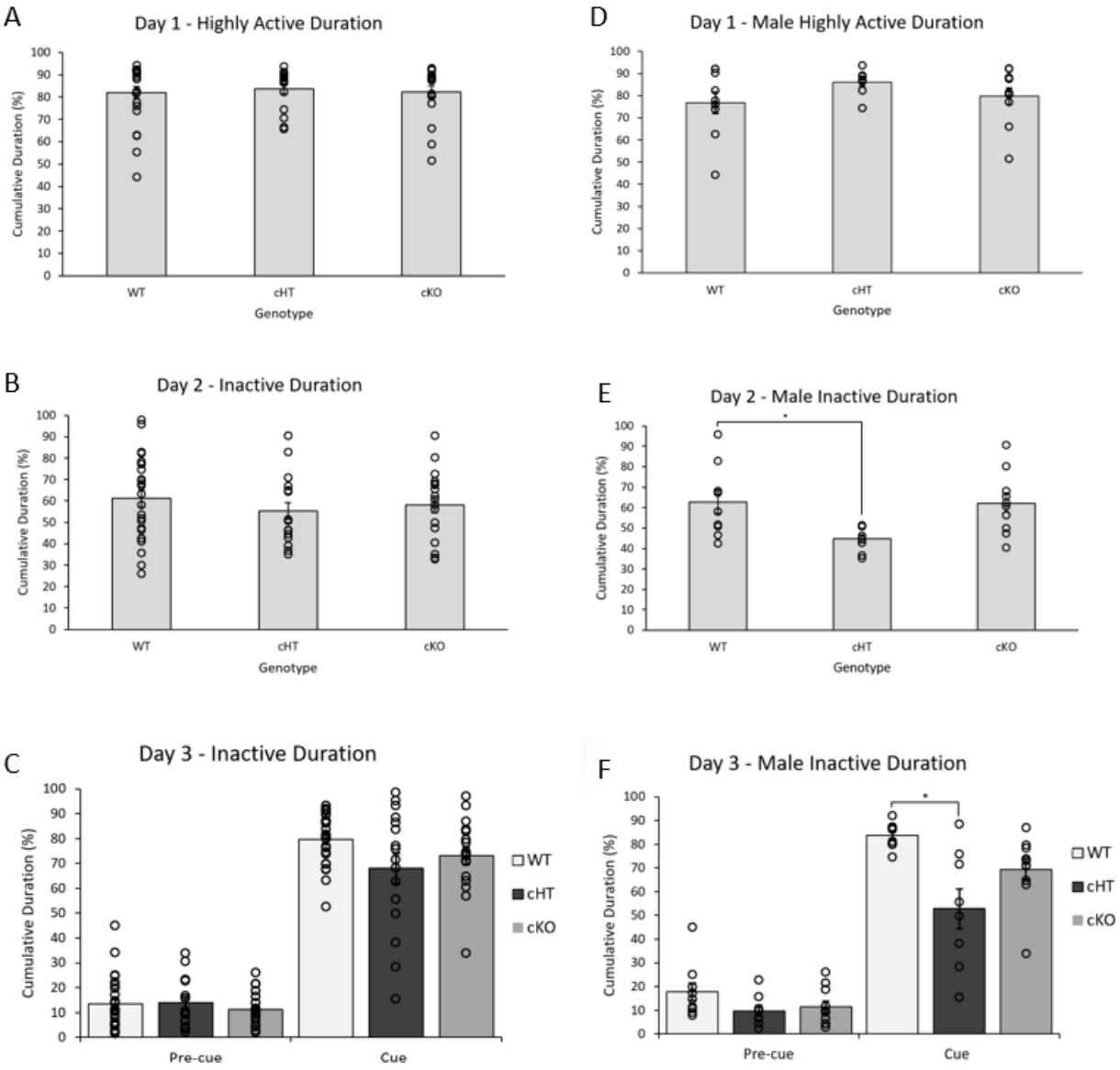


**Figure 22. No difference is seen in the fear conditioning test until males are analyzed separately.** The same outcome is seen for all genotypes when comparing the entire group (A-C). The males show no change in their activity when first put in the phenotyper box (D). On the second day, cHT males freeze less when put in the same context than their wildtype or cKO counterparts (E). When they are put in what they believe to be a novel context and the tone is played again the same decrease in freezing is seen in the cHT males (F). (Total n = 25, 16, 17, male n = 9, 8, 10 for WT, cHT, cKO respectively, one-way ANOVA with post-hoc Tukey-Kramer test).

# 4. Discussion

## 4.1. Forebrain-specific loss of Chd3 does not impair the survival or behaviour of the mice

Although *Chd3* has been examined in the neocortex through embryonic knockdown studies, never before has it been conditionally knocked out in the murine forebrain. We are aware of other groups looking at whole body knock outs of *Chd3* in mice, yet for a gene that is still not well understood these analyses are premature especially given that chromatin remodelers may act on many genes and thereby multiple systems within the body. Knockout with the *Emx1*-Cre driver easily allows for connection of observed phenotypes to their root cause. This is an important demonstration of the gene's role in cortical development and the consequential impact on the behaviour of the mice.

It was found that cKO mice were born in expected numbers (Table 6) with no impact on their size (Table 7, Figure 11) or development to weaning. These mice thus have no barrier in feeding from their mother or learning to obtain food from the wire bar pellet holder. Other knockout lines have shown increased aggression to their wildtype cage mates (238, 239), but there were no issues observed in cohabitation of the genotypes post-weaning. Moreover, cages with experimental litters of both sexes were kept past P100 without consequence.

When looking at the maturation of the brain, the gross morphology of the cortex through development is consistent with that of the wildtype animals (Figure 12). Furthermore, the increased activity with the steady decline seen across genotypes when put into the fresh cages of the beam break test demonstrates that the mutant animals have no defects in habituation to a novel environment (Figure 17). The nocturnal nature of mice gives expectations for this test such that there should be a drop in activity during light cycles with a concurrent rise during the dark

cycles. Even for those whose activity is elevated overall, this cyclic pattern was observed revealing normal and stable circadian rhythms in cHTs and cKOs. This test additionally shows that the mutants have no defects in locomotor abilities overall as the total number of beam breaks is relatively congruent with that of the wildtype animals. Moreover, though the wildtype animals were not viable as a control for the rotarod test, the cKOs still demonstrate a clear ability of motor learning in the performance of the test (Figure 18). Accordingly, though these assays were not testing for it, the open field test, adult social interaction, and Morris water maze still require stable locomotor ability or the results would otherwise be confounded. Since no such alterations were observed, we conclude that cHT and cKO mice have full locomotor abilities.

During the open field test under bright light conditions, mice are expected to spend more time in the dimly lit corners and less time in the bright centre of the box due to their nature as prey animals. A decrease in the duration in the centre could show an increase of anxiety behaviours, however an increase in the duration in the centre could also demonstrate a decrease of natural anxiety that tells the mice that the bright centre is the least safe. The mice all spend more than 50% of the test in the corners and less than 3% of the test in the centre (Figure 19). Furthermore, the speeds and total distances travelled throughout the duration of the test are all consistent. Thus, it can be gathered that the mutants display neither an inappropriate increase nor decrease in anxiety and as such are able to take apposite action in the interest of their safety.

An additional demonstration of average anxiety levels was seen in the Morris water maze test. It is believed that thigmotaxis, or circling of the pool, can occur due to increased anxiety since it may impair learning and memory (240-242). All genotypes spent about a quarter of the test in thigmotaxis, reinforcing that anxiety levels are consistent across genotypes (Figure 21).

Further, there was no indication of impairment of learning or memory due to all animals spending about half the test in the target quadrant and travelling the same distance overall.

Mice are also known to form social hierarchies, though this has been shown to be more dynamic in laboratory mice, it is the basis of the adult social interaction test (243-245). It is a requirement to be able to recognize members of the same species and further recognize sexual status, dominance, and colony identity. The social targets chosen are age-, sex-, and strain-matched such that the aforementioned factors will confound results as little as possible. The cHT and cKO mice show the same drop in distance travelled and increase in the time spent in the interaction zone in the presence of the social target as the wildtype mice (Figure 20). This indicates that their social recognition abilities are unhindered which is important for animals which live in colonies (244). This is in line with what was seen in the laboratory colonies whereby, as previously mentioned, the cHT and cKO mice displayed no difficulties in their home cages.

Taken together, the mutant animals display the physiological capabilities for survival as well as the necessary behavioural habits. Aside from being postnatally viable, they were able to steadily gain weight while breast feeding and learn how to access food and water from the cage system. They were able to maintain the social environment which was again demonstrated quantitatively in the adult social interaction test. No alterations were seen in locomotor ability nor motor learning which could make acquisition of resources necessary for survival difficult. Further, they had neither an increase in anxiety nor a decrease in anxiety that could make them more prone to hazardous behaviour. Overall, they not only demonstrate an adequate ability to survive in controlled conditions, but also indicate they have the same means as the wildtype animals for survival in nature.

These results are not unexpected given what has been seen in the other CHD subfamily II knockouts. For example, the *Chd4 Cmv*-Cre heterozygote females only showed a deficit in spatial and locomotor learning and memory (228). The *Chd4 Emx1*-Cre cKOs demonstrated behaviours equivalent behaviour to wildtype animals in the Morris water maze, beam break, and rotarod assays. Though there is a slight increase in significant behaviour in these mice from the *Chd3 Emx1*-Cre mice, *Chd4* has been shown to be expressed earlier and in more cell types than *Chd3* (197, 233). This suggests that the *Chd4* cKOs should be expected to have a further reaching phenotype than what may be seen in the *Chd3* cKOs which is what was observed.

Additionally, other mouse models which saw a deficit in upper layer neurons have yielded similar behavioural results as what was seen in our mice. Though the *Smarca5 Emx1*-Cre mice had a broader phenotype in the cortex than what was seen in the *Chd3 Emx1*-Cre mice, they too showed an impairment of contextual fear memory along with alterations in anxiety-like behaviours but no change to spatial learning and memory in the Morris water maze test (79).

### 4.2. Chd3 is required for proper migration of cells to the supragranular layers

Generation of the 6-layer murine cortex occurs in an inside-out fashion. Neocortical neurogenesis begins around E10.5 when the neuroepithelial cells in the ventricular zone (VZ) differentiate to the multipotent RGCs (246). In their proliferation, RGCs will divide symmetrically (with the cell division plane perpendicular to the ventricle) to generate two daughter RGCs, however when they divide asymmetrically one daughter RGC and one IPC or committed neuron is produced. This progenitor pool goes on to next form layer I which is comprised of Cajal-Retzius (CR) cells. From there, the layers are produced with layer VI first and subsequent layers having to travel through the existing layers to the top of the cortical plate (CP) (247).

Upon examination of E15.5 cortices, there was no noticeable difference in the populations of RGCs or IPCs. Investigation of cells in M phase with the mitosis marker pHH3 demonstrated equal numbers of actively dividing cells in each genotype (Figure 13). By staining for EdU on cortices that were dissected following a 1-hour EdU pulse, the proportion of cells in S-phase were also quantified. Similarly to the M-phase analysis, no change in the number of cells in S-phase was seen either. Together this suggests that Chd3-deficient cortical progenitors are still able to maintain normal cell cycle kinetics.

Following, P0 cortices show a consistent number of DAPI+ cells across genotypes (Figure 14). This indicates that there is no unexpected loss of cells by the time of birth. The number of DAPI+ cells in all genotypes is also consistent at P7, so it can be taken that the relative cell numbers are stable in the first week of life.

At this point it is known that the ~30% decrease in Satb2+ cells in layers II-IV of the cKOs cannot be attributed to loss of progenitors or changes in cell number in the CP, as both these parameters were normal in the Chd3 cKO mice. Additionally, there was no increase in the proportion of Ctip2+ cells in layer V or Tbr1+ cells in layer VI, further suggesting that cell fate was not the main reason for reduced Satb2+ cell numbers. Though Satb2 is used as a marker of the upper layers, Satb2+ cells may also be found in lower quantities in the lower layers. Quantification of Satb2+ cells in layer V revealed similar proportions between the genotypes, but there was a ~30% increase in Satb2+ cells in layer VI of the cKOs (Figure 15). Despite the clear defect in migration at P0, it is not clear if it is a defect or simply a delay as the cells do not complete migration until P7. Performing the same quantifications at P7 showed that the phenotype is improved but not resolved. These cortices exhibit a ~23% decrease in Satb2+ cells in layers II-IV and a ~20% increase in cells in layer VI.

To confirm an apparent migration defect behind the retention of the Satb2+ cells in the lower layers, we performed neuronal birthdating experiments by injecting pregnant dams with EdU at E15.5 and collecting the pups for dissection at P7 to track the migration of the upper layers. These mice not only show a clear paucity of EdU+ cells in the upper regions of the cortex, but also an accordant collection of EdU+ cells in the bottom region that is not present in the wildtype cortex (Figure 16). When comparing the co-labelled cells, the upper regions contain an 80% decrease in cKOs and 40% decrease in cHTs and the lower regions contain a ~233% increase in cHTs and a ~210% increase in cKOs. Though it should be noted that this is not a true disparity in co-labelling, but rather a facet of the difference in EdU+ and Satb2+ position between the genotypes. These data confirm a defect in migration of the superficial layers under the ablation of *Chd3*.

As the migration of the neurons rely on polarity of a tangentially oriented process to migrate radially along a radial glial fiber to its final position in the cortex (248), future work should examine the polarity of the Satb2+ cells that are being retained at the bottom of the CP. Knockdown of Chd3 at E15.5 with electroporation of a small hairpin RNA (shRNA) construct targeting Chd3 saw indications that cells retained in the lower layers remained multipolar (197). It is plausible that as these cells enter the CP they are not able to transition from multipolar to polar cells and as such do not migrate to their correct position within the cortex. As *Chd3* is a chromatin remodeler it is also possible that its loss prevents expression of other factors that are critical for regulation of radial migration. These factors can generally be placed into five categories – transcription factors, secreted molecules, cytoskeletal-regulating elements, neurotransmitters, and adhesion molecules (249). Looking at deficits in migration of late-born neurons, secreted guidance factors such as Semaphorin-3A (Sema3A) have been found to form a

descending gradient within the cortex in order to guide newborn neurons to the upper layers (250).

Defects in neuronal migration have been identified in other neurodevelopmental disorders. A variety of mutations have been found in ASD which result in a spectrum of migration defects of the cortex (251). Additionally, migration defects were seen in the knockdown of CHD subfamily II member Chd5 (197). As such, elucidation of the mechanism in the *Chd3 Emx1* cKO mice could provide important direction for the mechanisms of other genes as well.

### 4.3. Loss of Chd3 in the telencephalon produces memory defects in males

The fear conditioning test is a classic behavioural assay used on a multitude of animals to examine their ability to learn to predict adverse events by combining an aversive stimulus (the foot shock) with a neutral context (the phenotyper box) and a neutral stimulus (the tone). In mice the fear response is then measured with freezing behaviour to test if they have learned to associate the neutral context and/or stimulus with the aversive stimulus.

After training, the male cHTs showed a distinct 30% decrease in freezing compared to wildtype when exposed to the context again on the second day. They also only froze 50% of the time following the tone on the third day while wildtype froze 84%. As the open field test did not find reduced anxiety in these animals it indicates a reduction in contextual and associative memory of the cHT males thereby reducing their instinct to freeze when exposed to a previously adverse stimulus.

The amygdala is typically the first brain region associated with fear conditioning and is well established in its role in the acquisition of fear memories (252-255). However, increasing evidence suggests that it is the inhibitory neurons within the amygdala that regulate fear output

(256-260) which are outside the impact of the *Emx1*-Cre driver and therefore should not be affected in the cHTs.

The medial prefrontal cortex (mPFC) is associated with fear regulation which has been further resolved to contain two relevant subdivisions in rodents – the prelimbic cortex regulates fear expression and the infralimbic cortex regulates fear suppression (261-263). The prelimbic cortex and infralimbic cortex are both laminar structures. Though the analyses of cortical lamination performed in this thesis were outside of this region, it is possible that laminar defects may be present in other regions of the neocortex and future directions should include analysis of the lamination in the mPFC.

The hippocampus is involved with fear renewal or the return of fear when presented again with the neutral context or stimulus (264-266). It has been repeatedly shown that hippocampal inactivation leads to a drop in fear renewal (267-270). Further, the hippocampus has been demonstrated to be responsible for integrating contextual information during the training (271-274). Mouse brains dissected one hour after fear conditioning presented with 675 demethylated genes and 613 hypermethylated genes in the hippocampus (275). The lack of normal fear response could be due to the lack of Chd3 to respond to the change in methylation patterns. Confirmation of this hypothesis could provide molecular targets of Chd3 which remain largely unknown. Moreover, though knockdown studies did not see compensation from other subfamily II proteins in the embryonic cortex (197), upregulation of Chd3 and Chd5 has been observed in the cortex of Chd4 cKOs. Despite a lack of overlapping function in the cortex, it is not known if this is the case in the hippocampus. One confirmed mechanism of genetic compensation acts through nonsense-mediated decay (NMD) (276). NMD is triggered when mutant mRNAs contain premature termination codons (PTCs) such as those that are predicted to

occur in the *Chd3*-flox transcripts. Though the mechanism of upregulation of homologs upon mutant mRNA degradation is not resolved, the presence of the wildtype allele in cHTs could inhibit the animal from meeting a genetic threshold required for compensation that is not a barrier in the cKOs which have two mutant copies. This would explain the lack of diminished fear response in the cKO males despite the large reduction in cHT males.

However, this explanation does not explain why the same response is not then seen in the female cHTs. Perhaps it is a feature of differences in the transcriptomic landscape of the sexes in which one study identified 1415 differentially expressed genes between males, estrus females, and diestrus females (277). Importantly, one of the four regions sampled in this study was the medial amygdala which may point to the region altered in the cHT males which caused their reduced fear response. Whether this is a true alteration in the male cHT brains or, alternatively and effect of a small sample size, it highlights an area which warrants further exploration.

### 4.4. Chd3 Emx1 cKO as a model of SNIBCPS

In this thesis, the Emx1-Cre driver line was used to inactivate Chd3 in the developing telencephalon in order to generate as a first model of SNIBPC syndrome. As SNIBPC syndrome results in clinical manifestations across the body, a telencephalon cKO could not entirely recapitulate the syndrome. However, the mice may be assessed within the limits of the forebrain morphology and the neurologic conditions. For example, 58% of the original cohort had macrocephaly and of those that had magnetic resonance imaging (MRI) performed 33% showed widening of the cerebrospinal fluid (CSF) spaces. Further, intellectual disability and developmental delays may be tested for in behavioural assays that look at learning and memory. Another characteristic of SNIBCP syndrome is a speech delay or deficit which may be present in the mice as altered ultrasonic vocalizations in the pups.

Successful excision of exons 13-20 is seen upon Cre-mediated recombination (Figure 8, 9). The allele was designed with the expectation that it would lead to a frameshift causing a PTC (231). As the primary αChd3 antibody used in the western blot recognizes the N-terminus of the protein, if the excision simply removed the exons leaving the C-terminal end intact this truncated protein of approximately 190 kDa would have been identified by the antibody as well. In numerous blots no such band was observed. Furthermore, the same antibody was used for immunofluorescent staining and a clear loss of Chd3 is demonstrated both embryonically and perinatally which would not be seen if a truncated protein were still present (Figure 10). The RT-PCR and RT-qPCR identified both the connection of exons 12 to 21 and the loss of the intervening exons. Taken together, this validates the conditional deletion of the desired region.

When looking at the gross morphology of the brains, there was no indication of widened CSF spaces (Figure 12). Additionally, though behaviour results do not have a strong indication of a murine intellectual disability or developmental delay, there is evidence of learning and memory deficits in the male cHTs which should be explored further. Further, the ultrasonic vocalizations were not tested for and may recapitulate the speech difficulties seen in SNIBCPS patients.

Of interest, neuronal migration disorders are a spectrum of conditions that cause cortical malformations associated with defects in neuronal migration. Though the scope of symptoms in these disorders is wide, some common clinical presentations including developmental delay, intellectual disability, hypotonia, and difficulties with feeding are all seen in SNIBCPS as well (278). Although MRIs of SNIBCPS patients did not show some of the more severe malformations associated with some neuronal migration disorders such as lissencephaly or periventricular nodular heterotopias, it is possible that the migration defect seen in the cKO mice

is also present in SNIBCPS patients as it would not be visible on an MRI. If this were to be confirmed by clinicians, the *Chd3 Emx1* cKO mice would make an excellent SNIBCPS mouse model as they have no pre-existing issue with survival or behavioural abnormalities not associated with the syndrome. This would allow for easy exploration of treatments to resolve the migration defect.

Despite our mice not strongly mimicking the human syndrome, this is commonly seen in mouse mutants of chromatin remodelers. Given that chromatin remodelers act on a wide array of genes that may not always be well defined it can be difficult to predict where and how they will act. This is especially important when considering that gene expression is not identical between mice and humans. A study of matched cell types from human and mouse cortices compared 14553 orthologous genes and found that two-thirds had divergent expression in at least one of 37 homologous types or classes of genes (279). Beyond this, many mutations in human chromatin remodeling genes including *CHD3* are point mutations or deletions rather than the complete loss of function often generated in mouse models (Figure 4). Even deletion of an exon that leaves the rest of the sequence intact may affect tertiary structure and thereby the function of supposedly unaltered regions of the protein.

The results that seem somewhat nebulous in relation to its human disease in the *Chd3 Emx1*-Cre cKOs was also seen in the *Chd4 Emx1*-Cre cKOs where they too had a deficit in upper layers and variable behavioural results that did not entirely match the SIHIWE syndrome which it was intended to model (228). However, it was demonstrated in *Atrx* knockout mouse models that despite the lack of recapitulation of the syndromic phenotype, these mouse models can still serve to demonstrate important molecular mechanisms of the protein that would otherwise remain unknown (175-178). The *Atrx* mouse studies also exemplify that though conditional

deletions may not completely model the respective human syndrome, knock-in of patient mutations such as the *Atrx* R245C may (179). This highlights the success of these *Chd3 Emx1*-Cre models in providing insight into the understudied function of *Chd3* and support to the generation of a SNIBCPS patient mutation knock-in model to better understand its pathology.

## 4.5. Future Directions

The mice described here represent an important first look into cortical development as regulated by *Chd3*. *Chd3* is not a well described gene, and though many aspects of the development were unaffected this serves to better narrow the focus of its study and to give insight into where it may be dispensable.

One aspect which has been demonstrated in a knockdown and now knockout model of *Chd3* is the migration deficit of the upper layers (197). As the cells in the knockdown cortices showed evidence of multipolarity, further study should examine the polarity of the cells in the cKOs or *in vitro*. Additionally, there exist few suggested molecular targets of Chd3 and a study such as single cell RNA sequencing (scRNA-seq) could indicate other genes that may be involved in the action of the protein and the migration defect.

Furthermore, the presence of altered associative fear learning and memory in cHT males presents two avenues which warrant future study. First, the circuit of fear learning and memory involves the mPFC, the hippocampus, and the amygdala; all of which would have been affected by the *Emx1* Cre driver and none of which were examined in this thesis. Evidence from the literature described in a previous section (4.3.) suggests that any one or perhaps a combination of the three structures may have been altered in these mice. Secondly, the fear conditioning results in combination with the mild phenotype in the mice may indicate genetic compensation from

another CHD subfamily II member. This could be identified with an RNA-seq experiment as well as knocking out two or all three of the genes.

Finally, as seen in the *Atrx* R245C mice, a knock-in model of a patient mutation may be a better tool in which to study the pathogenesis of SNIBCPS. An excellent candidate would be the R985W mutation as it was observed in six children from five families (220). In addition, this residue was identified as a mutational hotspot as two other individuals were found to have mutations at the same location.

# 5. References


1. Inclusion Canada (2020). *Who We Are*. Retrieved from Inclusion Canada: https://inclusioncanada.ca/who-we-are/

2. Government of Canada (2017). *Canadian Survey on Disability.* Retrieved from Government of Canada: https://www.canada.ca/en/public-health/services/publications/diseases-conditions/infographic-developmental-disabilities-disorder-highlights-canadian-survey-2017.html

3. Kochinke K., Zweier C., Nijhof B., Fenckova M., …and Schenck A. (2016). Systematic Phenomics Analysis Deconvolutes Genes Mutated in Intellectual Disability into Biologically Coherent Modules. *Am J Hum Genet.* 98(1): 149-164.

4. D'Souza L., Channakkar A.S., Muralidharan B. (2021). Chromatin remodelling complexes in cerebral cortex development and neurodevelopmental disorders. *Neurochem. Int.* 147: 105055.

5. Adnani L., Han S., Li S., Mattar P., and Schuurmans C. (2018). Mechanisms of Cortical Differentiation. P. 223-320 *In* International Review of Cell and Molecular Bi\ology. Elsevier.

6. Wilkinson G., Dennis D., Schuurmans C. (2013). Proneural genes in neocortical development. P. 256-273 *in* Neuroscience Forefront Review. Elsevier.

7. Cecchi C. and Boncinelli E. (2000). Emx homeogenes and mouse brain development. *Trends in Neurosciences.* 23: 347-352.

8. Veritas Genetics. (2017, 07 28). *Size Matters: A Whole Genome is 6.4 Billion Letters.* Retrieved from Veritas Genetics: https://www.veritasgenetics.com/our-thinking/whole-story/

9. Toledo C. and Saltsman, K. (2012). *Genetics by the Numbers*. Retrieved from National Institute of General Medical Sciences: https://nigms.nih.gov/education/Inside-Life-Science/Pages/Genetics-by-the-Numbers.aspx

10. Marino-Ramirez L., Kann, M. G., Shoemaker, B. A., and Landsman, D. (2005). Histone structure and nucleosome stability. *Expert Rev Proteomics.* 2(5): 719-729.

11. Maeshima K., Ide S., Babokhov M. (2019). Dynamic chromatin organization without the 30-nm fiber. *Current Opinion in Cell Biology*. 58: 95-104.

12. Finch J. T. and Klug A. (1976). Solenoidal model for superstructure in chromatin. *Proc Natl Acad Sci USA*. 73: 1897-1901.

13. Song F., Chen P., Sun D., Wang M., Li G. (2014). Cyro-EM Study of the Chromatin Fiber Reveals a Double Helix Twisted by Tetranucleosomal Units. *Science*. 6182(344): 376-380.

14. Robinson P.J., Fairall L., Huynh V. A., Rhodes D. (2006). EM measurements define the dimensions of the “30-nm” chromatin fiber: Evidence for a compact, interdigitated structure. *Proc. Natl. Acad. Sci. U.S.A.* 103: 6506-6511.

15. Dorigo B., Schalch T., Kulangara A., Duda S., Schroeder R. R., Richmond T.J., (2004). Nucleosome arrays reveal the two-start organization of the chromatin fiber. *Science.* 306: 1571-1573.

16. Schalch T., Duda S., Sargent D.F., Richmond T.J. (2005). X-ray structure of a tetranucleosome and its implications for the chromatin fibre. *Nature.* 436: 138-141.

17. Sanborn A.L., Rao S.S., Huang S.C., Durand S.C., Huntley M.H., Jewett A.I., Bochkov I.D., Chinnapan D., Cutosky D., Li J *et al* (2015). Chromatin extrusion explains key features of loop and domain formation in wild-type and engineered genomes. *Proc. Natl. Acad. Sci. U.S.A.* 112: 6456-6465.

18. Ricci M.A., Manzo C., Garcia-Parajo M.F., Lakadamyali M., Cosma M.P. (2015). Chromatin fibers are formed by heterogeneous groups of nucleosomes in vivo. *Cell*. 160: 1145-1158.

19. Maeshima K., Ide S., Hibino K., Sasai M. (2016). Liquid-like behaviour of chromatin. *Current Opinion in Genetics and Development*. 37: 36-45.

20. Maeshima K., Rogge R., Tamura S., Joti Y., Hikima T., Szerlong H., Krause C., Herman J., Seidel E., DeLuca J., Tetsuya I., Hansen J.C. (2016). Nucleosomal arrays self-assemble into supramolecular globular structures lacking 30-nm fibers. *EMBO J.* 35: 1115-1132.

21. Maeshima K., Matsuda T., Shindo Y., Noji H., Oka K., Nagai T. (2018) A Transient Rise in Free $Mg^{2+}$ Ions Released from ATP-Mg Hydrolysis Contributes to Mitotic Chromosome Condensation. *Current Biology*. 28: 444-451.

22. Luger K and Richmond T.J. (1998) The histone tails of the nucleosome. *Curr. Opin. Genet. Dev.* 8:140-146

23. Dorigo B., Schalch T., …Richmond T.J. (2003). Chromatin fiber folding: requirement for the histone H4 N-terminal tail. *J. Mol. Biol.* 327: 85-96.

24. Zheng C., Lu X., … Hayes J.J. (2005). Salt-dependent intra- and inter-nucleosomal interactions of the H3 tail domain in a model oligonucleosomal array. *J. Biol. Chem.* 280: 33552-33557.

25. Millan-Zambrano G., Burton A., Bannister A.J., and Schneider R. (2022). Histone post-translational modifications – cause and consequence of genome function. *Nature Reviews Genetics* 23: 563-580.

26. Wang Z., Zang C., Rosenfeld J.A., Schones D.E., Barski A., …Zhao K. (2008). Combinatorial patterns of histone acetylations and methylations in the human genome. *Nat. Genet.* 40(7): 897-903.

27. Pradeepa M.M., Grimes G.R., Kumar Y., Olley G., …Bickmore W.A. (2016). Histone H3 globular domain acetylation identifies a new class of enhancers. *Nat. Genet.* 48(6): 681-686.

28. Creyghton M.P. Cheng A.W., Welstead G.G., Kooistra T., …Jaenisch R. (2010). Histone H3K27ac separates active from poised enhancers and predicts developmental state. *Proc. Natl. Acad. Sci. U.S.A.* 107(50): 21931-21936.

29. Koch C.M., Andrews R.M., …Dunham I. (2007). The landscape of histones across 1% of the human genome in five human cell lines. *Genome Research* 17: 691-707.

30. Lee H., Oh S., Ro D.H., Yoo H., and Kwon Y. (2020). The Key Role of DNA Methylation and Histone Acetylation in Epigenetics of Atherosclerosis. *J. Lipid Atheroscler.* 9(3): 419-434.

31. Byvoet P., Shepherd G.R., Hardin J.M., and Noland B.J. (1972). The distribution and turnover of labelled methyl groups in histone fractions of cultured mammalian cells. *Arch. Biochem. Biophys.* 148: 558-567.

32. Murray K. (1964) The occurrence of N-methyl lysine in histones. *Biochemistry* 3:10-15.

33. Fischle W., Franz H., Jacobs S.A., Allis C.D., Allis C.D., and Khorasanizadeh S. (2008). Specificity of the chromodomain Y chromosome family of chromodomains for lysine-methylated ARK(S/T) motifs. *J. Biol. Chem.* 283: 19626-19635.

34. Young N.L., Dimaggio P.A., and Garcia B.A. (2010). The significance, development and progress of high-throughput combinatorial histone code analysis. *Cell. Mol. Life Sci.* 67: 3983-4000.

35. Husmann D. and Gozani O. (2019). Histone lysine methyltransferases in biology and disease. *Nat. Struc. Mol. Biol.* 26: 880-889.

36. Rosenfeld J.A., Wang Z., Schones D., Zhao K., DeSalle R., and Zhang M. (2009). Determination of enriched histone modifications in non-genic portions of the human genome. *BMC Genomics*. 10: 143.

37. Barski A., Cuddapah S., Cui K., Roh T.Y., Schones D.E., Wang Z., Wei G., Chepelev I., and Zhao K. (2007). High-resolution profiling of histone methylations in the human genome.

38. Benevolenskaya E.V. (2007). Histone H3K4 demethylases are essential in development and differentiation. *Biochem. Cell Biol.* 85(4): 435-443.

39. Steger D.J., Lefterova M.I., Ying L., Stonestrom A.J., …Vakoc C.R. (2008). DOT1L/KMT4 recruitment and H3K79 methylations are ubiquitously coupled with gene transcription in mammalian cells. *Mol. Cell. Biol.* 28(8): 2825-2839.

40. Moore L.D., Le T., and Fan G. (2013). DNA Methylation and Its Basic Function. *Neuropsych.* 38: 23-38.

41. Henikoff S. and Smith M.M. (2015). Histone Variants and Epigenetics. *Cold Spring Harb. Perspect. Biol.* 7(1): a019364.

42. Talbert P.B. and Henikoff S. (2021). Histone Variants at a Glance. *J. Cell Sci.* 134(6): jcs244749.

43. Long M., Sun X., Shi W., Yanru A., Leung S.T.C., …Ausio J. (2019). A novel histone H4 variant H4G regulates rDNA transcription in breast cancer. *Nucleic Acid Res.* 47: 8399-8409.

44. Moore L.D., Le T., and Fan G. (2013). DNA methylation and Its Basic Function. *Neuropsychopharmacology.* 38: 23-38.

45. Uszczynska-Ratajczak B., Lagarde J., Frankish A., Guigo R, and Johnson R. (2018). Towards a complete map of the human long non-coding RNA transcriptome. *Nat. Rev. Genet.* 19: 535-548.

46. Fang S. (2018). NONCODEV5: a comprehensive annotation database for long non-coding RNAs. *Nucleic Acids Res.* 46: D308-D314.

47. Dueva R. (2019). Neutralization of the positive charges on histone tails by RNA promotes an open chromatin structure. *Cell Chem. Biol.* 26: 1436-1449.

48. Statello L., Guo C.-J., Chen L.-L., and Huarte M. (2021). Gene regulation by long non-coding RNAs and its biological functions. *Nat. Rev. Mol. Cell Biol.* 22: 96-118.

49. Martire S. and Banaszynski L.A. (2020). The roles of histone variants in fine-tuning chromatin organization and function. *Nat. Rev. Mol. Cell Biol.* 21:522-524.

50. Larrigan S., Shah S., Fernandes A., and Mattar P. (2021). Chromatin Remodeling in the Brain – a NuRDevelopmental Odyssey. *Int. J. Mol. Sci.* 22(9): 4768.

51. Tyagi M., Imam N., Verma K., and Patel A.K. (2016). Chromatin remodelers: We are the drivers!! *Nucleus* 3;7(4): 388-404.

52. Petty E. and Pillus L. (2013). Balancing chromatin remodeling and histone modifications in transcription. *Trends Genet.* 29: 621-629.

53. Clapier C.R. and Cairns B.R. (2009). The biology of chromatin remodeling complexes. *Ann. Rev. Biochem.* 78: 273-304.

54. Elfring L.K., During R., McCallum C.M., Peterson C.L., and Tamkun J.W. (1994). Identification and characterization of Drosophila relatives of the yeast transcriptional activator SNF2/SWI2. *Mol. Cell Biol.* 14: 2225-2234.

55. Goodwin L.R. and Picketts D.J. (2018). The role of ISWI chromatin remodeling complexes in brain development and neurodevelopmental disorders. *Molecular and Cellular Neuroscience* 87: 55-64.

56. Ito T., Bulger M., Pazin M.J., Kobayashi R., and Kadonaga J.T. (1997) ACF, and ISWI-containing and ATP-utilizing chromatin assembly and remodeling factor. *Cell* 90: 145-155.

57. Tsukiyama T. and Wu C. (1995) Purification and properties of an ATP-dependent nucleosome remodeling factor. *Cell*. 83:1011-1020.

58. Strohner R., Nemeth A., Jansa P., Hoffmann-Rohrer U., Santoro R., Langst G., Grummt I. (2001). NoRC – a novel member of mammalian ISWI-containing chromatin remodeling machines. *EMBO J.* 20: 4892-4900.

59. Poot R.A., Dellaire G., Hulsmann B.B., Grimaldi M.A., …Varga-Weisz P.D. (2000). HuCHRAC, a human ISWI chromatin remodeling complex contains hACF1 and two novel histone-fold proteins. *EMBO J.* 19: 3377-3387.

60. LeRoy G., Orphanides G., Lane W.S., Reinberg D. (1998). Requirement of RSF and FACT for transcription of chromatin templates in vitro. *Science*. 282: 1900-1904.

61. Hakimi M.A., Bochar D.A., Schmiesing J.A., Dong Y., …Shiekhattar R. (2002). A chromatin remodelling complex that loads cohesion onto human chromosomes. *Nature*. 418: 994-998.

62. Gushin D., Geiman T.M., Kikyo N., Tremethick D.J., Wolffe A.P., and Wade P.A. (2000). Multiple ISWI ATPase complexes from *Xenopus laevis*: functional conservation of an ACF/CHRAC homolog. *J. Biol. Chem.* 275: 35248-35255.

63. Barak O., Lazzaro M.A., Lane W.S., Speicher D.W., Picketts D.J., and Shiekhattar R. (2003). Isolation of human NURF: a regulator of engrailed gene expression *EMBO J.* 22:6089-6100.

64. Banting G.S., Barak O., Ames T.M., Burnham A.C., …Shiekhattar R. (2005). CECR2, a protein involved in neurulation, forms a novel chromatin remodeling complex with SNF2L. *Hum. Mol. Genet.* 14:513-524.

65. Bochar D.A., Savard J., Wang W., Lafleur D.W., … Shiekhattar R. (2000). A family of chromatin remodeling factors related to Williams syndrome transcription factor. *Proc. Nat. Acad. Sci. U.S.A.* 97: 1038-1043.

66. Bozhenok L., Wade P.A., and Varga-Weisz P. (2002). *WSTF-ISWI* chromatin remodeling complex targets heterochromatic replication foci. *EMBO J.* 21: 2231-2241.

67. Varga-Weisz P.D, Wilm M., Bonte E., Dumas K., Mann M., and Becker P.B. (1997). Chromatin remodeling factor CHRAC contains the ATPases ISWI and topoisomerase II. *Nature*. 388: 598-602.

68. Oppikofer M., Bai T., Gan Y., Hayley B., …Cochran A.G. (2017). Expansion of the ISWI chromatin remodeler family with new active complexes. *EMBO Rep.* 18:1697-1706.

69. Alvarez-Saavedra M., De Repentigny Y., Lagali P.S., Raghu Ram E.V., …Picketts D.J. (2014). Snf2h-mediated chromatin organization and histone H1 dynamics govern cerebellar morphogenesis and neural maturation. *Nat. Commun.* 5: 4181.

70. Li D., Wang Q., Gong N.N., Kurolap A., …Hakonarson H. (2021). Pathogenic variants in *SMARCA5*, a chromatin remodeler, cause a range of syndromic neurodevelopmental features. *Sci. Adv.* 7(20): eabf2066.

71. Drivas T.G., Li D., Nair D., Alaimo J.T., …Bhoj E. (2020). A second cohort of *CHD3* patients expands the molecular mechanisms known to cause Snijders Blok-Campeau syndrome. *Eur. J. Hum. Genet.* 28:1422-1431.

72. Mannino E.A., Miyakawa H., Santen G., and Schrier Vergano S.A. (2018). First data from a parent reported registry of 81 individuals with Coffin-Siris syndrome: Natural history and management recommendations. *Am. J. Med. Genet.* 176: 2250-2258.

73. Karaca E., Harel T., Pehilvan D., Jhangiani S.N., …Lupski J.R. (2015). Genes that Affect Brain Structure and Function Identified by Rare Variant Analyses of Mendelian Neurologic Disease. *Neuron.* 88:499-513.

74. Lopes F., Barbosa M., Ameur A., Soares G., …Maciel P. (2016). Identification of novel genetic causes of Rett syndrome-*like* phenotypes. *J. Med. Genet.* 53: 190-199.

75. Homann O.R., Misura K., Lamas E., Sandrock R.W., Nelson P., McDonough S.I., and DeLisi L.E. (2016). Whole-genome sequencing in multiplex families with psychoses reveals mutations in the SHANK2 and SMARCA1 genes segregating with illness. *Molecular Psychiatry*. 21:1690-1695.

76. Stankiewicz P., Khan T.N., Szafranksi P., Slattery L., …and Yang Y. (2017). Haploinsufficiency of the Chromatin Remodeler BPTF Causes Syndromic Developmental and Speech Delay, Postnatal Microcephaly, and Dysmorphic Features. *The American Journal of Human Genetics.* 101:503-515.

77. Gorski J.A., Talley T., Qiu M., Puelles L., Rubenstein J.L.R., and Jones K.R. (2002). Cortical Excitatory Neurons and Glia, But Not GABAergic Neurons, Are Produced in the Emx1-Expressing Lineage. *J. of Neuro.* 22: 6309-6314.

78. Alvarez-Saavedra M., Yan K., De Repentigny Y., Hashem L.E., …Picketts D.J. (2019). Snf2h Drives Chromatin Remodeling to Prime Upper Layer Cortical Neuron Development. *Front. Mol. Neurosci.* 12: 243.

79. Dahlstrand K., Lardelli M., and Lendahl U. (1995). Nestin mRNA expression correlates with the central nervous system progenitor cell state in many, but not all, regions of the developing central nervous system. *Brain Res. Dev. Brain Res.* 84(1): 109-29.

80. Yip D.J., Corcoran C.P., Alvarez-Saavedra M., DeMaria A., …Picketts D.J. (2012). Snf2l Regulates Foxg1-Dependent Progenitor Cell Expansion in the Developing Brain. *Dev. Cell* 22:871-878.

81. Zapata G., Yan K., and Picketts D.J. (2022). Generation of a mouse model of the neurodevelopmental disorder with dysmorphic facies and distal limb anomalies syndrome. *Hum. Mol. Genet.* 31(20): 3405-3421.

82. Carlson M., Osmond B.C., Neigeborn L., and Botstein D. (1984). A suppressor of SNF1 mutations causes constitutive high-level invertase synthesis in yeast. *Genetics*. 107: 19-32.

83. Stern M., Jensen R., and Herskowitz I. (1984). Five SWI genes are required for expression of the HO gene in yeast. *J. Mol. Biol.* 178: 853-868.

84. Marmorstein R. and Berger S.L. (2001). Structure and function of bromodomains in chromatin-regulating complexes. *Gene.* 272: 1-9.

85. Olave I.A., Reck-Peterson S.L., and Crabtree G.R. (2002). Nuclear actin and actin-related proteins in chromatin remodeling. *Ann. Rev. Biochem.* 71: 755-781.

86. Szerlong H., Saha A., and Cairns B.R. (2003). The nuclear actin-related proteins Arp7 and Arp9: a dimeric module that cooperates with architectural proteins for chromatin remodeling. *EMBO J.* 22: 3175-3187.

87. Rando O.J., Zhao K., Janmey P., and Crabtree G.R. (2002). Phosphatidylinositol-dependent actin filament binding by the SWI/SNFlike BAF chromatin remodeling complex. *Proc. Natl. Acad. Sci. U.S.A.* 99: 2824-2829.

88. Dietrich N., Trotter K., Ward J.M., and Archer T.K. (2023). BRG1 HSA domain interactions with BCL7 proteins are critical for remodeling and gene expression. *Life Sci. Alli.* 6(5): e202201770.

89. Euskirchen G., Auerbach R.K., and Snyder M. (2012). SWI/SNF Chromatin-remodeling Factors: Multiscale Analyses and Diverse Functions. *J. Biol. Chem.* 287(37): 30897-30905.

90. Alpsoy A., and Dykhuizen E.C. (2018). Glioma tumor suppressor candidate region gene 1 (GLTSCR1) and its paralog GLTSCR1-like form SWI/SNF chromatin remodeling subcomplexes *J. Biol. Chem.* 293: 3892-3903.

91. Mashtalir N., D'Avino A.R., Michel B.C., Luo J., …Kadoch C. (2018). Modular Organization and Assembly of SWI/SNF Family Chromatin Remodeling Complexes. *Cell*. 175(5): 1272-1288.e20.

92. Wanior M., Kramer A., Knapp S., and Joerger A.C. (2020). Exploiting vulnerabilities of SWI/SNF chromatin remodelling complexes for cancer therapy. *Oncogene.* 40: 3637-3654.

93. Alfert A., Moreno N., and Kerl K. (2019). The BAF complex in development and disease. *Epigenetics Chromatin.* 183: 802-817.

94. Wieczorek D., Bögershausen N., Beleggia F., Steiner-Haldenstätt S., …Wollnik B. (2013). A comprehensive molecular study on Cofn–Siris and Nicolaides–Baraitser syndromes identifies a broad molecular and clinical spectrum converging on altered chromatin remodeling. *Hum. Mol. Genet.* 22(25): 5121-5135.

95. Tsurusaki Y., Okamoto N., Ohashi H., Kosho T., …Matsumoto N. (2012). Mutations affecting components of the SWI/SNF complex cause Coffin-Siris syndrome. *Nat. Genet.* 44: 376–378.

96. Santen G.W.E., Aten E., Vulto-van Silfhout A.T., Pottinger C., …van Belzen M.J. (2013). Coffin–Siris syndrome and the BAF complex: genotype–phenotype study in 63 patients. *Hum Mutat.* 34:1519-1528.

97. Kosho T., Miyake N., and Carey J.C. (2014). Coffin-Siris syndrome and related disorders involving components of the BAF (mSWI/SNF) complex: historical review and recent advances using next generation sequencing. *Am. J. Med. Genet. C Semin. Med. Genet.* 166C: 241–251.

98. De Rubeis S., He X., Goldberg A.P., Poultney, C. S., …Buxbaum J.D. (2014). Synaptic, transcriptional, and chromatin genes disrupted in autism. *Nature* 515: 209–215.

99. Qian Y., Zhou Y., Wu B., Chen H., …Wang H. (2022). Novel Variants of the SMARCA4 Gene Associated with Autistic Features Rather Than Typical Coffin-Siris Syndrome in Eight Chinese Pediatric Patients. *J. Autism Dev. Disord.* 52(11): 5033-5041.

100. Miyake N., Abdel-Salam G., Yamagata T., Eid M., …Matsumoto N. (2016). Clinical features of SMARCA2 duplication overlap with Coffin–Siris syndrome. *Am. J. Med. Genet. A.* 170: 2662–2670.

101. Morin G., Villemain L., Baumann C., Mathieu M., Blanc N., and Verloes A. (2003). Nicolaides–Baraitser syndrome: confirmatory report of a syndrome with sparse hair, mental retardation, and short stature and metacarpals. *Clin. Dysmorphol.* 12: 237–240.

102. Ejaz R., Babul-Hirji R., and Chitayat D. (2016). The evolving features of Nicolaides–Baraitser syndrome – a clinical report of a 20-year follow-up. *Clin. Case Rep.* 4: 351–355.

103. Tang, S., Hughes, E., Lascelles, K., Euro EPINOMICS RES Myoclonic Astatic Epilepsy Working Group, Simpson, M. A., and Pal, D. K. (2017). New SMARCA2 mutation in a patient with Nicolaides–Baraitser syndrome and myoclonic astatic epilepsy. *Am. J. Med. Genet. A.* 173: 195–199.

104. Wolff, D., Endele, S., Azzarello-Burri, S., Hoyer, J., …Zweier C. (2012). In-frame deletion and missense mutations of the C-terminal helicase domain of SMARCA2 in three patients with nicolaides-baraitser syndrome. *Mol. Syndromol.* 2(6): 237–244.

105. Koga, M., Ishiguro, H., Yazaki, S., Horiuchi, Y., …Arinami T. (2009). Involvement of SMARCA2/BRM in the SWI/SNF chromatin remodeling complex in schizophrenia. *Hum. Mol. Genet.* 18: 2483–2494.

106. Loe-Mie Y., Lepagnol-Bestel A.-M., Maussion G., Doron-Faigenboim A., … Moalic J.-M. (2010). SMARCA2 and other genome-wide supported schizophrenia-associated genes: regulation by REST/NRSF, network organization and primate-specific evolution. *Hum. Mol. Genet*. 19: 2841–2857.

107. Bogershausen N. and Wollnik B. (2018). Mutational Landscapes and Phenotypic Spectrum of SWI/SNF-Related Intellectual Disability Disorders. *Front. Mol. Neurosci.* 11:252.

108. International Mouse Phenotyping Consortium. (ND). *Gene: Smarca2.* Retrieved from International Mouse Phenotyping Consortium: https://www.mousephenotype.org/data/genes/MGI:99603.

109. Bultman S.J., Gebuhr T.C., Yee D., La Mantia C., …Magnuson T. (2000) A Brg1 null mutation in the mouse reveals functional differences among mammalian SWI/SNF complexes. *Mol. Cell* 6: 1287-1295.

110. Sokpor G., Xie Y., Rosenbusch J., and Tuoc T. (2017). Chromatin Remodeling BAF (SWI/SNF) Complexes in Neural Development and Disorders. *Front. Mol. Neurosci.* 20: 243.

111. Matsumoto S., Banine F., Struve J., Xing R., …Sherman L.S. (2006). Brg1 is required for murine neural stem cell maintenance and gliogenesis. *Dev. Biol.* 289: 372–383.

112. Lessard J., Wu J. I., Ranish J. A., Wan M., …Crabtree G.R. (2007). An essential switch in subunit composition of a chromatin remodeling complex during neural development. *Neuron*. 55: 201–215.

113. Zhan X., Shi X., Zhang Z., Chen Y., and Wu J. I. (2011). Dual role of Brg chromatin remodeling factor in Sonic hedgehog signaling during neural development. *Proc. Natl. Acad. Sci. U.S.A.* 108: 12758–12763.

114. Ninkovic J., Steiner-Mezzadri A., Jawerka M., Akinci U., …Poot R. (2013). The BAF complex interacts with Pax6 in adult neural progenitors to establish a neurogenic cross-regulatory transcriptional network. *Cell Stem Cell*. 13: 403–418.

115. Doyle D.Z., Lam M.M., Qalieh A., Qalieh Y., Sorel A., Funk O.H., and Kwan K. (2021). Chromatin remodeler *Arid1a* regulates subplate neuron identity and wiring of cortical connectivity. *PNAS.* 118: e2100686118.

116. Liu X., Dai S.-K., Liu P.-P., and Liu C.-M. (2021). Arid1a regulates neural stem/progenitor cell proliferation and differentiation during cortical development. *Cell Proliferation.* 54: e13124.

117. Narayanan R., Pham L., Kerimoglu C., Stoykova A., …Tuoc T. (2018). Chromatin Remodeling BAF155 Subunit Regulates the Genesis of Basal Progenitors in Developing Cortex. *iScience*. 4: 109-126.

118. Tuoc T., Boretius S., Sansom S.N., Pitulsecu M.-E., Frahm J., Livesey F.J., and Stoykova A. (2013). Chromatin Regulation by BAF170 Controls Cerebral Cortical Size and Thickness. *Dev. Cell.* 25: 256-269.

119. Tuoc T., Dere E., Radyushkin L., Nguyen H., …Stoykova A. (2017). Ablation of BAF170 in Developing and Postnatal Dentate Gyrus Affects Neural Stem Cell Proliferation, Differentiation, and Learning. *Mol. Neurobiol.* 54(6): 4618-4635.

120. Ebbert R., Birkmann A., and Schuller H.J. (1999). The product of the SNF2/SWI2 paralogue INO80 of Saccharomyces cerevisiae required for efficient expression of various yeast structural genes is part of a high-molecular-weight protein complex. *Molecular microbiology* 32: 741-751.

121. Jonsson Z.O., Jha S., Wohlschlegel J.A., and Dutta A. (2004). Rvb1p/ Rvb2p recruit Arp5p and assemble a functional Ino80 chromatin remodeling complex. *Mol. Cell* 16: 465-477.

122. van Attikum H., Fritsch O., Hohn B., and Gasser S.M. (2004). Recruitment of the INO80 complex by H2A phosphorylation links ATP-dependent chromatin remodeling with DNA double-strand break repair. *Cell* 119: 777-788.

123. Tsukuda T., Fleming A.B., Nickoloff J.A., Osley M.A. (2005). Chromatin remodelling at a DNA double-strand break site in Saccharomyces cerevisiae. *Nature* 438: 379-383.

124. Morrison A.J., Highland J., Krogan N.J., Arbel-Eden A., Greenblatt J.F., Haber J.E., Shen X. (2004). INO80 and gammaH2AX interaction links ATP-dependent chromatin remodeling to DNA damage repair. *Cell* 119: 767-775.

125. Watanabe S., Radman-Livaja M., Rando O.J., and Peterson C.L. (2013). A histone acetylation switch regulates H2A.Z deposition by the SWR-C remodeling enzyme. *Science* 340: 195-199.

126. Wong M.M., Cox L.K., and Chrivia J.C. (2007). The chromatin remodeling protein, SRCAP, is critical for deposition of the histone variant H2A.Z at promoters. *J. Biol. Chem.* 282: 26132-26139.

127. Xu M., Yao J., Shi Y., Yi H., Zhao W., Lin X., and Yang Z. (2021). The SRCAP chromatin remodeling complex promotes oxidative metabolism during prenatal heart development. *Development* 148: dev199026.

128. Alazami A.M., Patel N., Shamseldin H.E., Anazi S., …Alkuraya F.S. (2014). Accelerating Novel Candidate Gene Discovery in Neurogenetic Disorders via Whole-Exome Sequencing of Prescreened Multiplex Consanguineous Families. *Cell Reports* 10: 148-161.

129. Hood R.L., Lines M.A., Nikkel S.M., Schwartzentruber J., …Boycott K.M. (2012). Mutations in SRCAP, Encoding SNF2-Related CREBBP Activator Protein, Cause Floating-Harbor Syndrome. *Am. J. Hum. Genet.* 90: 308-313.

130. International Mouse Phenotyping Consortium. (ND). *Gene: Ino80.* Retrieved from International Mouse Phenotyping Consortium: https://www.mousephenotype.org/data/genes/MGI:1915392.

131. Keil J.M., Doyle D.Z., Qalieh A., Lam M.M., …Kwan K.Y. (2020). Symmetric neural progenitor divisions require chromatin-mediated homologous recombination DNA repair by Ino80. *Nat Commun.* 11(1): 3839.

132. Bavley C.C., Rice R.C., Fischer D.K., Fakira A.K., …Rajadhyaksha A.M. (2018). Rescue of learning and memory deficits in the human nonsyndromic intellectual disability cereblon knock-out mouse model by targeting the AMP-activated protein kinase – mTORC1 translational pathway. *J. Neurosci.* 38(11): 2780-2795.

133. Ye B., Yang L., Qian G., Liu B., …Fan Z. (2020). The chromatin remodeler SRCAP promotes self-renewal of intestinal stem cells. *EMBO J.* 39: e103786.

134. Xu M., Yao J., Shi Y., Yi H., Zhao W., Lin X., and Yang Z. (2021). The SRCAP chromatin remodeling complex promotes oxidative metabolism during prenatal heart development. *Development.* 148(8): dev199026.

135. Ye B., Liu B., Yang L., Huang G., …Fan Z. (2017). Suppression of SRCAP chromatin remodelling complex and restriction of lymphoid lineage commitment by Pcid2. *Nature Commun.* 8: 1518.

136. Chen C.-W., Goodell M., Waldvogel S., and Zhang L. (2022). Srcap mutation promotes lymphoid bias in therapy-related clonal hematopoiesis. *Exp. Hem.* 111: S45-S164.

137. Timpano S. and Picketts D.J. (2020). Neurodevelopmental Disorders Caused by Defective Chromatin Remodeling: Phenotypic Complexity Is Highlighted by a Review of ATRX Function. *Front. Genet.* 11: 885.

138. Iwase S., Xiang B., Ghosh S., Ren T., …Shi Y. (2012). ATRX links atypical histone methylation recognition mechanisms to human brain function. *Nat. Struct. Mol. Biol.* 18(7): 769-776.

139. Argentaro A., Yang J. C., Chapman L., Kowalczyk M. S., …Rhodes D. (2007). Structural consequences of disease-causing mutations in the ATRX-DNMT3-DNMT3L (ADD) domain of the chromatin-associated protein ATRX. *Proc. Natl. Acad. Sci. U.S.A.* 104: 11939–11944.

140. Dhayalan, A., Tamas, R., Bock, I., Tattermusch, A., …Jeltsch A. (2011). The ATRX-ADD domain binds to H3 tail peptides and reads the combined methylation state of K4 and K9. *Hum. Mol. Genet*. 20: 2195–2203.

141. Eustermann, S., Yang, J. C., Law, M. J., Amos, R., …Neuhaus D. (2011). Combinatorial readout of histone H3 modifications specifies localization of ATRX to heterochromatin. *Nat. Struct. Mol. Biol*. 18: 777–782.

142. Allshire R.C. and Karpen G.H. (2008). Epigenetic regulation of centromeric chromatin: old dogs, new tricks? *Nat. Rev. Genet*. 9: 923–937.

143. Pidoux A.L. and Allshire R.C. (2005). The role of heterochromatin in centromere function. *Philos. Trans. R Soc. Lond. B Biol. Sci.* 360: 569–579.

144. McDowell T.L., Gibbons R.J., Sutherland H., O'Rourke D.M., …Higgs D.R. (1999). Localization of a putative transcriptional regulator (ATRX) at pericentromeric heterochromatin and the short arms of acrocentric chromosomes. *Proc. Natl. Acad. Sci. U.S.A*. 96: 13983–13988.

145. Goldberg A.D., Banaszynski L.A., Noh K.-M., Lewis P.W., …Allis C.D. (2010). Distinct factors control histone variant H3.3 localization at specific genomic regions. *Cell* 140: 678–691.

146. Mackenzie D., Watters A.K., To J.T., Young M.W., …Zhang D. (2021). ALT Positivity in Human Cancers: Prevalence and Clinical Insights. *Cancers.* 10: 2384.

147. Aguilera P. and Lopez-Contreras A.J. (2023). ATRX, a guardian of chromatin. *Trends in Genetics* 39(6): 505-519.

148. Law M.J., Lower K.M., Voon H.P., …Gibbons R.J. (2010). ATR-X syndrome protein targets tandem repeats and influences allele-specific expression in a size-dependent manner. *Cell* 143:367–378.

149. Bérubé N.G., Healy J., Medina C.F., Wu S., …Picketts D.J. (2008). Patient mutations alter ATRX targeting to PML nuclear bodies. *Eur. J. Hum. Genet.* 16: 192-201.

150. Bagheri-Fam S., Argentaro A., Svingen T., …Harley V.R. (2011). Defective survival of proliferating Sertoli cells and androgen receptor function in a mouse model of the ATR-X syndrome. *Hum. Mol. Genet.* 20: 2213–2224.

151. Xue Y., Gibbons R., Yan Z., Yang, D., …Wang W. (2003). The ATRX syndrome protein forms a chromatin-remodeling complex with Daxx and localizes in promyelocytic leukemia nuclear bodies. *Proc. Natl. Acad. Sci. U.S.A.* 100: 10635–10640.

152. Tang, J., Wu, S., Liu, H., Stratt, R., …Yang X. (2004). A novel transcription regulatory complex containing death domain-associated protein and the ATR-X Syndrome protein. *J. Biol. Chem*. 279: 20369–20377.

153. Hoelper D., Huang H., Jain A. Y., Patel D. J., and Lewis P. W. (2017). Structural and mechanistic insights into ATRX-dependent and -independent functions of the histone chaperone DAXX. *Nat. Commun.* 8: 1193.

154. Lewis P. W., Elsaesser S. J., Noh K. M., Stadler S. C., and Allis C. D. (2010). Daxx is an H3.3-specific histone chaperone and cooperates with ATRX in replication-independent chromatin assembly at telomeres. *Proc. Natl. Acad. Sci. U.S.A*. 107: 14075-14080.

155. Jang C.-W., Shibata Y., Starmer J., Yee D., and Magnuson T. (2015). Histone H3.3 maintains genome integrity during mammalian development. *Genes & Dev.* 29: 1377-1392.

156. Garrick D., Samara V., McDowell T.L., Smith A.J.H., …Gibbons R.J. (2004). A conserved truncated isoform of the ATR-X syndrome protein lacking the SWI/SNF homology domain. *Gene* 326: 23-34.

157. Vaisfeld A., Taormina S., Simonati A., and Neri G. (2022). Phenotypic Spectrum and Molecular Findings in 17 ATR-X Syndrome Italian Patients: Some New Insights. *Genes* 13(10): 1792.

158. Gibbons R.J. and Higgs D.R. (2000). Molecular-clinical spectrum of the ATR-X syndrome. *Am. J. Med. Genet.* 97: 204-212.

159. Martinez F., Tomas M., Millan J.M., Fernandez A., Palau F., and Prieto F. (1998). Genetic localisation of mental retardation with spastic diplegia to the pericentromeric region of the X chromosome: X inactivation in female carriers. *J. Med. Genet.* 35: 284-287.

160. Lossi A.M., Millan J.M., Villard L., Orellana C., …Martinez F. (1999). Mutation of the XNP/ ATR-X gene in a family with severe mental retardation, spastic paraplegia and skewed pattern of X inactivation: demonstration that the mutation is involved in the inactivation bias. *Am. J. Hum. Genet.* 65: 558-562.

161. Jezela-Stanek A., Fisher C., Szarras-Czapnik M., …Krajewska-Walasek M. (2009). X-linked alpha thalassaemia/mental retardation syndrome: a case with gonadal dysgenesis, caused by a novel mutation in ATRX gene. *Clin. Dysmorphol.* 18(3):168-171.

162. León N.Y. and Harley V.R. (2021). ATR-X syndrome: genetics, clinical spectrum, and management. *Hum. Genet.* 140: 1625-1634.

163. Wada T., Sugie H., Fukushima Y., and Saitoh S. (2005). Non-skewed X-inactivation may cause mental retardation in a female carrier of X-linked alpha-thalassemia/mental retardation syndrome (ATR-X): X-inactivation study of nine female carriers of ATR-X. *Am. J. Med. Genet. A.* 138:18-20.

164. Badens C., Martini N, Courrier S., …Edery P. (2006). ATRX syndrome in a girl with a heterozygous mutation in the ATRX Zn fnger domain and a totally skewed X-inactivation pattern. *Am. J. Med. Genet. A.* 140: 2212–2215.

165. Badens C., Lacoste C., Philip N., DesPortes V., …Levy P. (2006). Mutations in PHD-like domain of the ATRX gene correlate with severe psychomotor impairment and severe urogenital abnormalities in patients with ATRX syndrome. *Clin. Genet*. 70: F57-62.

166. Fulka H. and Langerova A. (2014). The maternal nucleolus plays a key role in centromere satellite maintenance during the oocyte to embryo transition. *Development*. 141: 1694-1704.

167. Garrick D., Sharpe J.A., Arkell R., Dobbie L., …Gibbons R.J. (2006). Loss of Atrx afects trophoblast development and the pattern of X-inactivation in extraembryonic tissues. *PLoS Genet.* 2: e58.

168. Bérubé N.G., Jagla M., Smeenk C., De Repentigny Y., Kothary R., and Picketts D.J. (2002). Neurodevelopmental defects resulting from ATRX overexpression in transgenic mice. *Hum. Mol. Genet.* 11(3): 253-261.

169. Bérubé N.G., Mangelsdorf M., Jagla M., Vanderluit J., …Picketts D.J. (2005). The chromatin-remodeling protein ATRX is critical for neuronal survival during corticogenesis. *J. Clin. Inv.* 115(2): 258-267.

170. Huh M.S., Ivanochko D., Hashem L.E., Curtin M., Delorme M., Goodall E., Yan K., and Picketts D.J. (2016). Stalled replication forks within heterochromatin require ATRX for protection. *Cell Death Dis.* 7(5): e2220.

171. Watson L.A., Solomon L.A., Li J.R., Jiang Y., Edwards M., Shin-ya K., Beier F., and Bérubé N.G. (2013). Atrx deficiency induces telomere dysfunction, endocrine defects, and reduced life span. *J. Clin. Invest.* 123(5): 2049-2063.

172. Teng Y.-C., Sundaresan A., O'Hara R., Gant V.U., Li M., Martire S., Warshaw J.N., Basu A., and Banaszynski L.A. (2021). ATRX promotes heterochromatin formation to protect cells from G-quadruplex DNA-mediated stress. *Nat. Commun.* 12: 3887.

173. Tamming R.J., Durneaux, Jiang Y., Qiu L.R., … Bérubé N.G. (2020). Atrx Deletion in Neurons Leads to Sexually Dimorphic Dysregulation of miR-137 and Spatial Learning and Memory Deficits. *Cell Rep.* 31: 107838.

174. Nogami T., Beppu H., Tokoro T., Moriguchi S., …Kitajima I. (2011). Reduced expression of the ATRX gene, a chromatin-remodeling factor, causes hippocampal dysfunction in mice. *Hippocampus.* 21(6): 678-687.

175. Shioda N., Beppu H., Fukuda, Li E., Kitajima I., and Fukunaga K. (2011). Aberrant Calcium/Calmodulin-Dependent Protein Kinase II (CaMKII) Activity is Associated with Abnormal Dendritic Spine Morphology in the ATRX Mutant Mouse Brain. *J. of Neurosci.* 31(1): 346-358.

176. Giustino T.F. and Maren S. (2015). The Role of the Medial Prefrontal Cortex in the Conditioning and Extinction of Fear. *Front. Behav. Neurosci.* 9:298.

177. Shioda N., Yakubi Y., Yamaguchi K., Onozato M., …Fukunaga K. (2018). Targeting G-quadruplex DNA as cognitive function therapy for ATR-X syndrome. *Nat. Med.* 24(6): 802-813.

178. Tillotson R., Yan K., Ruston J., DeYoung T., …Justice M.J. (2023). A new mouse model of ATR-X syndrome carrying a common patient mutation exhibits neurological and morphological defects. *Human Molecular Genetics* ddad05.

179. Micucci J.A., Sperry E.D., and Martin D.M. (2015). Chromodomain Helicase DNA-Binding Proteins in Stem Cells and Human Developmental Diseases. *Stem Cells and Development.* 24(8): 917-926.

180. Liu C., Kang N., Guo Y., and Gong P. (2021). Advances in Chromodomain Helicase DNA-Binding (CHD) Proteins Regulating Stem Cell Differentiation and Human Diseases. *Front. Cell Dev. Biol.* 9:710203.

181. Watson A. A., Mahajan P., Mertens H. D., Deer M. J., …Barkte T. (2012). The PHD and Chromo Domains Regulate the ATPase Activity of the Human Chromatin Remodeler CHD4. *J. Mol. Biol.* 433: 3-17.

182. Allen M.D., Bycroft M., and Zinzalla G. (2020). Structure of the BRK domain of the SWI/SNF chromatin remodeling complex subunit BRG1 reveals a potential role in protein-protein interactions. *Protein Sci.* 29(4): 1047-1053.

183. Hoffmeister, H., Fuchs A., Erdel F., Pinz S., …Hubier, C. (2017). CHD3 and CHD4 form distinct NuRD complexes with different yet overlapping functionality. *Nucleic Acids Research*. 45(18): 10534-10554.

184. Xue Y., Wong J., Moreno T., Young M., Cote J., and Wang W. (1998). NURD, a Novel Complex with Both ATP-Dependent Chromatin-Remodeling and Histone Deacetylase Activities. *Molecular Cell.* 2: 851-861.

185. Ho L. and Crabtree G. R. (2010). Chromatin remodelling during development. *Nature* 463: 474 - 484.

186. Lai A. Y., and Wade P. A. (2011). Cancer Biology and NuRD: a multifaceted chromatin remodeling complex. *Nature Reviews Cancer*. 11: 588-596.

187. Millard C.J., Varma N., Saleh A., Morris K., …Schwabe W.R. (2016). The structure of the core NuRD repression complex provides insights into its interaction with chromatin. *eLife*. 5: e13941.

188. Price J.D., Lindter S., Ypsilanti A., Binyameen F., …Rubenstein J.L.R. (2022). DLX1 and the NuRD complex cooperate in enhancer decommissioning and transcriptional repression. *Development.* 149(11): dev199508.

189. Wilczewski C.M., Hepperla A.J., Shimbo T., Wasson L., …Conlon F.L. (2018). CHD4 and the NuRD complex directly control cardiac sarcomere formation. *PNAS*. 115(26): 6727-6732.

190. Zhang X., Zhang C., Zhao Q., Wang S., …Ding W. (2023). Inhibition of Annexin A10 Contributes to ZNF281 Mediated Aggressiveness of Hepatocellular Carcinoma. *Journal of Hepatocellular Carcinoma.* 10: 553-571.

191. Vermunt M.W., Luan J., Zhang Z., Thrasher A.J., …Blobel G.A. (2023). Gene silencing dynamics are modulated by transiently active regulatory elements. *Molecular Cell*. 83(5): P715-P730.E6.

192. Nitarksa J., Smith J.G., Sherlock W.T., Wohlschlegel J.A., Mitter R., and Riccio A. (2016). A Functional Switch of NuRD Chromatin Remodeling Complex Subunits Regulates Mouse Cortical Development. *Cell Reports*. 17: 1683-1698.

193. Pilarowski G.O., Vernon H.J., Applegate C.D., Boukas L., …Bjornsson H.T. (2018). Missense variants in the chromatin remodeler CHD1 are associated with neurodevelopmental disability. *J. Med. Genet.* 55(8): 561-566.

194. Lamar K.M.J and Carvill G.L. (2018). Chromatin remodeling proteins in epilepsy: lessons from CHD2-associated epilepsy. *Frontiers in Molecular Neuroscience* 11: 208.

195. Yasin H. and Zahir F.R. (2020). Chromodomain helicase DNA-binding proteins and neurodevelopmental disorders. *J. Trans. Genet. Genom.* 4: 307-319.

196. Feng W., Fang F., Wang X., Chen C., Lu J., and Deng J. (2022). Clinical analysis of CHD2 gene mutations in pediatric patients with epilepsy. *Pediatr. Investig.* 6(2): 93-99.

197. Carvill G.L. and Mefford H.C. (2021). CHD2-Related Neurodevelopmental Disorders. In: Adam M.P., Mirzaa G.M., Pagon R.A., et al., editors. *GeneReviews* [Internet]. Seattle (WA): University of Washington, Seattle; 1993-2023.

198. Tucker T., Zahir F.R., Griffith M., Delaney A., …Friedman J.M. (2014). Single exon-resolution targeted chromosomal microarray analysis of known and candidate intellectual disability genes. *Eur. J. Hum. Genet.* 22: 792-800.

199. Hall B.D. (1979). Choanal atresia and associated multiple anomalies. *J. Pediatr.* 95: 395-398.

200. Hittner H.M., Hirsch N.J., Kreh G.M., and Rudolph A.J. (1979). Colobomatous microphthalmia, heart disease, hearing loss, and mental retardation – a syndrome. *J. Pediatr. Ophthalmol. Strabismus* 16:122-128.

201. Pagon R.A., Graham J.M., Zonana J., and Yong S.L. (1981). Coloboma, congenital heart disease, and choanal atresia with multiple anomalies: CHARGE association. *J. Pediatr.* 99: 223-227.

202. Weissberg O. and Elliot E. (2021). The Mechanisms of CHD8 in Neurodevelopment and Autism Spectrum Disorders. *Genes*. 12(8): 1133.

203. Wilkinson B., Grepo N., Thompson B.L., Kim J., Wang K., Evgrafov O.V., Lu W., Knowles J.A., and Campbell D.B. (2015). The autism-associated gene chromodomain helicase DNA-binding protein 8 (*CHD8*) regulates noncoding RNAs and autism-related genes. *Transl. Psychiatry.* 5: e568.

204. Cotney J., Muhle R.A., Sanders S.J., Liu L., …Noonan J.P. (2015). The autism-associated chromatin modifier CHD8 regulates other autism risk genes during human neurodevelopment. *Nature Commun.* 6: 6404.

205. Bernier R., Golzio C., Xiong B., Stessman H.A., …Eichler E.E. (2014). Disruptive *CHD8* Mutations Define a Subtype of Autism Early in Development. *Cell.* 158(2): 263-276.

206. Barnard R.A., Pomaville M.B., and O'Roak B.J. (2015). Mutations and Modeling of the Chromatin Remodeler CHD8 Define an Emerging Autism Etiology. *Front. Neurosci.* 9:477.

207. Yasin H., Gibson W.T., Langlois S., Stowe R.M., …Zahir F.R. (2019). A distinct neurodevelopmental syndrome with intellectual disability, autism spectrum disorder, characteristic facies, and macrocephaly is caused by defects in CHD8. *J Hum Genet*. 64(4):271-280.

208. Alvarez-Mora M.I., Sanchez A., Rodriguez-Revenga L., Corominas J., …Madrigal I. (2022). Diagnostic yield of next-generation sequencing in 87 families with neurodevelopmental disorders. *Orphanet Journal of Rare Diseases.* 17: 60.

209. Wu J., Yu P., Jin X., Xu X., Sun Z.H. (2018). Genomic landscapes of Chinese sporadic autism spectrum disorders revealed by whole-genome sequencing. *J. Genet. Genom*. 45(10): 527-538.

210. Li J., Wang L., Guo H., Shi L., Xia S. (2017). Targeted sequencing and functional analysis reveal brain-size-related genes and their networks in autism spectrum disorders. *Mol Psychiatry*. 22(9):1282-1290.

211. Lim E.T., Uddin M., De Rubeis S., Chan Y., …Walsh C.A. (2017). Rates, distribution and implications of postzygotic mosaic mutations in autism spectrum disorder. *Nat Neurosci*. 20(9): 1217-1224.

212. Sifrim A., Hitz M.P., Wilsdone A., Breckpot J., Turki S.H.A., Thienpont B., and Hurles M.E. (2016). Distinct genetic architectures for syndromic and nonsyndromic congenital defects identified by exome sequencing. *Nature Genetics.* 48: 1060-1065.

213. Weiss K., Terhal P., Cohen L., Bruccoleri M., Irving M., Martinez A.F., and Muenke M. (2016). De novo mutations in CHD4, an ATP-dependent chromatin remodeler gene, cause an intellectual disability syndrome with distinctive dysmorphisms. *American Journal of Human Genetics.* 99: 934-931.

214. Weiss K., Lazar H.P., Kurolap A., Martinez A.F., …Lachlan K. (2020). The CHD4-related syndrome: a comprehensive investigation of the clinical spectrum, genotype-phenotype correlations, and molecular basis. *Genetics in Medicine*. 22: 389-397.

215. Snijders Blok L., Rousseau J., Twist J., Ehresmann S., …Campeau P.M. (2018). CHD3 helicase domain mutations cause a neurodevelopmental syndrome with macrocephaly and impaired speech and language. *Nature Commum.* 9: 4619.

216. Coursimault J., Lecoquierre F., Saugier-Veber P., Drouin-Garraud V., …Brehin A.-C. (2021). Hypersociability associated with developmental delay, macrocephaly and facial dysmorphism points to CHD3 mutations. *Eur. J. Hum. Genet.* 64:104166.

217. van der Spek J., den Hoed J., Snijders Blok L., Dingemans A.J.M., …Kleefstra T. (2022). Inherited variants in CHD3 show variable expressivity in Snijders Blok-Campeau syndrome. *Genetics in Medicine.* 24(6): 1283-1296.

218. Parenti I., Lehalle D., Nava C., Torti E., …Mignot C. (2021). Missense and truncating variants in CHD5 in a dominant neurodevelopmental disorder with intellectual disability, behavioural disturbances, and epilepsy. *Human Genetics.* 140: 1109-1120.

219. Boulasiki, P., Tan X.W., Spinelli M., and Riccio A. (2023). The NuRD Complex in Neurodevelopment and Disease: A Case of Sliding Doors. *Cells*. 12:1179.

220. International Mouse Phenotyping Consortium. (ND). *Gene: Chd5.* Retrieved from International Mouse Phenotyping Consortium: https://www.mousephenotype.org/data/genes/MGI:1344395.

221. International Mouse Phenotyping Consortium. (ND). *Gene: Chd5.* Retrieved from International Mouse Phenotyping Consortium: https://www.mousephenotype.org/data/genes/MGI:3036258.

222. Yamada T., Yang Y., Hemberg M., YoshidaT., …Bonni A. (2014). Promoter Decommissioning by the NuRD Chromatin Remodeling Complex Triggers Synaptic Connectivity in the Mammalian Brain. *Neuron.* 83:133-134.

223. Larrigan S., Joshi S., and Mattar P. (2023). Modelling Sifrim-Hitz-Weiss Syndrome using mouse genetics. [Manuscript submitted for publication].

224. Zhuang T., Hess R.A., Kolla V., Higashi M., Raabe T.D., and Brodeur G.M. (2014). CHD5 is required for spermiogenesis and chromatin condensation. *Mech. Dev.* 131: 35-46.

225. Pisansky M.T., Young A.E., O'Connor M.B., Gottesman I.I., Bagchi A., and Gerwitz J.C. (2017). Mice lacking the chromodomain helicase DNA-binding 5 chromatin remodeler display autism-like characteristics. *Transl. Psychiatry.* 7: e1152.

226. Xie J., Schafer C., Colijn S., Muthukumar V., and Griffin C.T. (2020). The chromatin-remodeling enzyme CHD3 plays a role in embryonic viability but is dispensable for early vascular development. *PLoS ONE* 15(7): e0235799.

227. Buglo, E., Sarmiento, E., Martuscelli, N. B., Sant, D. W., Danzi, M. C., Abrams, A. J., Dallman, J. E., Zuchner, S. (2020). Genetic compensation in a stable *slc25a46* mutant zebrafish: A case for using F0 CRISPR mutagenesis to study phenotypes caused by inherited disease. *PLoS ONE*, 6309-6314.

228. Telley L., Agirman G., Prados J., Amberg N., …Jabaudon D. (2019). Temporal patterning of apical progenitors and their daughter neurons in the developing neocortex. *Science* 364 (6440): eaav2522.

229. Treit D. and Fundytus M. (1988). Thigmotaxis as a test for anxiolytic activity in rats. *Pharmacol Biochem Behav*. 31(4): 959-962.

230. Huang Y., Zhou W., and Zhang Y. (2012). Bright lighting conditions during testing increase thigmotaxis and impair water maze performance in BALB/c mice. *Behav Brain Res*. 226(1): 26-31.

231. Goodman J. and McIntyre C.K. (2017). Impaired spatial memory and enhanced habit memory in a rat model of post-traumatic stress disorder. *Front Pharmacol*. 8: 663.

232. Packard M.G. and Wingard J.C. (2004). Amygdala and "emotional" modulation of the relative use of multiple memory systems. *Neurobiol Learn Mem*. 82(3): 243-252.

233. Nelson R.J. and Chiavegatto S. (2000). Aggression in Knockout Mice. *ILAR Journal.* 41(3): 153-162.

234. Karpati A., Yoshikawa T., Naganuma F., Matsuzawa T., …Yanai K. (2019). Histamine H1 receptor on astrocytes and neurons controls distinct aspects of mouse behaviour. *Scientific Reports.* 9(1): 16451.

235. Hasu M., Lagace D., Grouleau M., and Kealey S. (2020). BEHAV-8 Adult Social Interaction. *uOttawa ACVS Standard Operating Procedure*.

236. Persson B.M., Ambrozova V., Duncan S., Wood E.R., O'Connor A.R., and Ainge J.A. (2022). Lateral entorhinal cortex lesions impair odor-context associative memory in rats. *J. Neurosci. Res.* 100(4): 1030-1046.

237. Kjelstrup K.G., Tuvnes F.A., Steffenach H.A., Murison R., Moser E.I., and Moser M.-B. (2002). Reduced fear expression after lesions of the ventral hippocampus. *PNAS*. 99(16): 10825-10830.

238. Varholick J.A., Pontiggia A., Murphy E., Daniele V., …Bailoo J.D. (2019). Social dominance hierarchy type and rank contribute to phenotypic variation within cages of laboratory mice. *Scientific Reports.* 9: 13650.

239. Williamson C.M., Franks B., and Curley J.P. (2016). Mouse Social Network Dynamics and Community Structure are Associated with Plasticity-Related Brain Gene Expression.

240. Wang F., Kessel H.W., and Hu H. (2014). The mouse that roared: neural mechanisms of social hierarchy. *Trends. Neurosci.* 37(11): 674-682.

241. Hatanaka Y., Zhu Y., Torigoe M., Kita Y., and Murakami F. (2016). From migration to settlement: the pathways, migration modes and dynamics of neurons in the developing brain. *Proc. Jpn. Acad. Ser. B. Phys. Biol. Sci.* 92(1): 1-19.

242. Noctor S.C., Cunningham C.L., and Kreigstein A.R. (2013). Radial Migration in the Developing Cerebral Cortex. P. 299-312 *in* Cellular Migration and Formation of Neuronal Connections: Comprehensive Developmental Neuroscience. Elsevier.

243. Chen G., Sima J., Jin M., Wang K., …Yuan X.-B. (2007). Semaphorin-3A guides radial migration of cortical neurons during development. *Nature Neuroscience.* 11: 36-44.

244. Pan Y.-H., Wu N., and Yuan X.-B. (2019). Toward a Better Understanding of Neuronal Migration Deficits in Autism Spectrum Disorders. *Front. Cell Dev. Biol.* 7: 205.

245. Maren S., and Quirk G.J. (2004). Neuronal signalling of fear memory. *Nat. Rev. Neurosci.* 5: 844-852.

246. Herry C., Ferraguti F., Singewald N., Letzkus J.J., Ehrlich I., and Lüthi A. (2010). Neuronal circuits of fear extinction. *Eur. J. Neurosci*. 31: 599-612.

247. Paré D., Quirk G.J., and Ledoux J.E. (2004). New Vistas on Amygdala Networks in Conditioned Fear. *J. Neurophysiol.* 92: 1-9.

248. Lee H., Heller A.S., van Reekum C.M., Nelson B., and Davidson R.J. (2012). Amygdala-prefrontal coupling underlies individual differences in emotional regulation. *Neuroimage.* 62(3): 1575-1581.

249. Nitecka L., and Ben-Ari Y. (1987). Distribution of GABA-like immunoreactivity in the rat amygdaloid complex. J. Comp. Neurol. 266: 45-55.

250. Paré D., and Smith Y. (1993). Distribution of GABA immunoreactivity in the amygdaloid complex of the cat. *Neuroscience* 57: 1061-1076.

251. Royer S., Martina M., and Paré D. (1999). An inhibitory interface gates impulse traffic between the input and output stations of the amygdala. *J. Neurosci*. 19: 10575-10583.

252. Lee S., Kim S.-J., Kwon O.-B., Lee J. H., and Kim J.-H. (2013). Inhibitory networks of the amygdala for emotional memory. *Front. Neural Circuits* 7:129

253. Wolff S.B.E., Gründemann J., Tovote P., Krabbe S., …Luthi A. (2014). Amygdala interneuron subtypes control fear learning through disinhibition. *Nature* 509: 453-458.

254. Riga D., Matos M.R., Glas A., Smit A.B., Spijker S., and Van den Oever M.C. (2014). Optogenetic dissection of medial prefrontal cortex circuitry. *Front. Syst. Neurosci*. 8:230.

255. Sotres-Bayon F., and Quirk G.J. (2010). Prefrontal control of fear: more than just extinction. *Curr. Opin. Neurobiol*. 20: 231-235.

256. Milad M.R. and Quirk G.J. (2012). Fear extinction as a model for translational neuroscience: ten years of progress. *Annu. Rev. Psychol.* 63: 129-151.

257. Maren S., Phan K. L., and Liberzon I. (2013). The contextual brain: implications for fear conditioning, extinction and psychopathology. *Nat. Rev. Neurosci*. 14: 417-428.

258. Vervliet B., Craske M.G., and Hermans D. (2013). Fear extinction and relapse: state of the art. *Annu. Rev. Clin. Psychol*. 9: 215-248.

259. Goode T. D. and Maren S. (2014). Animal models of fear relapse. *ILAR J.* 55: 246-258.

260. Corcoran K. A. and Maren S. (2001). Hippocampal inactivation disrupts contextual retrieval of fear memory after extinction. *J. Neurosci*. 21: 1720-1726.

261. Hobin J.A. and Maren, S. (2006). Ventral hippocampal muscimol disrupts context-specific fear memory retrieval after extinction in rats. *Hippocampus* 16: 174-182.

262. Zelikowsky M., Pham D.L., and Fanselow M.S. (2012). Temporal factors control hippocampal contributions to fear renewal after extinction. *Hippocampus* 22: 1096-1106.

263. Maren S., and Hobin J.A. (2007). Hippocampal regulation of context-dependent neuronal activity in the lateral amygdala. *Learn. Mem.* 14: 318-324.

264. Phillips R.G., and Ledoux J.E. (1992). Differential contribution of amygdala and hippocampus to cued and contextual fear conditioning. *Behav. Neurosci.* 106: 274-285.

265. Frankland P.W., Cestari V., Filipkowski R.K., McDonald R.J., and Silva A.J. (1998). The dorsal hippocampus is essential for context discrimination but not for contextual conditioning. *Behav. Neurosci.* 112: 863-874.

266. Wiltgen B.J., Sanders M.J., Anagnostaras S.G., Sage J.R., and Fanselow M.S. (2006). Context fear learning in the absence of the hippocampus. *J. Neurosci*. 26: 5484-5491.

267. Jin J., and Maren S. (2015). Fear renewal preferentially activates ventral hippocampal neurons projecting to both amygdala and prefrontal cortex in rats. *Sci. Rep*. 5:8388.

268. Halder R., Hennion M., Shomroni O., Rahman R., …Bonn S. (2015). DNA methylation changes in plasticity genes accompany the formation and maintenance of memory. *Nature Neuroscience.* 19: 102-110.

269. El-Brolosy M. A., Kontarakis, Z., Rossi, A., Kuenne C., …Stainier D.Y.R. (2019). Genetic Compensation triggered by mutant mRNA degradation. *Nature Research*, 568: 193-215.

270. Knoedler J.R., Inoue S., Bayless D.W., Yang T., …Shah N.M. (2023). A functional cellular framework for sex and estrous cycle-dependent gene expression and behaviour. *Cell.* 185(4): 654-671.

271. National Institute of Neurological Disorders and Stroke. (2023, 01 20). *Neuronal Migration Disorders*. Retrieved from National Institute of Neurological Disorders and Stroke: https://www.ninds.nih.gov/health-information/disorders/neuronal-migration-disorders

272. Hodge R.D., Bakken T.E., Miller J.A., Smith K.A., …Lein E.S. (2019). Conserved cell types with divergent features in human versus mouse cortex. *Nature.* 573: 61-68.